ABSORPTION SPECTROSCOPY AND SURFACE ENHANCED VIBRATIONAL TECHNIQUES FOR MONITORING DEPHOSPHORYLATION AND PHOSPHORYLATION REACTIONS IN MODEL COMPOUNDS

By

Kennedy Uchenna Eguzozie

Submitted in accordance with the requirements

For the degree of

DOCTOR OF PHILOSOPHY

In the subject

CHEMISTRY

At the

UNIVERSITY OF SOUTH AFRICA

SUPERVISOR: PROFESSOR FIKRU TAFESSE (PhD)

CO-SUPERVISOR: PROFESSOR SYLVIA PAUL (PhD)

JUNE 2012

DECLARATION

I, Kennedy Uchenna Eguzozie sincerely and solemnly declare that the work: ABSORPTION SPECTROSCOPY AND SURFACE ENHANCED VIBRATIONAL TECHNIQUES FOR MONITORING DEPHOSPHORYLATION AND PHOSPHORYLATION REACTIONS IN MODEL STUDIES is my work and that all sources that have been quoted have been indicated and acknowledged by means of complete references.

---------- ----------

DEDICATION

This research thesis is dedicated to:

The divine will of the Almighty God, my creator and redeemer

Lord, again take my silver and my gold

Not a mite would I withhold

Take my intellect, O Lord

And use it as thou shall choose.

What a divine and marvelous privilege

It has been to always sing your praise

And to be a laborer in your vineyard

To my loving parents, Mr. Denis Ugbedechi Eguzozie & Mrs. Evelyn Nnenna Eguzozie.

My brothers and sisters (Ngozi, Ada, Oby, Gladys, Chijioke, Harriet, Chinedu, Benson, Adaku, Emeka and Kelechi).

My loving wife Chioma Kennedy Eguzozie (an angel that heaven made specifically for me) and the mother of my children. I thank you so much baby for all the sacrifices that you have made toward me and our children. May the Almighty God continue to bless and prosper you all the days of your life. My

solemn prayer is for you to realize that you will always be beautiful in my eyes, as the coming years will show…. Love you my girl.

To my children (my gifts of love) Mmesoma Kennedy Eguzozie, Adamaka Kennedy Eguzozie and Chisimdi Kennedy Eguzozie. I can see in you my dreams come true. Daddy loves you more than you can ever imagine. Thanks guys for all the joy that you bring me

ACKNOWLEDGEMENT

I give my warmest gratitude to my supervisor Professor Fikru Tafesse not only for initiating the project, but also for his guidance and unwavering encouragement during the course of the project. Sir, thanks a lot for the mentoring. I will always remain grateful to you and your family.

My immeasurable thanks also go to my co-supervisor Professor Silvia Paul for all her very well directed and positive contributions during the course of this project. Your wealth of expertise especially in the field of Raman spectroscopy is well appreciated, and I thank you immensely.

I like to thank from the bottom of my heart, the head of the Department of Chemistry at the University Of South Africa (UNISA), Professor Jack Mphahlele for giving me the privilege and the opportunity to have a taste of higher chemistry. Prof thanks a lot for all the emotional and financial support all these years.

I owe my elder brother Mr. Nick Ngozi Eguzozie lots of thanks for all the sacrifices that he made to see me through my Bachelors degree program. Dede, thanks for the emotional, financial and inspirational support all these years. How good it feels to have shared the same womb with you, and to have suckled from the same breast as you did. We your siblings are so proud of you and we love so dearly.

My sincere gratitude also goes to the Department of Chemistry, College of Science, Engineering and Technology and the University Of South Africa (UNISA), for the financial assistance extended to me in the form of post graduate academic assistant.

My gratitude also goes to all staff members of the Department of Chemistry at UNISA, my office mates, Martin Enemchukwu and Augustine Makwakwa for their well appreciated contribution, and to everyone who has made this work possible by providing support. It does not matter how small the contribution has been, it is all highly appreciated.

Above all, I would like to give the greatest appreciation and adoration to our heavenly father Jesus Christ for all his favors and blessings towards me and my family ever since I came to South Africa. Lord again; take all my silver and my gold, not a mite will I withhold. Take my intellect O Lord, and use it as thou shall choose. My faith and trust in you, have moved the highest mountain, turn a desert into a fountain, and have parted the waters of the deepest sea. My faith in you Lord, has made my broken heart to mend, and has now brought the rains from heaven. It has been an immeasurable privilege laboring in your vineyard dear Lord.

ABSTRACT

Mechanistic aspects of phosphorylation, dephosphorylation, pyrophosphorylation and depyrophosphorylation reactions that mimic phosphorylases, dephosphorylases, pyrophosphorylases and depyrophosphorylases have been studied in the biologically important middle pH region. The different systems monitored are; (a) the reactions between $[\{CoN_4(OH)(OH_2)\}]^{2+}$ and $[HPO_4]^-$ for 1:1, 2:1 and 3:1 $[\{CoN_4(OH)(OH_2)\}]^{2+}$ to $[HPO_4]^{2-}$ ratios. (b) the reactions between $[\{CoN_4PO_4]$ and $[O_2NC_6H_4O]^-$ (abbreviated as NP^-) for 1:1, 2:1 and 3:1 $[\{CoN_4PO_4]$ to $[O_2NC_6H_4O]^-$ ratios. (c) the reactions between $[\{CoN_4(OH)(OH_2)\}]^{2+}$ and $[O_2NC_6H_4PO_4]^{2-}$ (abbreviated as NPP^{2-}) for 1:1, 2:1 and 3:1 $[\{CoN_4(OH)(OH_2)\}]^{2+}$ to $[O_2NC_6H_4PO_4]^{2-}$ ratios. (d) the reactions between $[\{CoN_4(OH)(OH_2)\}]^{2+}$ and $[H_2P_2O_7]^{2-}$ for 1:1, 2:1 and 3:1 $[\{CoN_4(OH)(OH_2)\}]^{2+}$ to $[H_2P_2O_7]^{2-}$ ratios. (e) the reactions between $[\{CoN_4P_2O_7\}]^-$ and $[O_2NC_6H_4O]^-$ for 1:1, 2:1 and 3:1 $[\{CoN_4P_2O_7\}]^-$ to $[O_2NC_6H_4O]^-$ ratios.

Significant phosphorylation was noted for systems containing 1:1 molar ratio $[\{CoN_4PO_4]$ and $[O_2NC_6H_4O]^-$. Enhanced phosphorylation was depicted for system containing 1:1 molar ratio of $[\{CoN_4(OH)\}_2PO_4]^+$ and $[O_2NC_6H_4O]^-$. Pyrophosphorylation was noted for reactions of 1:1 molar

ratio of $[\{CoN_4P_2O_7\}]^-$ and $[O_2NC_6H_4O]^-$· The rate of pyrophosphorylation was substantially reduced for systems that were 2:1 in molar ratio of $[\{CoN_4P_2O_7\}]^-$ and $[O_2NC_6H_4O]^-$. No appreciable pyrophosphorylation was noted for systems, which has a 3:1 molar ratio of $[\{CoN_4P_2O_7\}]^-$ and $[O_2NC_6H_4O]^-$. Specific mechanistic features and the possible roles metal ions play in phosphorylase, dephosphorylase and pyrophosphorylase are highlighted from results of UV-Visible spectroscopy, ^{31}P $\{^1H\}$ NMR spectroscopy and Surface Enhanced Raman Scattering (SERS) studies.

** For the structures of complexes formed in solution, see chapter 3, table 1*

TABLE OF CONTENTS

LIST OF TABLES

LIST OF FIGURES

LIST OF REACTION SCHEMES

CHAPTER ONE

Project background

Reversible phosphorylation/dephosphorylation and pyrophosphorylation/depyrophosphorylation reactions play critical roles in mediating cellular responses to extracellular or intracellular stimuli. They initiate multiple levels of protein phosphorylation/dephosphorylation and pyrophosphorylation/depyrophosphorylation reactions that activate and deactivate specific carbohydrate and protein targets. Examples include, *trans*-cytoplasmic signalling to the nucleus by the nitrogen-activated protein kinase pathway[1], cell cycle regulation mediated by the action of kinases[2], and the regulation of metabolic enzymes such as glycogen phosphorylases, glycogen dephosphorylases, glycogen synthases and acetyl-CoA carboxylases through the second messenger cAMP[3]. Accordingly, these reactions are also known to play major role in the biological world by linking the processes of respiration and fermentation with other cellular reactions.

These biochemical processes are accomplished by phosphorylases, dephosphorylases, pyrophosphorylases, and depyrophosphorylases.
Phosphorylases/dephosphorylase catalyze the addition/removal of a phosphate group to/from an acceptor while pyrophosphorylases/depyrophosphorylases catalyze the addition/removal of a pyrophosphate group to/from an acceptor. A typical example of this process is found in the liver, muscle and other tissues in living organisms. The liver secretes glucose into

to keep blood glucose level constant. Liver, muscles and other tissues also store glucose as glycogen. Glycogen synthesis begins with glucose-1-phosphate which can be synthesized from glucose-6-phosphate by the phosphorylating action of the enzyme phosphoglucomutase. Reversibly, glycogen is broken down principally by glycogen phosphorylase. This enzyme (usually known simply as “phosphorylase”) uses the cofactor pyridoxal 5’ phosphate (PLP) to cleave glycogen. Note that the reaction is not hydrolytic as no water is used in the cleavage reaction. Instead, inorganic phosphate combines with the non-reducing terminal glucose residue to give glucose-1-phosphate[4]. Glycogen phosphorylase cleaves only glucose residue attached to glycogen via alpha (α 1, 4-linkage). Lysis of the C_1-O bond provides sufficient energy to produce glucose-1-phosphate without the expenditure of adenosine triphosphate (ATP). This makes the storage of carbohydrate as glycogen more energy efficient, since ATP is not required to form glucose-6-phosphate. It is also worth mentioning that one of the first enzymes for which reversible phosphorylation and dephosphorylation reactions were established as a control mechanism was muscle phosphorylases[4]. Structural studies on the nonphosphorylated and phosphorylated forms of the rabbit muscle glycogen phosphorylase led to an understanding of the structural basis of its activation by phosphorylation and deactivation by dephosphorylation as has been reported[5]. Protein phosphorylation is not always an activation mechanism; however, an example of the opposite response is given by isocitrate dehydrogenase, which is inhibited by phosphorylation[6]. In mammals, the phosphorylase

enzyme 3-hydroxy-3-methyl-glutaryl-Coenzyme A (HMG.CoA reductase) catalyzes the rate limiting step in the biosynthesis of isoprenoids, isoprenoid derivatives and cholesterol. On the cellular level the activity of phosphorylase in higher eukaryotes is regulated post-translationally by reversible phosphorylation reactions[7]. The mechanism for its down regulation by phosphorylation/dephosphorylation is simple and in this case no change in conformation is involved. Instead, inhibition is achieved by phosphorylation or dephosphorylation of the serine residue (Ser 113), at the start of an α helix. The negatively charged phosphorylated and dephosphorylated group block access to the catalytic site by the anionic isocitrate substrate through steric and electrostatic effects. These cascades of enzyme catalyzed dephosphorylation and phosphorylation reactions have also been reported[8] to be essential in the energy balance for all living organisms, especially in the cellular control mechanisms of glycolysis, glucogenesis, glucogenolysis and gluconeogenesis.

Many of the enzymes involved in dephosphorylation, phosphorylation, pyrophosphorylation, depyrophosphorylation reactions are metalloenzymes that require metal ions for their reactivity. Divalent metal ions have been known as promoters for the dephosphorylation and phosphorylation reactions[9,10]. Divalent metal ions are substitutionally labile and therefore form a variety of complexes, many of which are in rapid equilibrium. As result it has been quite difficult to define any particular complex or binding mode as being responsible for the observed rate enhancement. In spite of these difficulties, considerable progress has now been made in this area.

Different modes of cleavage of phosphate moieties in dephosphorylation and related phosphoryl group transfer involve the cleavage within the P-O or O-C framework as shown below.

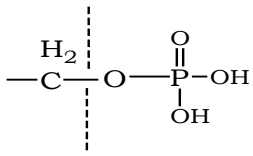

if the rapture is at the O - C bond, there will be a whole group phosphate transfer

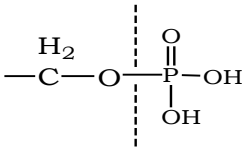

if the rupture is at the P - O bond there will be a whole phosphoryl group transfer

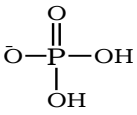

a phosphate group

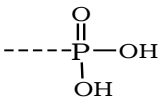

a phosphoryl group

Substitution lability is an essential requirement for efficient catalysis and it is for this reason that enzymes primarily use first row transition metal ions as cofactors. A number of these enzymes and enzymatic models have been studied[11-14] in considerable details and various proposals have been advanced regarding the role of metal ions in catalyzing or promoting these biochemical reactions. It has been reported by previous investigators that phosphorylase activation requires Mn^{2+} and ATP. The activity is attributed to the production of cyclic AMP in the reaction. A protein kinase which is stimulated by cAMP is responsible not only for activating phosphorylase, but also for inactivating glycogen synthase[15]. The nonphosphorylated form of the enzyme "phosphorylase b" is less active than the phosphorylated form "phosphorylase a". Phosphorylase a then convert's glycogen to glucose-1-phosphate. The end

result in this phosphorylation and dephosphorylation reactions is an increased energy supply for metabolism.

Some of the various proposals which have been advanced regarding the role of metal ions in catalyzing or promoting the dephosphorylation/phosphorylation and pyrophosphorylation/depyrophosphorylation reactions are discus- see below.

(1) Charge neutralization or shielding: like protons metal ions are Lewis acids or electrophiles. They can serve as a general acid catalyst for reactions catalyzed by protons. Secondly phosphate derivatives usually carry many negative charges so that the approach of a negatively charged nucleophile such as a hydroxide ion is not favoured on electrostatic grounds. Therefore the neutralization or shielding of these negative charges is very necessary for a perfect dephosphorylation or phosphorylation by the electrophilic activation of the phosphorus metal centre.

(2) Strain induction: The bidentate coordination of a phosphate monoester to a metal ion could result in the formation of a strained chelate ring thus facilitating a nucleophilic attack at the phosphorus centre.

(3) Template formation for orientating substrate in optimum stereochemical position: Metal ions enhance the optimal stereochemical orientation for intramolecular hydrolytic attack by the nucleophile.

(4) Generation of coordinated nucleophile at biological pH: Hydroxide is a better nucleophile than water but its concentration would be low at pH 6.5. This problem is overcome by the simultaneous coordination of water and phosphate esters to a metal atom. Coordinated hydroxide then acts as a Nucleophile to promote hydrolysis.

The mechanisms employed by enzymes to catalyze dephosphorylation/ phosphorylation and pyrophosphorylation/depyrophosphorylation reactions are not well understood despite the advance in research in the area of enzymology. It has been suggested that complexation with a metal ion could change the mechanistic features of these biochemical processes from a largely dissociative mechanism observed in the absence of a metal ion to an associative mechanism with more nucleophilic involvement in the transition state[16-20]. A change from a dissociative to an associative mechanism would allow for catalysis to occur by induced intramolecularity in an enzymatic reaction. This is because reactions with stable transition states have stricter requirements for alignment than reactions with unstable transition states [21-23]. This is due to the increased bond formation by the nucleophile in the transition state. It is worth mentioning, that the specific mechanistic features and the possible roles which metal ions play

in these biochemical processes are still not well understood. This research project is geared towards having a better insight into specific mechanistic features by mimicking the possible roles which metal ions play in the associated enzymes by employing of UV-Visible spectroscopy, ^{31}P NMR spectroscopy and Surface Enhanced Vibrational techniques in model compounds.

1.1 Mechanisms of phosphorylation/dephosphorylation and pyro-phosphorylation /depyrophosphorylation reactions.

A comparison of the reaction mechanisms of phosphorylases, dephosphorylases, pyrophosphorylases and depyrophosphorylases, with those of the uncatalysed analogues, have been the focus of considerable study[24-26]. The postulated mechanisms involved in these biochemical reactions are discussed below.

1.1.1 Dissociative mechanism: This is otherwise known as the D mechanism (S_N1). It proceeds via an extremely reactive three coordinate metaphosphate intermediate.

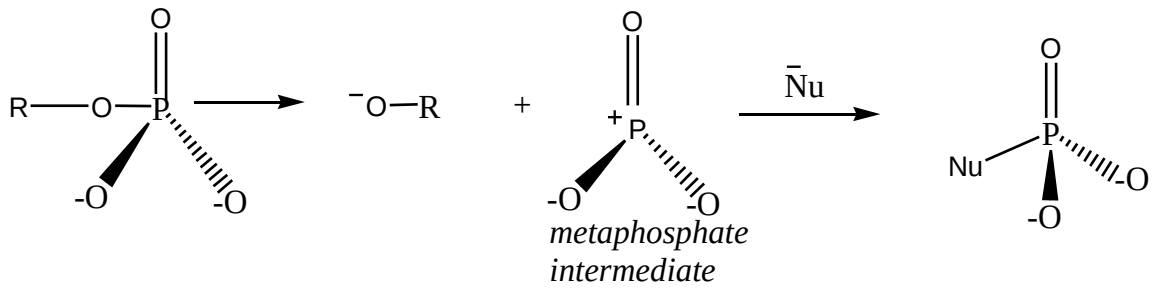

The nascent trigonal metaphosphate species could, if free, react with a nucleophile on either face to give a racemic product. The monomeric metaphosphate anion has also been directly observed in the gas phase by mass spectrometry.

1.1.2 Associative mechanism*:* This is called the A mechanism (S_N2) and would give an inversion of configuration. It proceeds by the addition of a nucleophile at the phosphorus to generate a five coordinate intermediate or transition state because the phosphorus atom can readily expand its coordination number by use of its d-orbital. An attacking nucleophile such as hydroxide adds to four coordinate phosphorus molecule to give a pentacoordinate phosphorane. Normally the phosphorane will have a trigonal bipyramidal stereochemistry, but spirocyclic phosphoranes appear to favour square pyramidal structures.

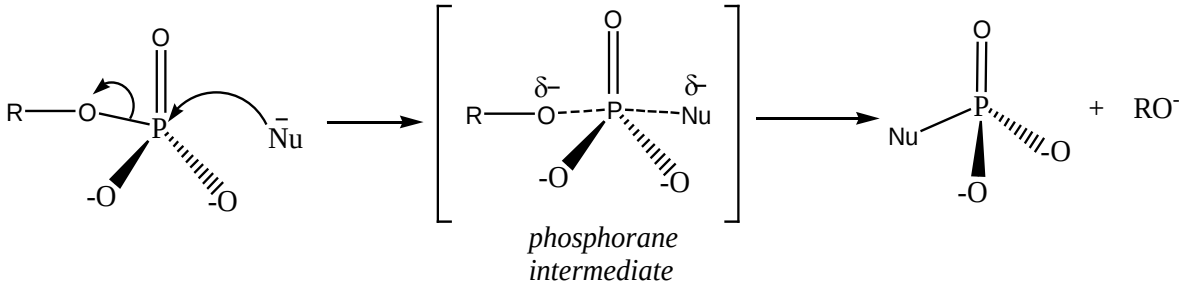

The associative mechanism can be further explained using the inline addition and the adjacent addition mechanisms but in all a phosphorane intermediate is formed. Both methods only shed light on the state of the intermediate as displacement and rearrangement within the molecule is achieved.

1.1.2.1 ***In-Line Associative Addition***: This process gives rise to a pentacoordinate stable intermediate with fully formed bonds. The displacement occurs with inversion of configuration as with S_N2 mechanism.

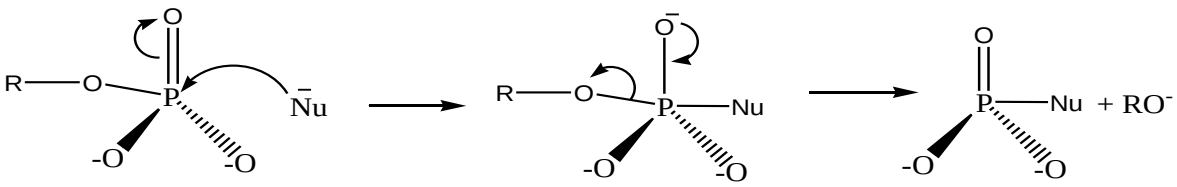

1.1.2.2 Adjacent Associative Addition-Displacement: This mechanism gives rise to retention of configuration via an adjacent associative mechanism. The pentacoordinate stable intermediate must pseudo-rotate (swop ligands about the P atom between apical and equatorial positions) so that the nucleophile leaves from the apical position.

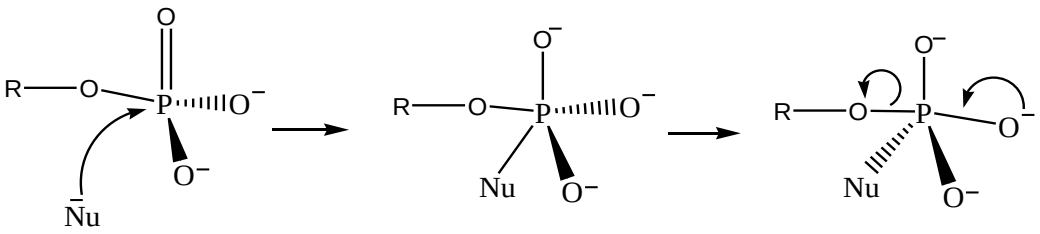

1.1.3 Concerted mechanism: This is known as interchange mechanism, otherwise called I mechanism. It can be either the I_a type (interchange associative) or the I_d type (interchange dissociative). Interchange mechanisms are characterized by the interchange of ligands X and Y between inner and outer coordination spheres of the metal. When the

replacement rate of an outgoing ligand depends on the nature and concentration of the entering ligand, the associative and the I_a mechanisms are possible. If the replacement rate is independent of the nature of the entering ligand, then the mechanism is dissociative or I_d. The D and I_d mechanisms are difficult to distinguish because the differences depend on the energy well of the intermediate. If the intermediate is relatively stable and lives long enough (on the scale probably longer than 10^{-10} s), to be able to distinguish the entering ligand, it will react with the ligands at different rates. This is a condition for D mechanism. Thus, if two entering ligands Y' and Y" are present (competitive reactions), the products will not be formed statistically (e.g. 50% MY' and 50% MY"), but one of the products will predominate which strongly indicates that the D mechanism is operative. On the other hand, if the intermediate is exceedingly short lived (shorter than10^{-10} s); it cannot discriminate between the entering ligands. The free coordination position is then occupied statistically, namely according to entering ligands' concentration. This is so called 'accidental bimolecularity'. Here the reaction rate depends on the entering ligands concentration and not on its nature (this statement disregards the ligands solvation effect, steric effects and electric dipole charges effects, which usually ought not to be neglected). The ligand X leaves the coordination shell and enters the solvation shell. The return from the solvation shell into the coordination shell is possible, but not if the entering ligand is in great excess and dominates the solvation shell. This is commonly the case because replacements are usually carried out under pseudo-first order conditions. In an I_d process, the reaction rate depends on the entering ligand

concentration, but not on its nature[26]. Phosphate di- and tri-esters react exclusively via the associative mechanism. Phosphate monoesters however, can react by both associative and dissociative mechanisms depending on their state of protonation[27]. Neutral esters $P(O)(OH_2)(OR)$ always appear to react by the associative pathway.

Probing dephosphorylation/phosphorylation and pyrphosphorylation/depyrophosphorylation reactions in biological systems is very difficult because of the already mentioned problems associated with the complex structure of enzymes. Current efforts aimed at having a better understanding of the mechanistic features and the possible roles played by metal ions in these processes employ *in vitro* techniques in the presence of model compounds. The present research employs model compounds to mimic the enzymes and substrates that operate in life processes.

1.2 PROJECT AIMS

1. To utilize UV-Visible spectroscopic techniques in probing the rate of phosphorylation, dephosphorylation, pyrophosphorylation and depyrophosphorylation reactions in model compounds.
2. To use ^{31}P NMR spectroscopy to elucidate the reaction mechanisms and other mechanistic features of phosphorylation, dephosphorylation, pyrophosphorylation and depyrophosphorylation reactions in model compounds.

3. To investigate the applicability of vibrational techniques such as SERS in monitoring phosphorylation, dephosphorylation, pyrophosphorylation and depyrophosphorylation reactions in model compounds to provide insights into both the structure and dynamic processes involved in these biochemical processes.

1.4 THESIS STRUCTURE

Chapter One

Project background: The chapter describes the project background, project aims, choice of model system, as well as the thesis organization.

Chapter Two

Literature review: The chapter describes the biochemical processes of dephosphorylation, phosphorylation, pyrophosphorylation and depyrophosphorylation reactions in living systems. It also gives a general insight into the importance of enzyme catalyzed dephosphorylation and phosphorylation reactions in living systems focusing on the processes of glucose metabolism, cholesterol metabolism, RNA synthesis and DNA replication.

Chapter Three

Application of UV–Visible absorption spectroscopic technique for monitoring phosphorylation, dephosphorylation, pyrophosphorylation and depyro-phosphorylation reactions in model systems: The chapter attempts to give a general overview of UV-Visible absorption spectroscopy, the reasons why it was adopted as one the preferred analytical techniques, experimental results, discussions and conclusions.

Chapter Four

The use of ^{31}P NMR spectroscopic technique for monitoring phosphorylation, dephosphorylation, pyrophosphorylation and depyrophosphorylation reactions in model systems: The chapter gives a general overview of ^{31}P NMR spectroscopy, the reasons for adopting it as one of the analytical technique, experimental, results, discussions and conclusions.

Chapter Five

Monitoring Phosphorylation, dephosphorylation, pyrophosphorylation and depyrophosphorylation reactions by surface enhanced Raman scattering (SERS) in model compounds: The chapter gives a general overview of Surface Enhanced Raman Scattering (SERS) spectroscopy, the reasons why it was adopted as an alternative vibrational analytical technique, results, experimental, discussions and conclusions.

Chapter Six

General conclusions and future outlook: This chapter draws a comparison between all the results derived from the different analytical techniques adopted in the investigation, and some insights into future investigations.

References

CHAPTER TWO

Literature review

Phosphate esters are ubiquitous in the living world. Our genetic materials, DNA and RNA are phosphodiesters. Phosphoric acid is particularly suited for its role in nucleic acids because it can link two nucleotides with a very stable bond and remain negatively charged at physiological pH. The chemistry of phosphate and pyrophosphate esters make them particularly suited for the basis of a regulatory mechanism. While the dephosphorylation of a phosphate monoester, such as serine phosphate or methyl phosphate is thermodynamically favourable, the activation energy is high. Under physiological conditions (neutral pH, 25^{o} C), methyl phosphate has an estimated half-life for uncatalysed hydrolysis of about 500,000 years[28,29]. The balance between phosphorylation and dephosphorylation on one hand and pyrophosphorylation and depyrophosphorylation reactions on the other have been shown to regulate a wide range of biochemical processes which includes metabolism, DNA transcription and replication, cell differentiation and immune responses[30]. Despite the fact that phosphorylation and/or dephosphorylation and pyrophosphorylation and/or depyrophosphorylation processes often take place far from active sites, they function as a control between active and inactive states for many enzymes. Regulation is often accomplished by significant conformational changes that result from these processes. The resulting conformational changes have been documented[30] by structural studies on the presumption that the activation effects can be

enhanced, often resulting in the rate acceleration of 10^2-10^5fold. The importance of enzyme catalyzed dephosphorylation, phosphorylation, pyrophosphorylation and depyrophosphorylation reactions is described in the next paragraph.

2.1 Phosphorylation, dephosphorylation, pyrophosphorylation and de-pyrophosphorylation reactions in living systems

In biological systems, enzyme catalyzed reactions involving both dephosphorylation and phosphorylation reactions are of enormous importance especially in the storage and utilization of energy as observed in the condensation and breakdown of ATP[30]. Generally, phosphorylation is a chemical process of transferring a phosphoryl group (PO_3^{2-}) from a phosphate ester or anhydride to an acceptor (nucleophile), while the removal of a phosphoryl group from a donor (phosphate ester anhydride) to an acceptor is termed dephosphorylation. Dephosphorylation reactions are catalyzed by phosphatases, while phosphorylation reactions utilize phosphorylases. A short review of biochemical and structural information which has been established on enzymatic dephosphorylation/ phosphorylation and pyrophosphorylation/depyrophosphorylation reactions is provided below.

2.1.1. Alkaline phosphatase (AP): Alkaline phosphatase catalyzes the dephosphorylation of phosphate monoesters with a rate maximum near pH 7. The enzyme which has been isolated from E.coli is a dimer with molecular

weight 94000 and it contains at least two to four Zn^{2+} ions and Mg^{2+} ions per dimer. The metal ions appear to play two roles in the enzymes. Two Zn^{2+} ions are required for activity. The other two Zn^{2+} ions and the two Mg^{2+} ions, tend to enhance the activity of the enzyme in addition to stabilizing its tertiary and quaternary structure[31]. Several proposals for the mechanism of dephosphorylation reactions by alkaline phosphatases have been advanced. The usual role of the metal ion is considered to involve activation of the substrate by coordination, thereby increasing the electrophilicity at the phosphorus centre, and or activation of the nucleophile. Even with several of such proposals, the roles of the metal ions in the mechanisms are still unclear and the degree of involvement of the other functional groups surrounding the enzyme is yet to be established.

2.1.2. Yeast inorganic pyrophosphatases (YIP): Yeast Inorganic Pyrophosphatases consist of two identical sub-units with a molecular weight of 6400 for the dimer. YIP catalyses the reversible dephosphorylation of pyrophosphate. In the presence of Mg^{2+}, YIP is specific to pyrophosphate. However, when other metal ions are involved, the enzyme becomes less specific and it will now hydrolyse a number of pyrophosphate esters[32]. In the absence of phosphate, the native dimer binds divalent metal ions. Three divalent metal ions are bound with high affinity in the presence of phosphate. Metal ions like Mg^{2+}, Mn^{2+}, Co^{2+}, Zn^{2+}, Fe^{2+} and Cd^{2+} are presumed to activate the substrate. Other metal ions like $Ba^{2+}$and $Ca^{2+}$are presumed to inhibit it[33].

Several observations show that one metal ion is required to form the substrate and at least one other divalent ion is required for activity. Proposals

have been forwarded to explain the mechanism of YIP. The basic features include: metal binding to the pyrophosphate to produce a substrate; production of a metal bound hydroxo ligand as a nucleophile by an adjacent basic amino residue; and stabilization of the substrate by interaction with cationic amino acid residue[34].

2.1.3. Purple acid phosphatases (PAP): Purple Acid Phosphatases constitute diiron carboxylate proteins which hydrolyse orthophosphate monoesters under acidic conditions. The exact physiological function of Purple Acid Phosphatase is unknown. The enzyme exist in two forms, the reduced and the oxidized form

Reduced form (active) [Fe(III)-OH-Fe(II)]

Oxidized form (inactive) [Fe(III)-OH-Fe(III)

Fe(II) of the reduced PAP is labile and can be substituted by the other divalent metal ions ; e.g. Zn^{2+} retaining its catalytic activity. Purple Acid Phosphatases are iron containing non-heme proteins that catalyze the hydrolysis of the activated phosphoric esters. Though their *in vivo* function has not been established, it has been speculated that these enzymes may be involved in the various cell regulation mechanisms in living systems that includes glucose metabolism, cholesterol metabolism, RNA synthesis and DNA replication[35,36]. Additionally, certain amino acids and fatty acids can also undergo phosphoryl transfer reactions to form pyruvate and Acetyl CoA respectively which goes into the Krebs cycle in the mitochondria for the production of ATP as depicted below.

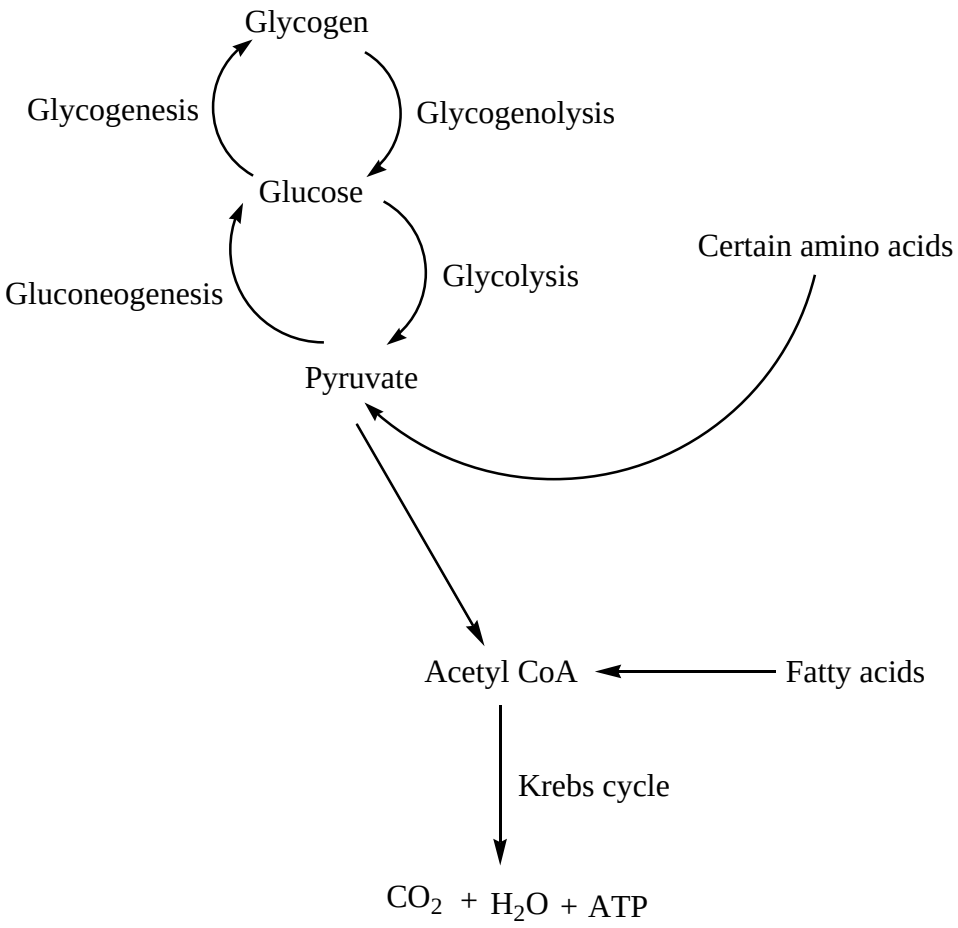

2.2. Glucose metabolism

The critical role played in regulating metabolism by phosphorylation and the counterbalancing roles played by dephosphorylating action of phosphatases and kinases is well established[37]. In glycogenolysis, glycogen phosphorylase catalyses the breakdown of glycogen in response to adrenalin (epinephrine). The enzyme catalyzes the transfer of a glucose unit from the end of the glycogen chain to inorganic phosphate, producing glucose-1-phosphate. This leads to the formation of a glucose molecule[37].

Subsequently, excess glucose is stored as glycogen in our bodies. In the process of glycolysis, a glucose molecule becomes phosphorylated to form glucose-6-phosphate. This undergoes further phosphorylation to produce glucose-1,6-biphosphate. The end product is the formation of glycogen as depicted below.

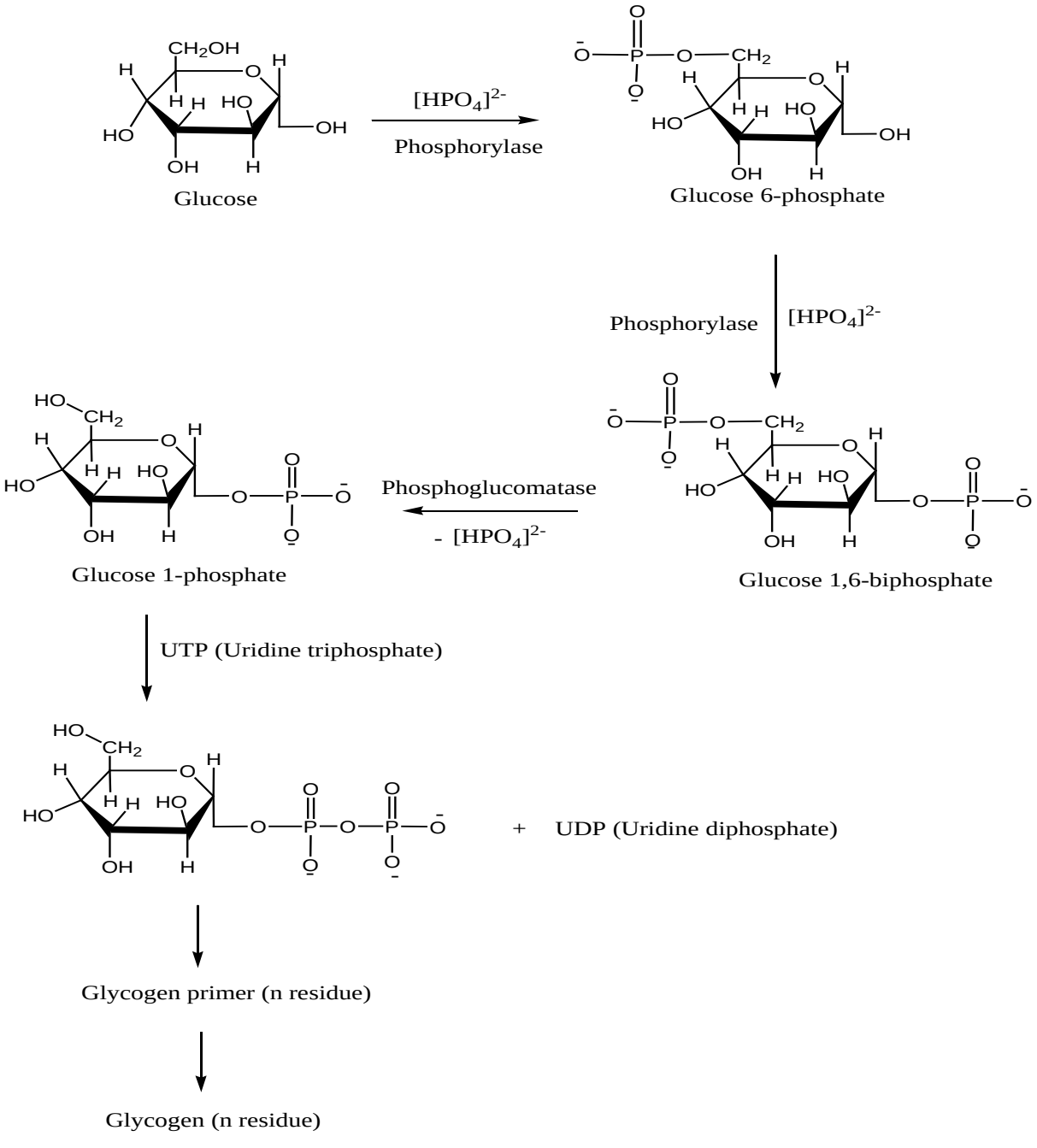

Additionally, the importance of phosphorylation and dephosphorylation reactions in biochemical processes of glucogenesis and gluconeogenesis is also crucial in the regulation of glucose levels in living systems.

2.3 Cholesterol metabolism

The building blocks of cholesterol are isoprenes, which are made of acetate. The basic isoprene subunits consist of isopentenyl pyrophosphate and dimethyl allyl pyrophosphate arranged in an alternating pattern to form polyprenyl chains. Farnesyl (15 carbon chain) and geranyl (20 carbon chains) are ubiquitous[38]. Cholesterol biosynthesis takes place in the cytosol and consists of four stages. In the first stage, three molecules of acetyl-CoA are used to make mevalonate, a C_6 compound that is the product of the reaction catalyzed by the highly regulated enzyme HMGCoA reductase. Mevalonate is then phosphorylated and decarboxylated in stage 2 to form the activated C_5 isoprenoid intermediate, isopentenyl pyrophosphate[38]. This important metabolite is an intermediate in a number of other biosynthetic reactions including those of plant chlorophylls and plant hormones. Isopentenyl pyrophosphate then undergoes isomerization to form dimethyl allyl pyrophosphate. In the third stage, three molecules of isopentenyl pyrophosphate are combined to form farnesyl pyrophosphate (C_{15}). Squalene, a C_{30} cholesterol precursor generated from this process. Squalene then cyclises to form a four-ringed molecule which is then modified by a number of reactions. This ultimately results in the loss of three methyl groups to generate cholesterol (C_{27}), a four-ringed sterol molecule[38].

2.4 RNA synthesis

RNA polymerase catalyzes the DNA-directed coupling of the nucleoside triphosphate (NTPs), adenosine triphosphate (ATP), cytidine triphosphate (CTP), guanosine triphosphate (GTP), and uridine triphosphate (UTP) in a reaction that involves pyrophosphorylation. Scheme 1 depicts this process. RNA synthesis proceeds in a stepwise manner in the 5'→ 3'direction, that is, the incoming nucleotide is appended to the free 3'-OH groups of the growing RNA chain[39]. All cells contain RNA polymerase. In bacteria, one species of this enzyme synthesizes nearly all of the cell's RNAs. Eukaryotic cells contain four or five different types of RNA polymerases that each synthesizes a different class of RNA.

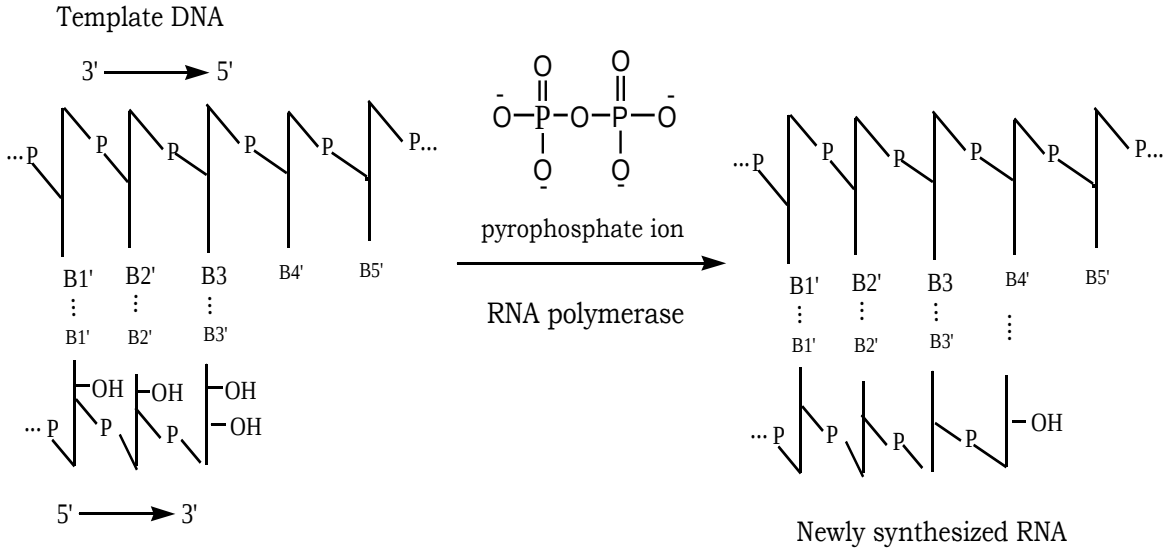

Scheme 1 Action of RNA polymerase

2.5 DNA replication

The chemical pathway by which DNA is replicated is identical to that of RNA synthesis as depicted in Scheme 2, but with two major differences: firstly deoxynucleoside triphosphates (dNTPs) rather than nucleoside triphosphates are the reactants and secondly, the enzyme that catalyzes the reaction is DNA polymerase rather than RNA polymerase. The properties of DNA polymerase result in a third major difference between RNA and DNA synthesis, whereas RNA polymerase can link together two nucleotides on a DNA template, DNA polymerase can only extend (in the 5' to 3' direction) an existing polynucleotide that is base paired to the DNA's template strand. Thus, whereas RNA polymerase can initiate RNA synthesis from the beginning, DNA polymerase requires an oligonucleotide primer, which it lengthens[39].

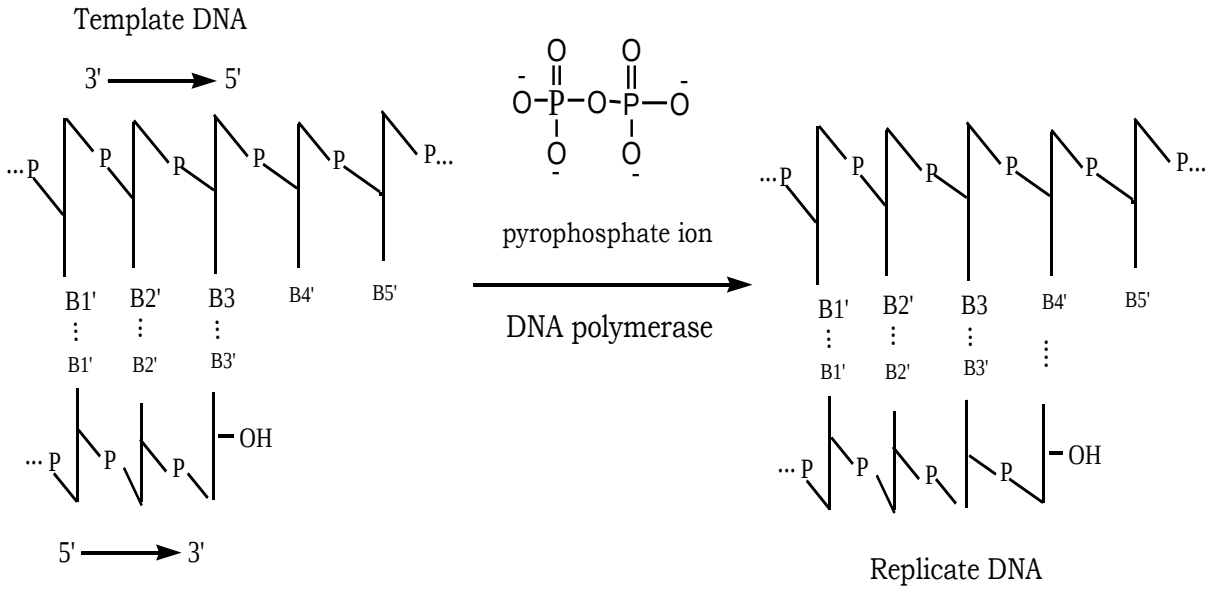

Scheme 2 Action of DNA polymerase

It is to be noted that because of the importance of the biochemical processes of dephosphorylation and phosphorylation in living organisms, our research group has had a modest interest in such reactions. It has been reported[40-42] that oxidizing VO_2 complexes of polyphosphates and ATP produce a 10^3 fold increase in the rate of dephosphorylation induced by VO_2^+. The report also concluded that there was also a rate enhancement in the dephosphorylation reaction catalyzed by the complex $[N_4Co(OH)(H_2O)]^{2+}$ with polyphosphates using ^{31}P NMR. This gave rise to structural information on precursor complexes, intermediates and products in the reaction[42]. Through such reactions, it is possible to compare the behaviour of labile, semi-labile and inert metal ions. The structural and kinetic factors promoting or inhibiting dephosphorylation and phosphorylation processes can also be ascertained from such reactions.

CHAPTER THREE

UV-Visible absorption spectroscopic techniques for probing phosphorylation, dephosphorylation and pyrophosphorylation reactions in model compounds

This chapter describes some of the advantages inherent in the use of UV-Visible absorption spectroscopy as an analytical technique used in the study of phosphorylation, dephosphorylation, pyrophosphorylation and depyrophosphorylation reaction in model systems. It also gives a general insight on the principles of UV-Visible absorption spectroscopy. The experimental procedures adopted in the preparation and characterization of all the different species, are also discussed in the chapter. The chapter also describes the results and discussions obtained from the study.

3.1 The principle of UV-Visible absorption spectroscopy

The principle of UV-Visible absorption spectroscopy is based on the fact that molecules have the ability to absorb ultraviolet or visible light. This absorption corresponds to the excitation of outer electrons in the molecules concerned. When a molecule absorbs energy, an electron is promoted from the Highest Occupied Molecular Orbital (HOMO) to the Lowest Unoccupied Molecular Orbital (LUMO). It should be noted that occupied molecular orbital's with the lowest energy are the δ orbital's. At a slightly higher energy are the π orbital's and non-bonding orbital's (those with unshared

pair of electrons) still at a higher energy[43,44]. The highest energy orbital's belong to π* and δ*. The δ→δ* and n→ δ* transitions require relatively high energy, and are therefore associated with shorter wavelength radiation (ultraviolet). Lower energy n→π* and π→π* are ultraviolet or visible induced transitions. The difference in energy levels associated with vibration and rotation are much smaller than those involved in electronic transitions. Excitations therefore occur at corresponding longer wavelengths[45-47]. For most absorbing species in solution, absorption peaks do not appear as sharp lines at highly differentiated wavelengths, but rather as bands of absorption over a range of wavelengths. A principal reason is that an electronic transition is frequently accompanied by vibrational transitions between electronic levels – "vibrational fine structure". In some way, each vibrational level may have associated rotational levels so that an absorption spectrum due to an electronic transition may well be a complex structure with contributing components from vibrational and rotational absorption. Each electron in a molecule has unique ground state energy. The discrete levels to which it may jump are also unique. It follows that there will be a finite and predictable set of transitions possible for the electrons of a given molecule. Each of the transitions requires the absorption of a quantum of energy. If that energy is derived from electromagnetic radiation, there will be a direct relationship between the wavelengths of the radiation at the particular transition that it stimulates. That relationship is known as specific absorption. A plot of those points along the wavelength scale at which a given substance shows absorption 'peak' or maxima is called an absorption spectrum. The absorption spectrum of a compound is one of its

most useful physical characteristics, both as a means of identification (qualitative analysis) and of estimation (quantitative analysis). A detailed discussion on preferred absorption range, spectral bandwidth and slit width follows.

3.1.1 Preferred absorption range

The ability of a spectrophotometer to measure accurately throughout its absorption range could be impaired by a number of factors, chief of which is the inherent noise in the detector. Instruments equipped with photo-emissive detectors (phototube or photomultiplier) have minimum relative error when absorbance = 0.86. In practice, the error will not be significant for any absorbance between 0.8 - 1.5 A^o except where light levels are low[46]. Spectrophotometers like the Super Aquarius 9000 series used in this study that is equipped with a silicon diode detector do not suffer from this limitation. In such an instrument, performance limits are usually dependent on stray light and measures absorbance up to 3 A^o with accuracy and reliability.

3.1.2 Spectral bandwidth and slit width

The resolution of a spectrophotometer (the minimum separation between narrow absorption bands that can be observed) is usually limited by the spectral purity and intensity of the monochromator light output and detector sensitivity at that wavelength. Most instruments using diffraction

gratings take advantage of the linear dispersion and provide fixed slit width to give known and controlled bandwidth at the exit slit of the monochromator. In practice, the unwanted effects of spectral bandwidth on peak absorbance measurement can be eliminated by constructing a set of calibration curves at known concentrations. Provided Beer's law is obeyed, a plot of concentration against absorbance at a given wavelength will yield a straight line from which unknown concentrations can be accurately determined if absorbance is measured at the same condition.

3.2 Experimental

3.2.1 Instruments and reagents

All reagents used were either analytical reagents grade or the purest available commercially and were used without further purification. Measurement of pH was made with the Metrohm 635-pH meter equipped with a combination electrode. The pH electrode was conditioned prior to use in a pH range 4 to 9. The pH of the reaction mixture was maintained by adding drops of 0.1 M, 0.01 M and 0.001 M of NaOH or $HClO_4$, using different marked dotting glass rods in a simple technique referred to as glass stick dotting. The temperature of the reaction was controlled using a thermostated water bath, which allows the water to circulate via a jacketed reaction vessel maintained at 25^{o} C. A super Aquarius 9000 series UV-Visible spectrophotometer from Cecil instruments was used to collect spectra and rate data.

3.2.2 Choice of model systems

3.2.2.1 Co(III) complexes as an enzyme model

Co(III) amine complexes were used as the enzyme model because of the following advantages which the model posses:

(1) Model systems based on cobalt(III) complexes are especially advantageous in that metal coordination sites open for phosphate substitution can be limited, permitting studies of a type not readily available using labile metal centres. They are exchange inert and so its complexes are thermodynamically stable, thus making the mechanisms and kinetics of Co(III) complexes to be well understood. They are semi labile, and generally undergo ligand-exchange reactions relatively slowly. Large fraction of our knowledge of the isomerism, modes of reaction and general properties of octahedral complexes as a class is based upon studies of Co(III) complexes.

(2) The (Co-N bonds) in Co(III) amine and polyamine complexes retain their integrity in an aqueous medium for a long time. They show a particular affinity for nitrogen donors. Majority of its complexes contain amines such as 1,3-diamninopropane, nitro groups, or even nitrogen-bonded SCN groups as well as water molecules.

(3) Co(III) complexes are easy to synthesize and are kinetically robust, thereby permitting the characterization of all the species present in solution[48].

3.2.2.2 Nitrophenol as substrate model

(1) The use of nitrophenol (NP) as a substrate model allows one to monitor the reaction at 400 nm without any interference from nitrophenylphosphate (NPP) which only absorbs at 310 nm as has been reported[49]. The rate of dephosphorylation and phosphorylation can be determined either by measuring the rate of depletion of nitrophenol at 400 nm, or by measuring the rate of formation of nitrophenylphosphate at 310 nm. It is expected that the calculations will afford comparable values in both scenarios.

The structures of the complexes encountered in this study are given in Table1.

Table 1. Structures of Complexes encountered in this study

Structural Formula	Chemical Formula	Comment
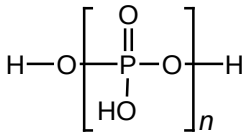	$[\{HO(PO_2OH)_n\ H\}]$	This is the accepted structural form of the polyphosphoric acids where *n* can be 1, 2 or 3 for phosphoric, pyrophosphoric and tripolyphosphoric acids respectively.
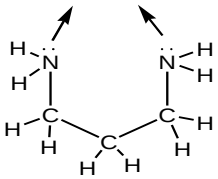	$NH_2CH_2CH_2CH_2NH_2$	Trimethylenediamine abbreviated as tn. Some authorities recommend pn (propylenediamine). In our study, we use tn for convenience and conformation with earlier studies. 2 molecules of tn are abbreviated as N_4.
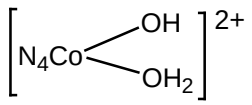	$[\{CoN_4(OH)(OH_2)\}]^{2+}$	The cis aquohydroxo complex is one of the reactive species in solution.
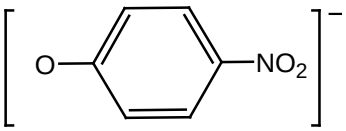	$[O_2NC_6H_4O]^-$ Abbreviated as $[NP]^-$	Nitrophenolate anion is the predominant specie under the experimental condition.
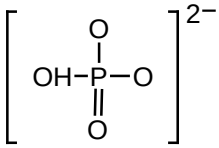	$[HPO_4]^{2-}$	The hydrogen phosphate anion is the predominant species in the middle pH region (pH region of 6.5-7.0) in the reacting solution.
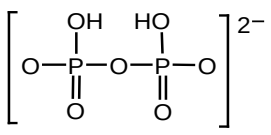	$[H_2P_2O_7]^{2-}$	The dihydrogen phosphate anion is the predominant specie in solution under the experimental conditions.

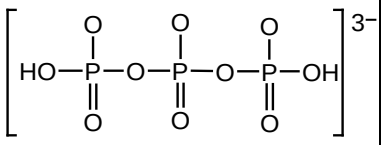	$[H_2P_3O_{10}]^{3-}$	The predominant tripolyphosphate ion in solution under the experimental condition. The pyro and tripoly-phosphate behave as typical polyprotic acids and thus protonation degree varies with pH. Between pH 6.5 and 7.0 triphosphates exists mainly as $[H_2P_3O_{10}]^{3-}$ in solutions.
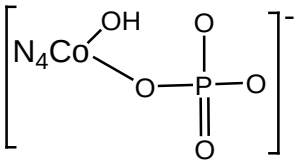	$[\{CoN_4(OH)PO_4\}]^{-}$	Monocordinated phosphate complex formed during the early stages of the reaction between $[\{CoN_4(OH)(OH_2)\}]^{2+}$ and $[HPO_4]^{2-}$. It should be noted that the monocordinated phosphates $[\{CoN_4(OH)PO_4\}]^{-}$ and the bicordinated phosphates $[\{(CoN_4)PO_4\}]$ exists in reaction solutions. The charge inherent on each depends on the degree of protonation. Example, the same complex can be positively charged,$[\{CoN_4(OH)OPO(OH)_2\}]^{+}$.
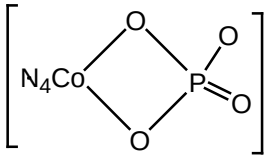	$[\{CoN_4PO_4\}]$	

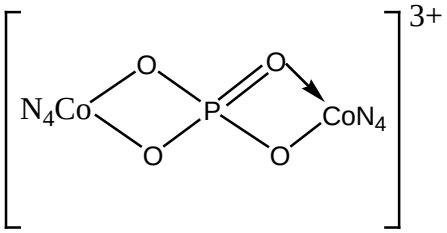	$[\{(CoN_4)_2PO_4\}]^{3+}$	Bicordinated phosphate complex formed after 30 minutes of the reaction. Monodentate species may also be depicted as $[\{(CoN_4(OH)O)_2P(O)OH\}]^{+}$.
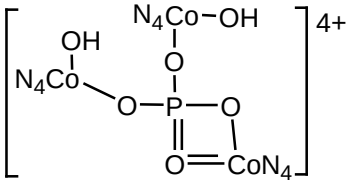	$[\{(CoN_4)_3(OH)_2PO_4\}]^{4+}$	A four membered phosphate ring complex formed from the reaction between $[\{CoN_4(OH)(OH_2)\}]_3^{2+}$ and $[HPO_4]^{2-}$. Monocordinated chelate of this reaction can also be written as $[\{(CoN_4(OH)\}_3PO_4]^{3+}$.
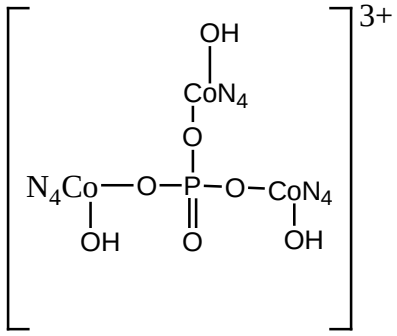	$[\{(CoN_4)_3(OH)_3PO_4\}]^{3+}$	Monocoordinated complex formed from the reaction between $[\{CoN_4(OH)(OH_2)\}]_3^{2+}$ and $[HPO_4]^{2-}$.
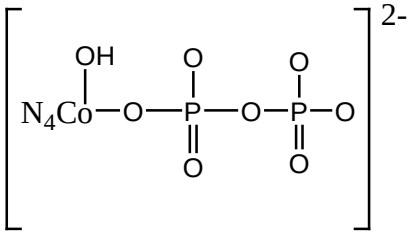	$[\{CoN_4(OH)P_2O_7]^{2-}$	Monocordinated pyrophosphate complexes formed during the early the early stages of the reaction between $[\{CoN_4(OH)(OH_2)\}]^{2+}$ and$[H_2P_2O_7]^{2-}$

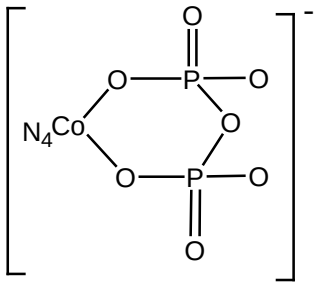	$[\{CoN_4P_2O_7\}]^-$	Six membered ring phosphate chelate formed after 30 minutes of reaction time. Different complexes have been reported in the literature.
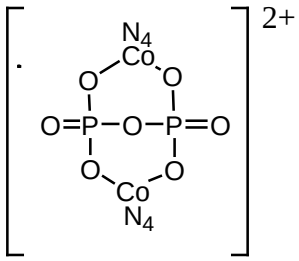	$[\{(CoN_4\}_2P_2O_7\}]^{2+}$	A double six-membered ring phosphate chelate formed as a result of the reaction between $[\{CoN_4(OH)(OH_2)\}_2]^{4+}$ and $[H_2P_2O_7]^{2-}$. Other racemic and meso forms have been reported in the literature.
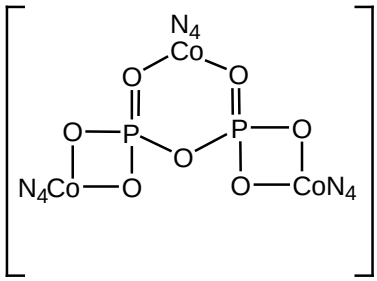	$[\{(CoN_4)\}_3P_2O_7\}]^{5+}$	A double four-membered and a single six-membered ring phosphate complex formed as a result of saturated reaction between $[\{CoN_4(OH)(OH_2)\}]_3^{2+}$ and $[H_2P_2O_7]^{2-}$Other suggested structures can be found in the literatures.
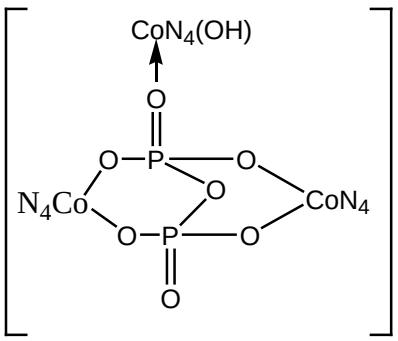	$[\{(CoN_4)\}_3(OH)P_2O_7\}]^{4+}$	A double six-membered ring phosphate complex formed as a result of saturated reaction between $[\{CoN_4(OH)(OH_2)\}]_3^{2+}$ and $[H_2P_2O_7]^{2-}$Other suggested structures can be found in the literatures.

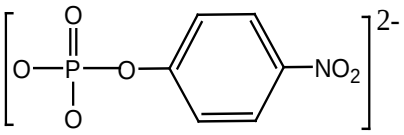	$[O_2NC_6H_4PO_4)]^{2-}$ Abbreviated as NPP^{2-}	Nitrophenylphosphate anion prevalent in the solution at pH 7.0
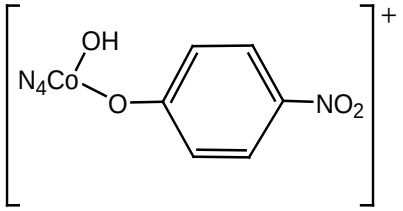	Abbreviated as $[\{CoN_4(OH)NP\}]^{+}$	This is the product of the reaction between $[\{CoN_4(OH)(OH_2)\}]^{2+}$ and $[O_2NC_6H_4O]^{-}$.
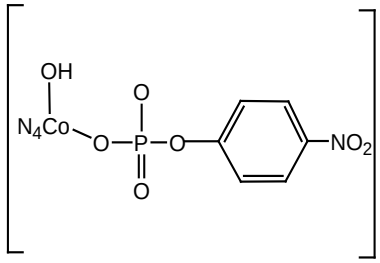	Abbreviated as $[\{CoN_4(OH)NPP\}]$	Monocordinated complex formed during the early stages of the reaction between $[\{CoN_4(OH)(OH_2)\}]^{2+}$ and $[O_2NC_6H_4OPO_2(O)]^{2-}$
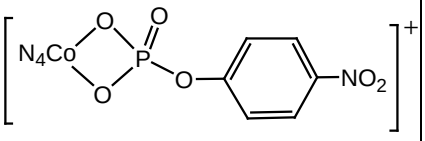	Abbreviated as $[\{CoN_4NPP\}]^{+}$	A bicoordinated phosphate complex attached to the NPP^{2-} formed after 30 minutes of reaction time.
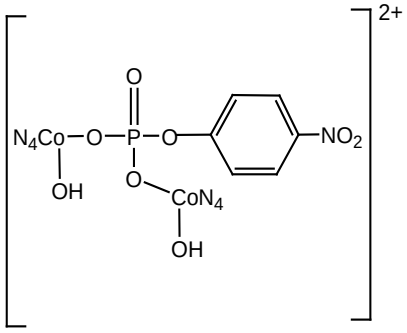	Abbreviated as $[\{(CoN_4(OH)\}_2NPP\}]^{2+}$	The reaction between $[\{CoN_4(OH)(OH_2)\}_2]^{2+}$ and NPP^{2-} to produce $[\{CoN_4(OH)\}_2NPP\}]^{2-}$. Other structural conformations can be found in the literatures.
	Abbreviated as	The reaction between $[\{CoN_4(OH)(OH_2)\}_3]^{2+}$ and NPP^{2-} to produce $[\{CoN_4(OH)\}_3NPP\}]^{4+}$.

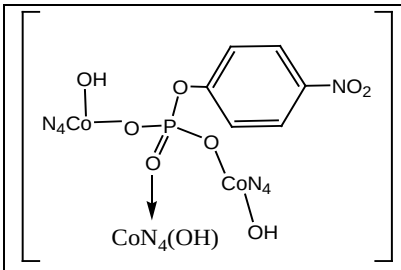	$[\{(CoN_4(OH)\}_3NPP\}]^{4+}$	

3.2.3 Calibration curve studies of nitrophenol and nitrophenyl-phosphate

Calibration curve studies were done by preparing a series of 4-nitrophenylphosphate and 4-nitrophenol solutions ranging from a concentration of 10^{-3} to 10^{-6} M, and the pH adjusted to 7. The spectra are depicted in figures 1and 2. Under the pH of study, the 4-nitrophenol is deprotonated to form the 4-nitrophenolate ion, which is bright yellow and has an absorbance maximum at 400 nm, quite distinct from NPP, which has an absorbance maximum at 310 nm.

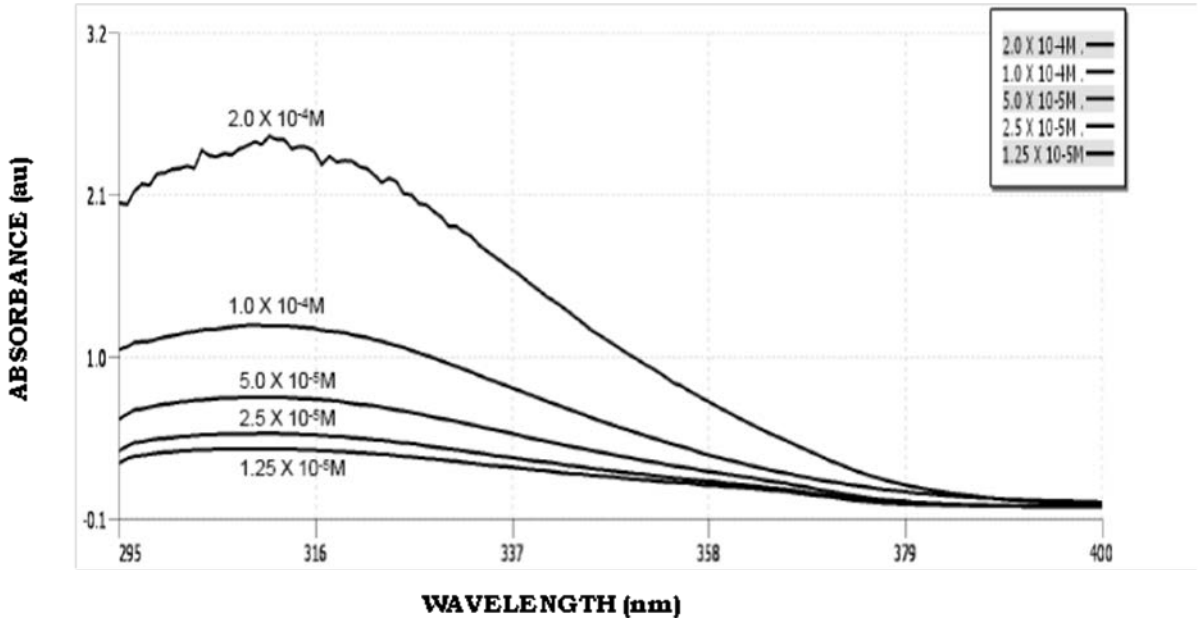

Figure 1. Absorption spectra of different concentrations of nitrophenyl-phosphate solutions at pH 7 and 25° C

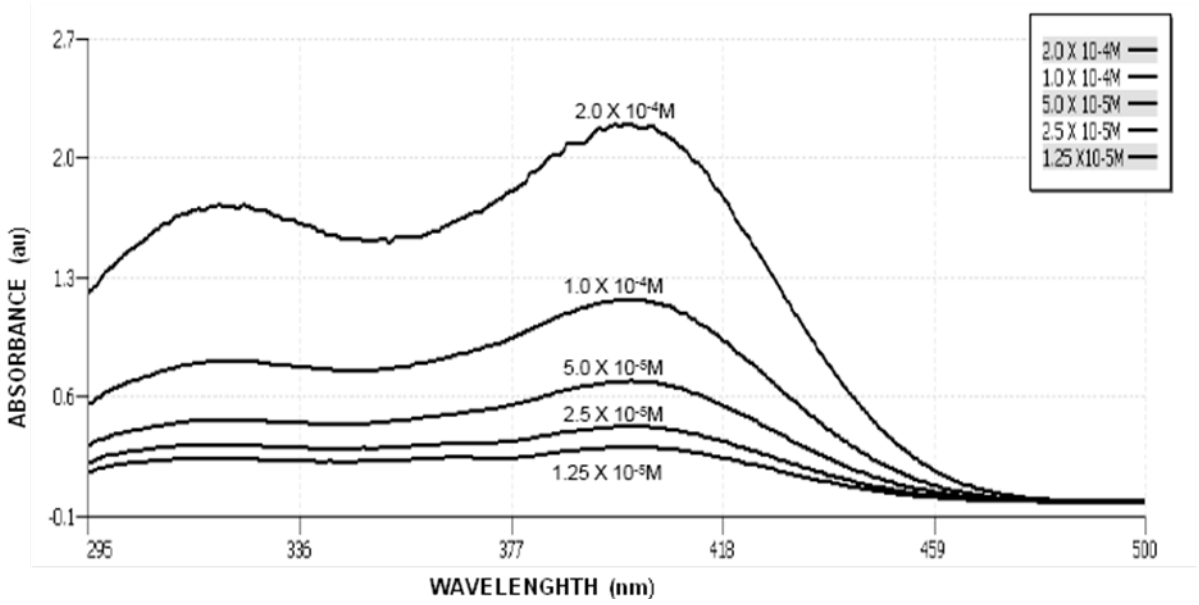

Figure 2. Absorption spectra of different concentrations of nitrophenol solution at pH 7 and 25° C

In a system where the pH is maintained, the ratio of the concentration of the p-nitrophenolate ion to the p-nitrophenol would be constant allowing for Beers law to operate. The absorbance values at 310 and 400 nm were plotted against concentration and the molar absorptivity (ε) determined. The molar absorptivity ε for 4-nitrophenol at 310 and 400 nm were calculated from the plots as 6398.9 $LMol^{-1}cm^{-1}$ and 8876.3 $LMol^{-1}cm^{-1}$. Similarly, the molar absorptivity value for nitrophenylphosphate at 310 nm was found to be 11098 $LMol^{-1}cm^{-1}$. Triplicate analysis was done for each reaction. The standard deviation for the triplicate analysis ranged from 0.1 to 0.2. The average value was used for analysis of the data.

3.2.4 Phosphorylation studies

The diaqua complexes $[CoN_4(H_2O)_2]^{3+}$ were prepared and characterized in solution from the carbonato cobalt(II) complexes $[CoCO_3N_4]$ using published protocols [50-52]. The conversion of the carbonatocobalt(II) species to the carbonatocobalt(III) species is the precursor for the preparation of a representative group of cobalt(III) amine coordination compounds used as the enzyme model. The different systems monitored for the phosphorylation studies are; (a) the reactions between $[HPO_4]^{2-}$ and $[O_2NC_6H_4O]^-$ for 1:1, 2:1 and 3:1 $[HPO_4]^{2-}$ to $[O_2NC_6H_4O]^-$ ratios. (b) the reaction between $[\{CoN_4(OH)(OH_2)\}]^{2+}$ and $[HPO_4]^{2-}$ for 1:1, 2:1 and 3:1 $[\{CoN_4(OH)(OH_2)\}]^{2+}$ to $[HPO_4]^{2-}$ ratios. (c) the reaction of $[CoN_4(OH)PO_4]^-$ and $[O_2NC_6H_4O]^-$ for 1:1, 2:1 and 3:1 $[CoN_4(OH)PO_4]^-$ to $[O_2NC_6H_4O]^-$ ratios.

3.2.4.1 Systems monitored for the phosphorylation studies

Reactions between $[HPO_4]^{2-}$ and $[O_2NC_6H_4O]^-$

The protocol employed in the reaction of 1:1 molar ratio of $[HPO_4]^{2-}$ and $[O_2NC_6H_4O]^-$ consist of mixing 2 mL of an aqueous solution of nitrophenol and 2 mL of an aqueous solution of sodium dihydrogen phosphate hetptahydrate ($Na_2HPO_4.7H_2O$) with the required concentration in the thermostated reaction vessel at 25^o C. 6 mL of deionized water was added to

it and the pH maintained at 7 for the whole duration of the reaction under constant stirring. After 30 minutes of reaction, aliquots were withdrawn for the recording of UV-Visible spectra. For 1:2 and 1:3 $[O_2NC_6H_4O]^-$ to $[HPO_4]^{2-}$ ratios, the amount of $[O_2NC_6H_4O]^-$ is held constant (2 mL) and that of $[HPO_4]^{2-}$ varied in the total reaction solution of 10 mL.

Reactions between $[CoN_4(OH)(OH_2)]^{2+}$ and $[HPO_4]^{2-}$

The procedure employed in the reaction of 1:1 molar ratio of $[CoN_4(OH)(OH_2)]^{2+}$ and $[HPO_4]^{2-}$ consist of mixing 2 mL of an aqueous solution of aquohydroxo cobalt amine complex and 2 mL of an aqueous solution of sodium dihydrogen phosphate hetptahydrate ($Na_2HPO_4.7H_2O$) with the required concentration in the thermostated reaction vessel at 25° C. 6 mL of deionized water was added to it and the pH maintained at 7 for the whole duration of the reaction under constant stirring. After 30 minutes of reaction, aliquots were withdrawn for the recording of UV-Visible spectra. For 1:2 and 1:3 $[CoN_4(OH)(OH_2)]^{2+}$ to $[HPO_4]^{2-}$ ratios, the amount of $[HPO_4]^{2-}$ is held constant (2 mL) and that of $[CoN_4(OH)(OH_2)]^{2+}$ varied in the total reaction solution of 10 mL.

Reactions between $[CoN_4(OH)PO_4]^-$ and $[O_2NC_6H_4O]^-$

The method employed in the reaction of 1:1 molar ratio of $[CoN_4(OH)PO_4]^-$ and $[O_2NC_6H_4O]^-$ consist of mixing 2 mL of an aqueous solution of

nitrophenol and 2 mL of an aqueous solution of $[CoN_4(OH)PO_4]^-$ with the required concentration in the thermostated reaction vessel at 25° C. 6 mL of deionized water was added to it and the pH maintained at 7 for the whole duration of the reaction under constant stirring. After 30 minutes of reaction, aliquots were withdrawn for the recording of UV-Visible spectra. For 1:2 and 1:3 $[CoN_4(OH)PO_4]^-$ to $[O_2NC_6H_4O]^-$ ratios, the amount of $[O_2NC_6H_4O]^-$ is held constant (2 mL) and that of $[CoN_4(OH)PO_4]^-$ varied in the total reaction solution of 10 mL.

3.2.5 Dephosphorylation studies

The different systems monitored for the dephosphorylation studies are;

the reactions between $[\{CoN_4(OH)(OH_2)\}]^{2+}$and $[O_2NC_6H_4OPO_2(O)]^{2-}$ (abbreviated as NPP) for 1:1, 2:1 and 3:1 $[\{CoN_4(OH)(OH_2)\}]^{2+}$ to $[O_2NC_6H_4OPO_2(O)]^{2-}$ ratios.

3.2.5.1 Systems monitored for the dephosphorylation studies

Reactions between $[O_2NC_6H_4OPO_2(O)]^{2-}$ and $[CoN_4(OH)(H_2O)]^{2+}$

Two mL of nitrophenylphosphate solution and two mL of the aquohydroxo cobalt(III)amine complex $[CoN_4(OH)(H_2O)]^{2+}$ in the required concentration are mixed in a thermostated reaction vessel maintained at 25° C. Six mL of deionized water was added to it. The pH of the solution was kept at 7 for the whole duration of the reaction under constant stirring. After 30 minutes of

reaction, aliquots were withdrawn for the recording of the UV-Visible spectra. For 1:2 and 1:3 $[O_2NC_6H_4OPO_2(O)]^{2-}$ to $[CoN_4(OH)(H_2O)]^{2+}$ratios, the amount of $[O_2NC_6H_4OPO_2(O)]^{2-}$ is held constant (2 mL) and that of $[CoN_4(OH)(H_2O)]^{2+}$varied in the total reaction solution of 10 mL.

3.2.6 Pyrophosphorylation studies

The different systems monitored for the pyrophosphorylation studies are; (a) the reactions between $[O_2NC_6H_4O]^-$ and $[(OH)_2(PO_2)_2O]^{2-}$ (abbreviated as $[H_2P_2O_7]^{2-}$) for 1:1, 2:1 and 3:1 $[(OH)_2(PO_2)_2O]^{2-}$ to $[O_2NC_6H_4O]^-$ ratios. (b) the reaction between $[\{CoN_4(OH)(OH_2)\}]^{2+}$ and $[(OH)_2(PO_2)_2O]^{2-}$ for 1:1, 2:1 and 3:1 $[\{CoN_4(OH)(OH_2)\}]^{2+}$ to $[(OH)_2(PO_2)_2O]^{2-}$ ratios. (c) reaction of $[CoN_4P_2O_7]^-$ and $[O_2NC_6H_4O]^-$ for 1:1, 2:1 and 3:1 $[CoN_4P_2O_7]^-$ to $[O_2NC_6H_4O]^-$ ratios·

3.2.6.1 Systems monitored for the pyrophosphorylation studies

Reactions between $[O_2NC_6H_4O]^-$ and $[(OH)_2(PO_2)_2O]^{2-}$

The protocol employed in the reaction of 1:1 molar ratio of $[O_2NC_6H_4O]^-$ and $[(OH)_2(PO_2)_2O]^{2-}$ consist of mixing 2 mL of an aqueous solution of $[O_2NC_6H_4O]^-$ and 2 mL of an aqueous solution $[(OH)_2(PO_2)_2O]^{2-}$ with the required concentration in the thermostated reaction vessel at 25^o C. 6 mL of deionized water was added to it and the pH maintained at 7 for the whole

duration of the reaction under constant stirring. After 30 minutes of reaction, aliquots were withdrawn for the recording of UV-Visible spectra. For 1:2 and 1:3 $[O_2NC_6H_4O]^-$ to $[(OH)_2(PO_2)_2O]^{2-}$ ratios, the amount of $[O_2NC_6H_4O]^-$ is held constant (2 mL) and that of $[(OH)_2(PO_2)_2O]^{2-}$ varied in the total reaction solution of 10 mL.

Reactions between $[CoN_4(OH)(OH_2)]^{2+}$ and $[(OH)_2(PO_2)_2O]^{2-}$

The procedure employed in the reaction of 1:1 molar ratio of $[CoN_4(OH)(OH_2)]^{2+}$ and $[(OH)_2(PO_2)_2O]^{2-}$ consist of mixing 2 mL of an aqueous solution of aquohydroxo cobalt amine complex and 2 mL of an aqueous solution of $[(OH)_2(PO_2)_2O]^{2-}$ with the required concentration in the thermostated reaction vessel at 25^o C. 6 mL of deionized water was added to it and the pH maintained at 7 for the whole duration of the reaction under constant stirring. After 30 minutes of reaction, aliquots were withdrawn for the recording of UV-Visible spectra. For 2:1 and 3:1 $[CoN_4(OH)(OH_2)]^{2+}$ to $[(OH)_2(PO_2)_2O]^{2-}$ ratios, the amount of $[(OH)_2(PO_2)_2O]^{2-}$ is held constant (2 mL) and that of $[CoN_4(OH)(OH_2)]^{2+}$ varied in the total reaction solution of 10 mL.

Reactions between $[CoN_4P_2O_7]^-$ and $[O_2NC_6H_4O]^-$

The method employed in the reaction of 1:1 molar ratio of $[CoN_4P_2O_7]^-$ and $[O_2NC_6H_4O]^-$ consist of mixing 2 mL of an aqueous solution of nitrophenol

and 2 mL of an aqueous solution of $[CoN_4P_2O_7]^-$ with the required concentration in the thermostated reaction vessel at 25^o C. 6 mL of deionized water was added to it and the pH maintained at 7 for the whole duration of the reaction under constant stirring. After 30 minutes of reaction, aliquots were withdrawn for the recording of UV-Visible spectra. For 2:1 and 3:1 $[CoN_4P_2O_7]^-$ to $[O_2NC_6H_4O]^-$ ratios, the amount of $[O_2NC_6H_4O]^-$ is held constant (2 mL) and that of $[CoN_4P_2O_7]^-$ varied in the total reaction solution of 10 mL.

3.3 Results and discussion from the phosphorylation studies

The percentage phosphorylation was calculated from the net absorbance values of the aliquots at different times over the absorbance value of the same concentration of nitrophenylphosphate assuming 100% phosphorylation. One may also use the molar absorptivity constant of nitrophenylphosphate to determine the percentage phosphorylation from Beers law. All absorbances were taken against a solvent blank. Interference from other species in the analyte solution was not detected. Alternatively, the absorbance values at 400nm for the various aliquots over the absorbance value of the same concentration of nitrophenol may be used to determine the percentage phosphorylation. Note that in the first case, it is the increase in the amount of nitrophenylphosphate that is being monitored, while in the latter case, it is the decrease in the amount of nitrophenol that is measured. The calculations afforded comparable values in both scenarios. It is worth mentioning that from the results of the different spectra obtained, the different cobalt-

phosphate complexes do not affect the UV-Visible spectra of the measured nitrophenol and nitrophenylphosphate as they are not UV active in the wavelength of interest at millimolar concentrations. Table 2 summarizes the results obtained

Table 2. Percentage phosphorylation for the reactions of $[\{CoN_4OH\}_xPO_4]$ (Where x = 1,2,3) with $[O_2NC_6H_40]^-$ at 25° C and pH 7.0

REACTION SOLUTION COMPOSITION	FINAL CONCENTRATION	PERCENTAGE PHOSPHORYLATION CALCULATED AT 400 nm	PERCENTAGE PHOSPHORYLATION CALCULATED AT 310 nm
$[O_2NC_6H_4O]^-$ + $[CoN_4PO_4]$ (1:1)	2×10^{-3}	33.50	36.40
	1×10^{-3}	32.10	35.70
	2×10^{-4}	25.60	31.70
	1×10^{-4}	22.20	22.20
	2.5×10^{-5}	17.20	17.40
	1.25×10^{-5}	15.00	15.20
$[O_2NC_6H_4O]^-$ + $[CoN_4PO_4]$ (1:2)	2×10^{-3}	70.00	72.70
	1×10^{-3}	68.40	71.40
	2×10^{-4}	60.30	60.70
	1×10^{-4}	56.80	56.90
	2.5×10^{-5}	40.10	40.10
	1.25×10^{-5}	34.60	34.90
$[O_2NC_6H_4O]^-$ + $[CoN_4PO_4]$ (1:3)	2×10^{-3}	32.40	37.30
	1×10^{-3}	25.30	29.80
	2×10^{-4}	22.40	22.50
	1×10^{-4}	20.40	24.50
	2.5×10^{-5}	14.50	14.80
	1.25×10^{-5}	12.90	12.90

The following is deduced from the above studies

(1) It was observed that freshly prepared solutions containing *cis*-aquahydroxo bistrimethylenediaminecobalt(III) ions exhibit different visible spectral characteristics from those that were prepared and kept in the refrigerator for several days.

(2) No significant amount of phosphorylation was observed in the reaction between the unactivated $[HPO_4]^{2-}$ (in the absence of metal ion) and nitrophenol. This could be attributed to the fact that, activation of the phosphate in the presence of the metal ion is required for phosphorylation to occur.

(3) Enhanced differences in the visible spectra were noted at increased concentrations. This is presumably attributed to dimerization of the *cis*-hydroxoaquaions by olation resulting in the formation of singly and doubly bridged μ-hydroxo products. Addition of $[CoN_4(OH)(H_2O)]^{2+}$ at pH 7.0 to $[HPO_4]^{2-}$ at 1:1 molar ratio, results in rapid water substitution to form the monodentate complex $[CoN_4(OH)(PO_4)]^-$ which can then form a four membered bidentate chelate $[CoN_4(PO_4)]$ as depicted in table 1. The later has been shown to be more stable than the ring opened monodentate complex at pH 7.0 as has been reported[53]. An increase of the pH during the formation of the $[CoN_4(PO_4)]$ is attributed to the release of OH^- from the monodentate complex to produce the four membered chelate. However, complete quantitative formation of the 1:1 chelates, even in relatively concentrated solutions, may not be achievable because of (i) olation of aquahydroxo ions, which decrease the effective concentration of the

monomeric aquahydroxo species; and (ii) formation of higher metal to phosphate complexes which accompany the formation of the 1:1 complexes.

(4) Addition of $[CoN_4(OH)(H_2O)]^{2+}$ at pH 7 to $[HPO_4]^{2-}$ at 2:1 and 3:1 molar ratio result in the formation of several chelates of which the predominant species are $[\{CoN_4(OH)\}_2(PO_4)]^+$ and $[\{CoN_4(OH)\}_3(PO_4)]$ respectively. A mixture of these chelate species is anticipated in the reaction solution. The presence of the different species in the solution has been detected by ^{31}P NMR studies[53].

(5) The addition of $[O_2NC_6H_4O]^-$ to the preformed $[(CoN_4(PO_4]$ under the experimental condition showed a decrease in the absorbance maxima at 400 nm and an increase at 310 nm. These changes are consistent with the assertion that nitrophenol is being depleted and nitrophenylphosphate being formed in the solution. Formation of the complex results in a decrease of electron density on the phosphorus centre increasing its electrophillic character. Hence, the attacks of the phosphorus centre by oxygen of the nitrophenolate ion. A plausible reaction pathway is given below.

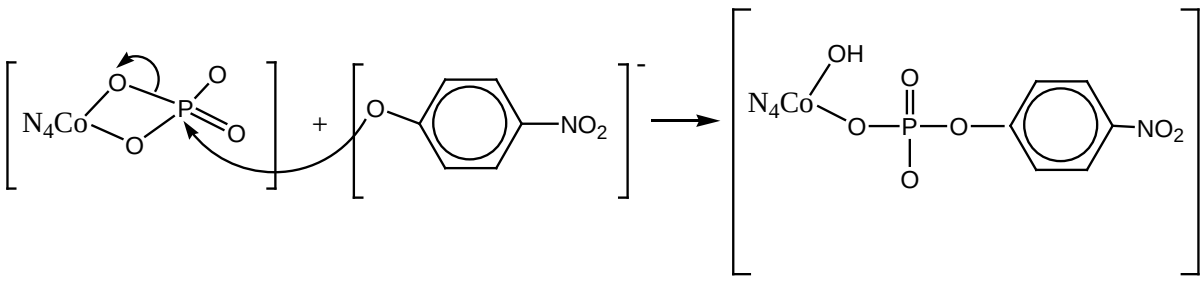

(6) The addition of 2:1 and 3:1 molar ratio of [($CoN_4(PO_4$] and $[O_2NC_6H_4O]^-$ under the experimental condition is presumed to produce $[\{CoN_4(OH)\}_2NPP]^{2+}$and $[\{CoN_4(OH)\}_3NPP)]^{4+}$ respectively as depicted in table 1. In these complexes, the additional metal ions per phosphate will force the phosphorus centre to adapt an increased electrophillic character, thereby facilitating the attack of nitrophenol on phosphorus.

(7) A decrease in the percentage phosphorylation observed for the 3:1 molar ratio $[CoN_4PO_4]$ and $[O_2NC_6H_4O]^-$ is a result of both dephosphorylation and phosphorylation reactions occurring simultaneously in the reaction solution.

3.4 Results and discussion from the dephosphorylation studies

The absorbance of the reactions at each concentration was measured at 310 nm and 400 nm respectively. The amount of phenolate ion produced was determined from the calibration curves and the percent dephosphorylation was calculated assuming 100% nitrophenol production for complete dephosphorylation. The percentage dephosphorylation was then calculated from the net absorbance values at 310 nm for the various aliquots over the absorbance value of the same concentration of nitrophenol at the same wavelength. Alternatively, the absorbance values at 400 nm for the various aliquots over the absorbance value of the same concentration of nitrophenylphosphate may be used to determine the percentage dephosphorylation. Again it should be noted that in the first case, it is an increase in the amount of nitrophenol that is being monitored, while in the

latter case, it is the depletion of nitrophenylphosphate that is measured. The calculations afforded comparable values in both scenarios. The results for the dephosphorylation reaction are summarized in table 3 below.

Table 3. Percentage dephosphorylation for the reactions of $[(CoN_4(OH)(OH_2)]^{2+}$ with nitrophenylphosphate at 25^o C and pH 7

REACTION SOLUTION COMPOSITION	FINAL CONCENTRATION	PERCENTAGE DEPHOSPHORYLATION CALCULATED AT 400 nm	PERCENTAGE DEPHOSPHORYLATION CALCULATED AT 310 nm
$[CoN_4(OH))OH_2)]^{2+}$ + $[O_2NC_6H_4PO_4]^{2-}$ (1:1)	2×10^{-3}	30.82	33.94
	1×10^{-3}	29.80	31.70
	2×10^{-4}	23.58	24.62
	1×10^{-4}	20.49	20.94
	2.5×10^{-5}	18.44	19.50
	1.25×10^{-5}	16.29	18.50
$[CoN_4(OH))OH_2)]^{2+}$ + $[O_2NC_6H_4PO_4]^{2-}$ (2:1)	2×10^{-3}	50.82	53.99
	1×10^{-3}	49.07	51.25
	2×10^{-4}	43.03	45.18
	1×10^{-4}	41.01	41.99
	2.5×10^{-5}	39.98	40.09
	1.25×10^{-5}	36.92	38.03
$[CoN_4(OH))OH_2)]^{2+}$ + $[O_2NC_6H_4PO_4]^{2-}$ (3:1)	2×10^{-3}	49.50	50.49
	1×10^{-3}	48.44	49.45
	2×10^{-4}	42.99	43.95
	1×10^{-4}	40.90	41.95
	2.5×10^{-5}	37.90	37.98
	1.25×10^{-5}	35.84	35.89

The important highlights deduced from the study are:

(1) It is presumed that at pH around 6.5 to 7.0, the aquohydroxo species is predominant. The values for pK_1 and pK_2 as determined by potentiometric

titration under conditions where *cis-trans* isomerism had proceeded to equilibrium are 4.94 and 7.20 for complexes[54]. Diaquabis(ethylenediamine) cobalt(III) in solution will be a mixture of *cis a*nd *trans* isomers as reported by previous investigators[55]. The enhanced reactivity for the aquohydroxo ions in comparison to the dihydroxo and diaquo species was noted for the system and this is in line with literature reports[56]. In the middle pH region, the reactivity of the aquohydroxo complex has been attributed to the presumption that the electron freed from the diaqua complex by the loss of a proton to form the aquohydroxo moiety, will labilize the coordinated water. The following reaction pathway highlights the course of the reaction.

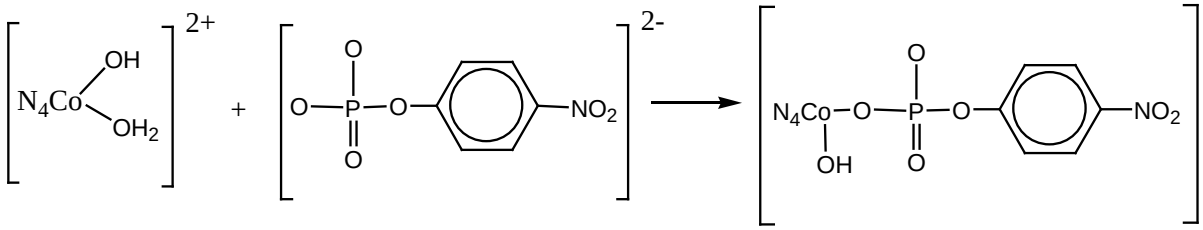

An attack of the phosphorus center by the coordinated hydroxide results in dephosphorylation, giving rise to free nitrophenol as depicted in the plausible pathway below.

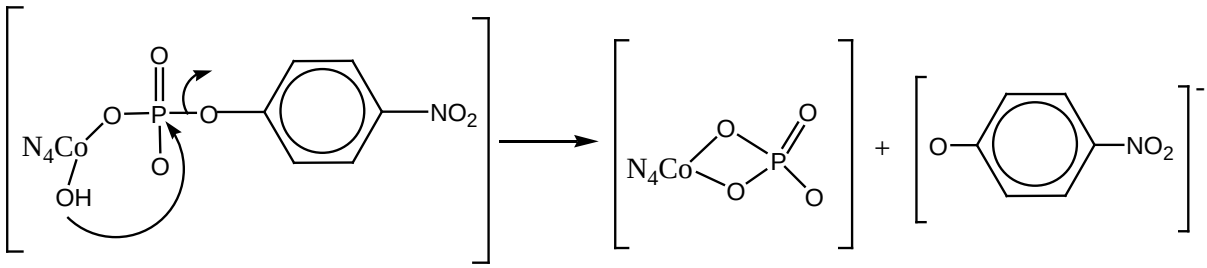

The coordinated hydroxide should be in *cis* position for effective intramolecular nucleophilic attack at the phosphorous centre[57]. Addition of $[CoN_4(OH)(H_2O)]^{2+}$ to NPP^{2-} results in the formation of a monodentate complex which then undergo intramolecular attack by the coordinated water or hydroxide of the metal complex on the phosphorus centre, thereby effecting dephosphorylation of NPP. In previous reports[58-60], the formation of a four membered chelate ring system has been noted for related systems along with ring opened monodentate species resulting in the formation of nitrophenol and the metal coordinated phosphate.

(2) An enhancement of the rate of dephosphorylation was noted in reaction solution that contained 2:1 aquahydroxo bistrimethylenediaminecobalt(III) species to NPP^{2-} ratio. This can be explained by the fact that the second metal ion coordinates to one of the available oxygen on the NPP, thereby creating a possibility of intramolecular attack on the phosphorus centre by coordinated water or hydroxide of the metal ion as depicted in the following plausible reaction pathway. The coordinated OH on the cobalt complex will have a

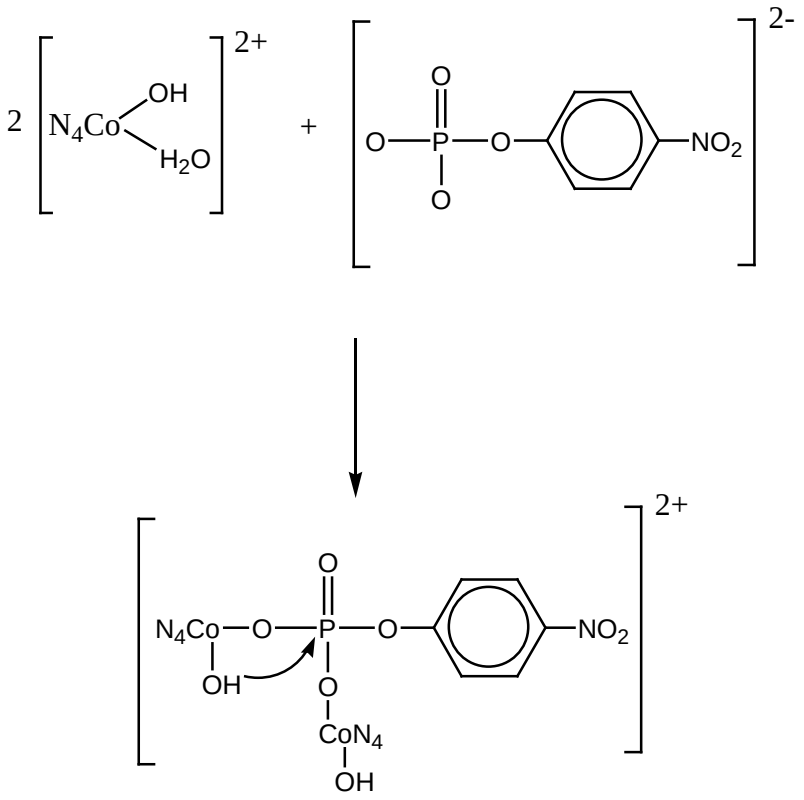

better chance of attack at the phosphorous center thereby increasing the degree of dephosphorylation of the NPP^{2-}.

(3) No significant additional amount of dephosphorylation was observed for reaction solutions that contained more than 3:1 metal-to-NPP^{2-} ratio. Since the reaction is presumed to be stoichiometric and not catalytic, it is anticipated that with an increase in the metal-to-phosphate ratio, the rate of dephosphorylation should increase. As is evident from the previous plausible reaction pathway, all of the oxygen moieties will be coordinated at 2:1 $[CoN_4(OH)(H_2O)]^{2+}$ to NPP^{2-} ratio. Hence the additional cobalt center will have no additional effect to enhance dephosphorylation of NPP^{2-}. Furthermore, above 3:1 $[CoN_4(OH)(H_2O)]^{2+}$ to nitrophenylphosphate ratio,

the concentration of the aquahydroxo species in the system becomes large, presumably triggering an olation reaction resulting in unreactive dimeric species in the solution, as has been reported in similar studies[54]. The absence of reactive aquahydroxo moieties explains the rate saturation in system containing large metal-to-phosphate ratios.

3.5 Results and discussion from the pyrophosphorylation studies

Quantification of the percent pyrophosphorylation was possible by determining the net absorbance decrease at 400 nm which depicts the depletion of nitrophenol in the reaction solution. The increase of the net absorbance at 310 nm was also utilized as an alternative for determining the percent pyrophosphorylation. In this case, an assumption was made that due to the similarities in structure of nitrophenylphosphate and nitrophenylpyrophosphate, the molar absorptivity value of nitrophenylphosphate can be applied for the calculation. Literature evidences support the above hypothesis to be correct as previous work reported the formation of nitrophenylpyrophosphate *in situ*[61]. Table 4 summarizes the results obtained.

Table 4. Percentage pyrophosphorylation for the reactions of $[\{CoN_4(OH)\}x(H_2P_2O_7)]$ (where x = 1, 2, 3) with NP at 25° C and pH 7.0

REACTION SOLUTION COMPOSITION	FINAL CONCENTRATION	PERCENTAGE PYROPHOSPHORYLATION CALCULATED AT 400 nm	PERCENTAGE PYROPHOSPHORYLATION CALCULATED AT 310 nm
$[\{CoN_4P_2O_7\}]^-$ + $[O_2NC_6H_4O]^-$ (1:1)	1×10^{-3}	61.25	60.55
	5×10^{-4}	48.99	51.05
	2.5×10^{-4}	45.29	47.20
	1.25×10^{-4}	30.99	30.42
	6.25×10^{-5}	25.42	24.88
$[\{CoN_4P_2O_7\}]^-$ + $[O_2NC_6H_4O]^-$ (2:1)	1×10^{-3}	16.99	16.96
	5×10^{-4}	11.29	13.46
	2.5×10^{-4}	11.04	10.18
	1.25×10^{-4}	7.25	8.85
	6.25×10^{-5}	6.09	6.02
$[\{CoN_4P_2O_7\}]^-$ + $[O_2NC_6H_4O]^-$ (3:1)	1×10^{-3}	0.92	0.82
	5×10^{-4}	0.79	0.70
	2.5×10^{-4}	0.09	0.08
	1.25×10^{-4}	0.04	0.02
	6.25×10^{-5}	0.02	0.00

The following is deduced from the above investigation

(1) In solution that were 1:1 in $[CoN_4(OH)(H_2O)]^{2+}$ to $[H_2P_2O_7]^{2-}$ ratio, the initial reaction was the formation of the monodentate complex $[CoN_4(OH)(H_2P_2O_7]$ by the loss of water from the $[CoN_4(OH)(H_2O)]^{2+}$ species. Chelate formation can take place through the attack of the phosphorus centers by the coordinated water with entry of the pyrophosphate oxygen.

The formation of the six-membered chelate is expected to be the major product as shown by the pathway.

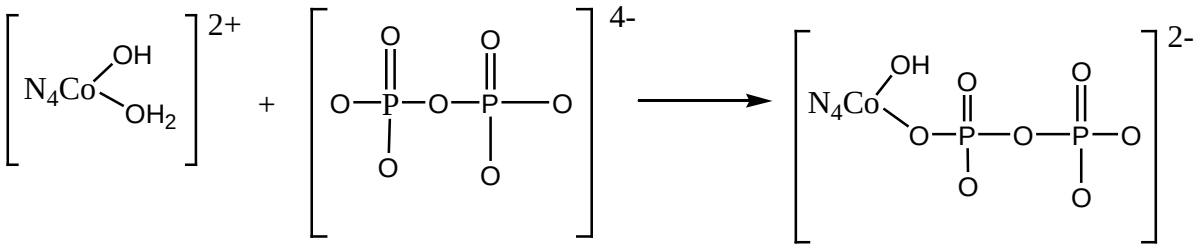

The coordinated hydroxide can then attack the phosphorus center leading to hydrolysis of the pyrophosphate. Alternatively, the coordinated hydroxide will pick up H^+ from the solution to form coordinated H_2O, which is a good leaving group. An attack of the cobalt center by the oxygen of pyrophosphate then results in the formation of both four and six membered chelates.

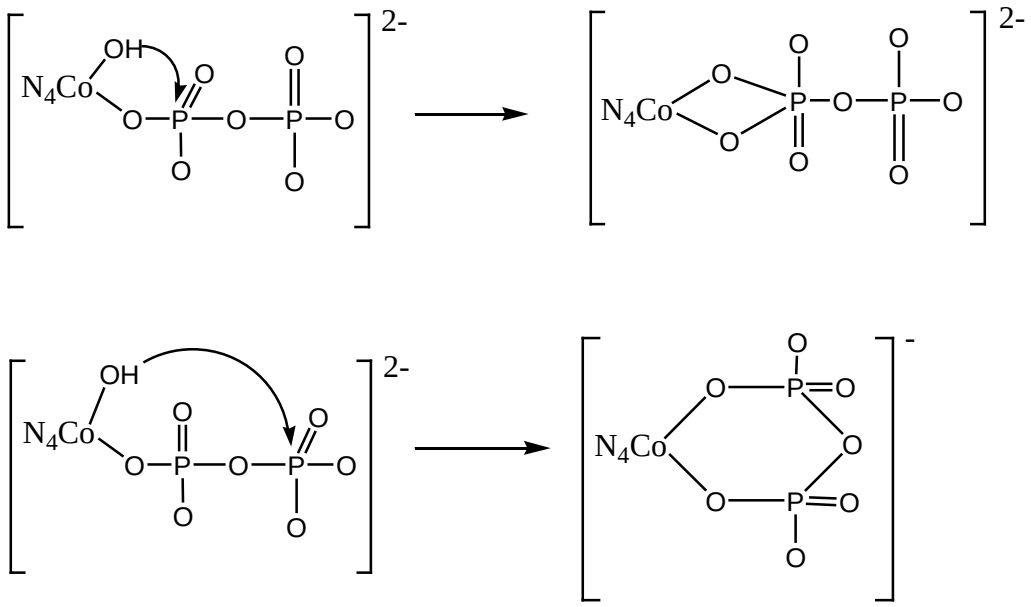

(2) The addition of 1 mole ratio of $[CoN_4(OH)(H_2O]^{2+}$ species to the preformed six membered chelate, $[CoN_4(OH)(P_2O_7)]^{2-}$, results in the formation of doubly six-membered chelates in a manner analogous to that described earlier. The existence of the single and double six-membered chelates in solution has been shown by previous ^{31}P NMR studies [59]. The chelates are relatively stable in solution at room temperature in the middle pH region, as evidenced by the slow degree of hydrolysis for solutions that predominantly contain these species. The plausible reaction pathway is given below,

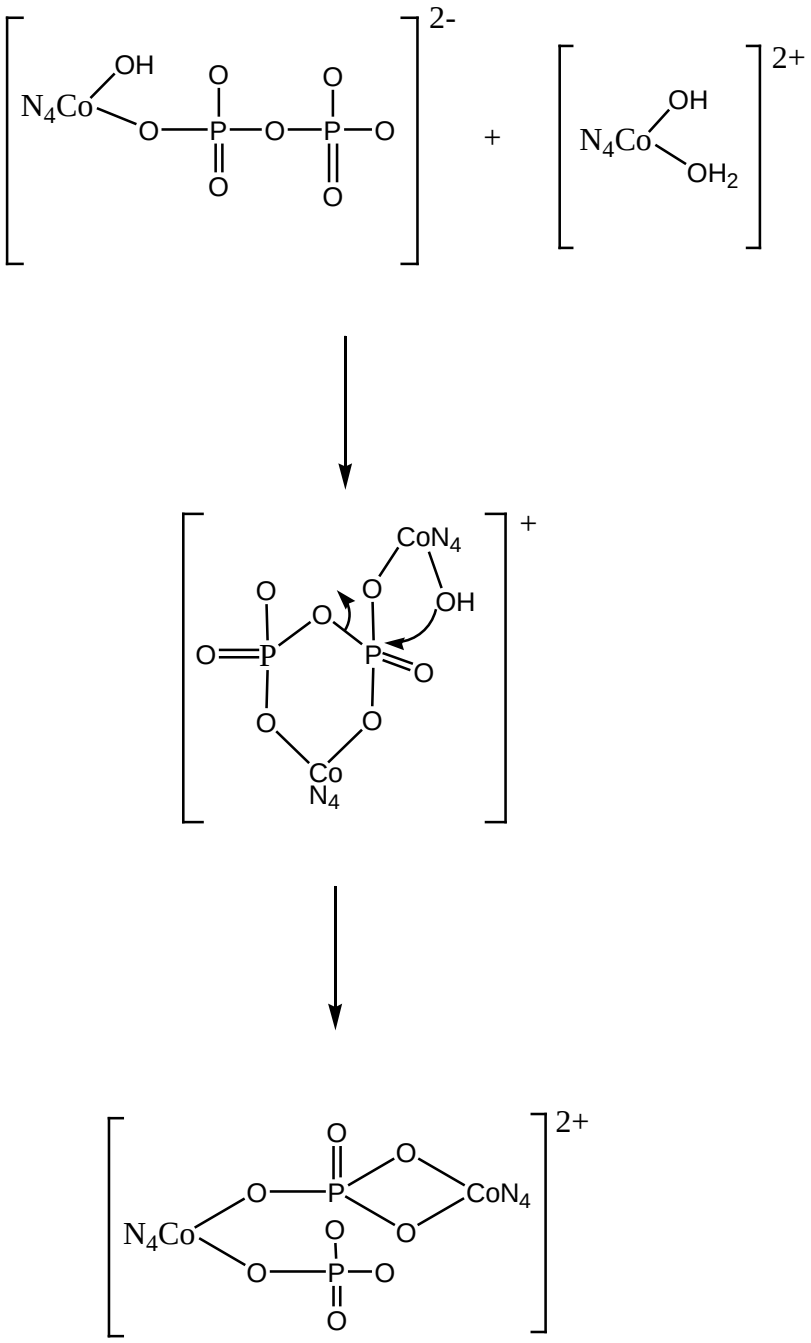

(3) The addition of NP^- to the preformed $[CoN_4(OH)(P_2O_7)]^{2-}$ showed a decrease in the absorbance at 400 nm and an increase at 310 nm. The decrease in absorbance at 400 nm is consistent with the assertion that nitrophenol is being depleted in the solution. The absorbance increase at

310 nm is indicative of the formation of either nitrophenylphosphate or nitrophenylpyrophosphate in the solution. Since the conditions of the experiment do not warrant for the hydrolysis of the pyrophosphate, we can safely assume that the species that prevails in the solution is nitrophenylpyrophosphate. It is to be expected from structural similarities that both nitrophenylphosphate and nitrophenylpyrophosphate behave similarly in their UV-Visible profile[61]. The plausible reaction pathway which results from the above is as follows.

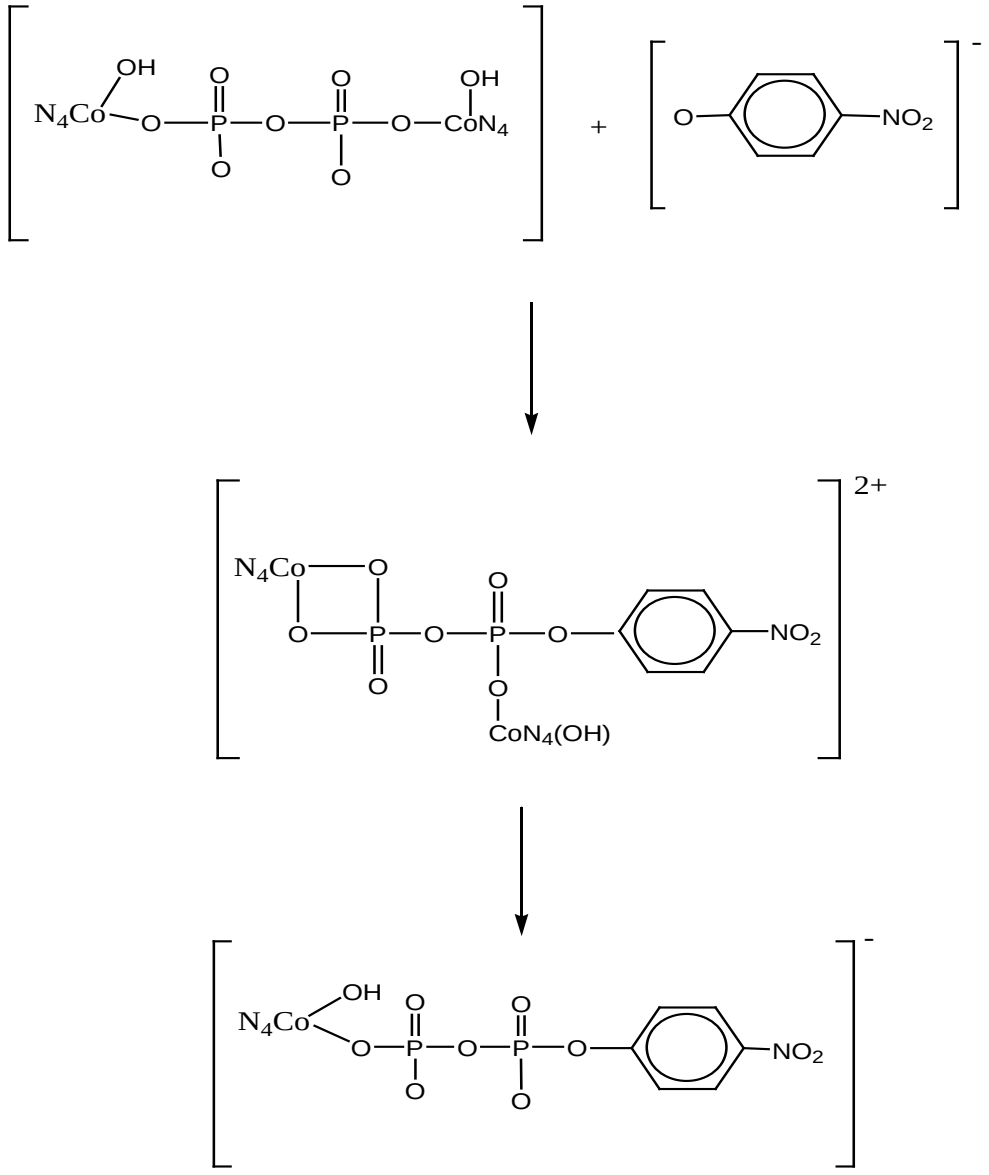

$[CoN_4(OH)(OH_2)]]^{2+}$ presumably cleave from the structure, producing nitrophenylpyrophosphate as depicted below

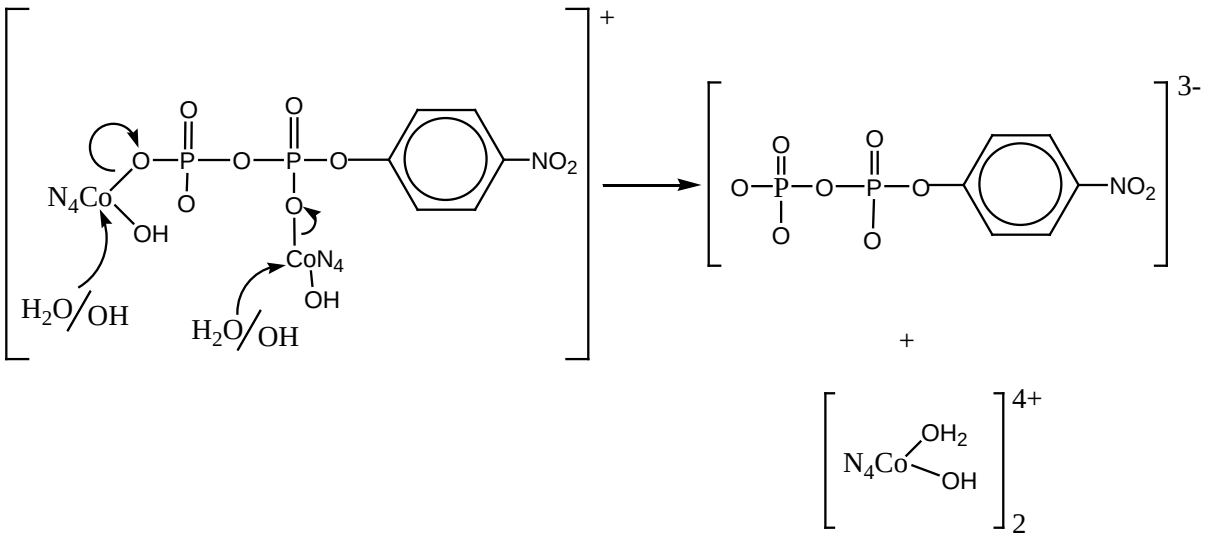

Earlier reports have suggested the synthesis of colourless crystals of dinitrophenyl dimethylpyrophosphate[61,62]. We were unable to obtain nitrophenylpyrophosphate commercially, but the ^{31}P $\{^1H\}$ NMR chemical shift, we have observed in situ gives an additional proof of its formation in the reaction solution.

(4) The reaction of 1 molar ratio of nitrophenol to 1 molar ratio of the preformed double six-membered chelate, $[\{CoN_4(OH)\}_2P_2O_7]$ showed a decreased rate of pyrophosphorylation (about 17%) compared to the one already discussed. Though the system produces stronger electrophilic phosphorus atoms due to the coordination of the pyrophosphate to two metal ions, the steric crowding does not enable the oxygens of the

nitrophenol to attack those centres effectively. The double six membered chelate is presumably thermodynamically stable.

CHAPTER FOUR

^{31}P NMR spectroscopic techniques for probing phosphorylation, dephosphorylation and pyrophosphorylation reactions in model compounds

With the advent of higher frequency instruments and Fourier transform NMR spectrophotometers; sensitivity was sufficiently increased, so that ^{31}P NMR studies of enzymatic models like ours become feasible. In considering the mechanism of enzymatic model reactions, it is first necessary to establish the ^{31}P NMR characteristics of reactants and products. Then, the more subtle characterization of the all phosphate species in the solution will possibly be attained. As will be discussed later, the parameters of interest from the ^{31}P NMR studies are (i) chemical shifts δ, (ii) spin-spin coupling constants (J).

The chemical shift of a nucleus represents change in its resonance frequency for a given value of the external magnetic field, due to shielding from its environment. δ is obtained relative to the resonance of 85% H_3PO_4. The magnetic interaction between P nuclear spins mediated by the electronic environment was observable in high-resolution as fine structure in the resonance. From the fine structure, the strength of the interaction, represented as J was deduced. In model investigations[63] which pertain to enzyme-substrate interactions, in which ^{31}P NMR spectra of the substrate

molecules were observed in their enzyme-bound complexes, δ and J may depend on the environment of the substrate on the enzyme model. The measurements of δ and J in the preformed complexes were thus potentially capable of providing information on e.g. the stoichiometric, state of metal chelation, the ionization state of the substrate, and possibly the conformational changes in the substrate produced by interaction with the metal ion. The application of ^{31}P NMR as a non perturbing method for determining equilibrium constants between phosphorus-containing compounds (both for the overall reaction and the interconversion steps between the metal ion bound species) have been described by previous investigators[63]. The chemical shifts δ and the spin-spin coupling constants J are the two spectral parameters that are measured from different peak positions in the high-resolution ^{31}P NMR spectra. The change in chemical shift could be attributed to the formation of a complex between the substrate and the metal ion in the enzyme. The stoichiometry of the different species present in solution can potentially be deduced from the variation of the chemical shift with concentration of the complex. If the chemical shift of a nucleus in a particular moiety on the substrate changes with pH, a comparison of δ vs pH of the metal ion bound substrate with that in free substrate is expected to shed light on the environment at the binding site in the complex. It might even be tempting to speculate on the basis of such comparison, which ionic species might be the true complex formed in the reaction, particularly when the pH dependence disappears in the bound state. In general, when a chemical shift is observed in a metal ion complex, the shift may be due to both a change in environment and a change in the

structure (or conformation) of the complex formed with the metal ion. If a distinction between such effects is made, it will be of considerable value to the understanding of the mechanism. The same argument applies to changes in spin-spin coupling constants. It may likely be due to conformational changes produced in the metal ion complex as has been reported[64]. In this respect, ^{31}P NMR suffers from a serious drawback in that no reliable theory applicable to molecules of biological interest is available either for δ or J that would allow meaningful correlations between δ and J measurements and molecular structure. The theoretical difficulties associated with δ and J of ^{31}P NMR compounds has been discussed by Letcher and Van Wazer[64,65]. It has been known for nearly two decades that many biological molecules possess characteristic ^{31}P NMR spectra, and some of these spectra are sensitive to important parameters like pH, metal ion chelation and so on, making ^{31}PNMR a useful technique for studying these systems. The volume of research being done with ^{31}P NMR and the variety and depth of information being extracted on biochemical systems testifies to the promise the method holds.

4.1 EXPERIMENTAL

4.1.1 INSTRUMENTS AND REAGENTS

All reagents used were either analytical reagents grade or the purest available commercially and were used without further purification. Measurement of pH was made with the Metrohm 635-pH meter equipped

with a combination electrode. The pH electrode was conditioned prior to use in a pH range 4 to 9. The pH of the reaction mixture was maintained by adding drops of 0.1 M, 0.01 M and 0.001 M of NaOH or $HClO_4$. The temperature of the reaction was controlled using a thermostated water bath, which allows the water to circulate via a jacketed reaction vessel maintained at 25^{o}C. ^{31}P NMR spectra were determined using a Varian Mercury 300MHz Fourier transform NMR spectrometer complete with 2 – channel mercury console, L600 PFG Varian 900 temperature controller and Varian 300 auto SW PFG 4 Nuc 30 – 122 MHz probe with multiple nuclei capacity operating at 121.47MHz.

The same protocol adopted in the UV-Visible studies in the preparation of both the enzyme and substrate model compounds and the reactions of the different systems were also employed in the ^{31}P NMR studies. The initial stoichiometric concentrations of phosphates (or pyrophosphates) were always 10^{-1}M. Higher concentrations caused solubility problems and lower concentrations would require many more accumulations which may lead to sample deterioration. The final concentration after mixing was 10^{-2} M. All spectra were taken at ambient temperature. The spectra from the literature were routinely proton decoupled, although decoupling made no noticeable difference in the spectra as reported[66-68]. For our experiments, the spectra were not proton decoupled. This could be attributed to the fact that effects of coupling are minimal in mono and diphosphates. Also, since the spectra were not integrated, there was no need for decoupling.

Phosphorous chemical shifts are referenced to an external standard of 1M H_3PO_4. Within experimental error, this standard has the same chemical shift as 85% H_3PO_4 with increasing values towards low fields, but the ^{31}P NMR spectrum of 1M H_3PO_4 is a much narrower line. Typical parameters used were as follows: spectrum width 10010.0Hz (414ppm), offset frequency 121.47MHz, pulse sequence s2pul, acquisition time 1.598 secs, number of repetitions 32000. The internal lock was accomplished by using 25% D_2O in the solvent.

4.1.2 Phosphorylation studies

The different systems monitored for the phosphorylation studies are; (a) the reactions between $[HPO_4]^{2-}$ and $[O_2NC_6H_4O]^-$ for 1:1, 2:1 and 3:1 $[HPO_4]^{2-}$ to $[O_2NC_6H_4O]^-$ ratios. (b) the reaction between $[\{CoN_4(OH)(OH_2)\}]^{2+}$ and $[HPO_4]^{2-}$ for 1:1, 2:1 and 3:1 $[\{CoN_4(OH)(OH_2)\}]^{2+}$ to $[HPO_4]^{2-}$ ratios. (c) reaction of $[CoN_4PO_4]$ and $[O_2NC_6H_4O]^-$ for 1:1, 2:1 and 3:1 $[CoN_4PO_4]$ to $[O_2NC_6H_4O]^-$ ratios.

4.1.2.1 Systems monitored for the phosphorylation studies

Reactions between $[HPO_4]^{2-}$ and $[O_2NC_6H_4O]^-$

Five mL of an aqueous solution of $[O_2NC_6H_4O]^-$ was mixed with five mL of an aqueous solution of $[HPO_4]^{2-}$ in the thermostated reaction vessel at 25° C. The concentration of the two reactant solutions was identical (10^{-1} M). The

final concentration after mixing was 10^{-2} M. The pH was maintained at 7 for the whole duration of the reaction under constant stirring. After 30 minutes of reaction, aliquots were withdrawn for the recording of ^{31}P $\{^1H\}$ NMR spectra. For 1:2 and 1:3 $[O_2NC_6H_4O]^-$ to $[HPO_4]^{2-}$ ratios, the amount of $[O_2NC_6H_4O]^-$ is held constant and that of $[HPO_4]^{2-}$ varied in the total reaction solution of 10 mL.

Reactions between $[CoN_4(OH)(OH_2)]^{2+}$ and $[HPO_4]^{2-}$

The procedure employed in the reaction of 1:1 molar ratio of $[CoN_4(OH)(OH_2)]^{2+}$ and $[HPO_4]^{2-}$ consist of mixing five mL of an aqueous solution of $[CoN_4(OH)(OH_2)]^{2+}$ with five mL of an aqueous solution of $[HPO_4]^{2-}$ in the thermostated reaction vessel at 25° C. The concentration of the two reactant solutions was identical (10^{-1} M). The pH was maintained at 7 for the whole duration of the reaction under constant stirring. After 30 minutes of reaction, aliquots were withdrawn for the recording of ^{31}P {1H} NMR spectra. For 2:1 and 3:1 $[CoN_4(OH)(OH_2)]^{2+}$ to $[HPO_4]^{2-}$ ratios, the amount of $[HPO_4]^{2-}$ is held constant and that of $[CoN_4(OH)(OH_2)]^{2+}$ varied in the total reaction solution of 10 mL.

Reactions between $[O_2NC_6H_4O]^-$ and preformed $[CoN_4PO_4]$ complexes

The method employed in the reaction of 1:1 molar ratio of the preformed complex $[CoN_4PO_4]$ and $[O_2NC_6H_4O]^-$ consist of mixing 5 mL of an aqueous

solution of $[O_2NC_6H_4O]^-$ and 5 mL of an aqueous solution of the preformed complex $[CoN_4PO_4]$ in the thermostated reaction vessel at 25° C. The concentration of the two reactant solutions was identical. The final concentration after mixing was 10^{-2} M. The pH was maintained at 7 for the whole duration of the reaction under constant stirring. After 30 minutes of reaction, aliquots were withdrawn for the recording of ^{31}P $\{^1H\}$ NMR spectra. For 2:1 and 3:1 $[CoN_4PO_4]$ to $[O_2NC_6H_4O]^-$ ratios, the amount of $[O_2NC_6H_4O]^-$ is held constant and that of $[CoN_4PO_4]$ varied in the total reaction solution of 10 mL.

4.2 Results and discussion for the phosphorylation studies

The chemical shifts observed in the different systems studied denoted as δ* for the various phosphorylated species are depicted in table 5. Comparison with literature data[66-68] leads to a plausible interpretation of all major signals.

Table 5. ^{31}P $\{^{1}H\}$ NMR chemical shifts for various phosphorylated species (0.01 M, 25° C and pH 7.0)

Structure	Chemical shifts (δ ppm)
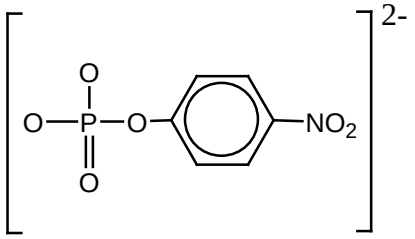	0.53*, 0.38 [66]
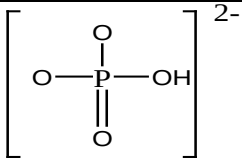	2.58*, 2.5 [66], 2.2 [67]
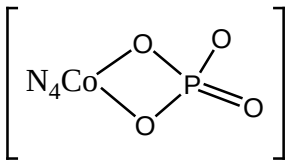	25.55*, 25.0 [66], 24.5 [67], 23.9 [68]
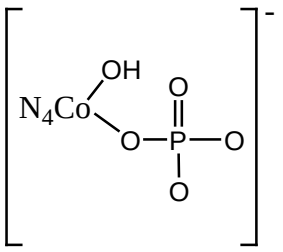	13.88*, 13.0 [66], 13.90 [67], 13.70 [68]
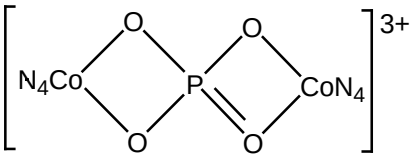	25.0*, 25.0 [67], 25.0 [68]

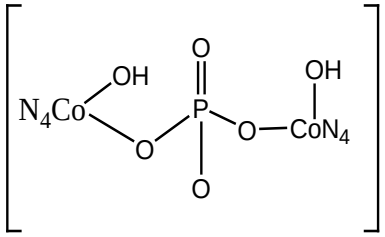	13.0*, 13.0 [67], 13.05 [68]
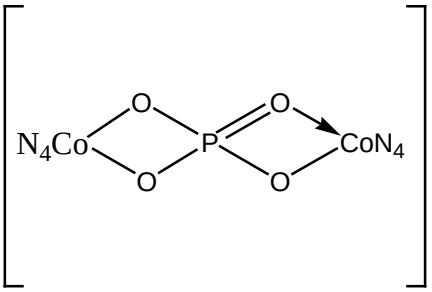 or 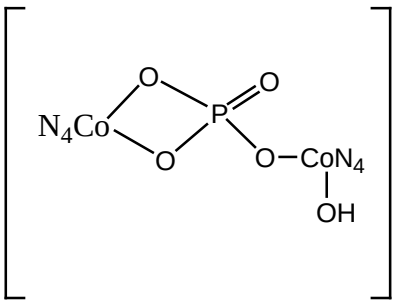	34.15*, 35.0 [67] 34.0, [68]
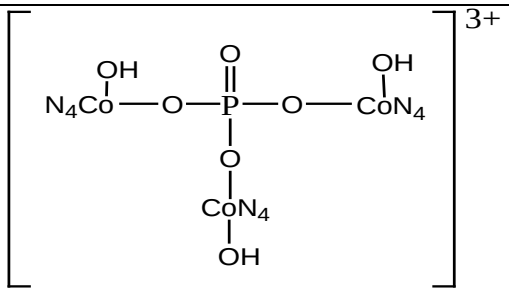	12.30*, 12.2 [68]

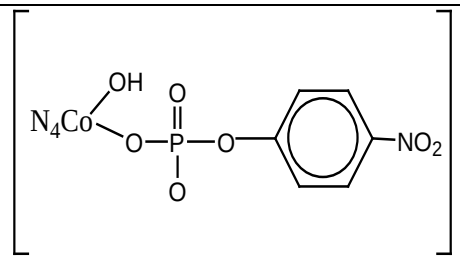	6.88*

Note: δ* is chemical shifts observed in our study

The important highlights deduced from the investigation are:

(1) The $^{31}P\{^{1}H\}$ NMR spectra of the solution that contained 1:1 $[CoN_4(OH)(H_2O)]^{2+}$: $[HPO_4]^{2-}$ showed two recognizable peaks at 13.88 and 25.55 ppm, in addition to a weak peak at 2.58 ppm. The chemical shift values are consistent with the formation of two types of complexes and depletion of $[HPO_4]^{2-}$ in the solution. Literature evidence[66-68] reveal that this is due to the formation of monodentate coordinated phosphate species and bidentate four member chelate species as shown below,

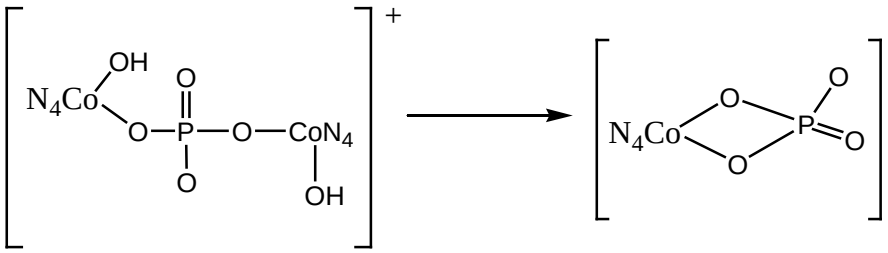

The phosphorus oxygen presumably attacks the cobalt center with concomittal release of the coordinate H_2O into the solution. The attack of the phosphorus center by the coordinated hydroxide results in the four membered chelate as depicted below,

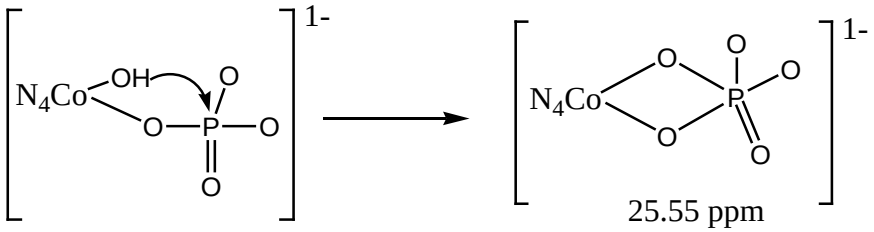

(2) For reaction solution that were 2:1 with respect to the enzyme model to phosphate ratio, showed additional signals around 25.0 ppm and 34.15 ppm. Analysis of the reaction leads to the following plausible reaction pathway,

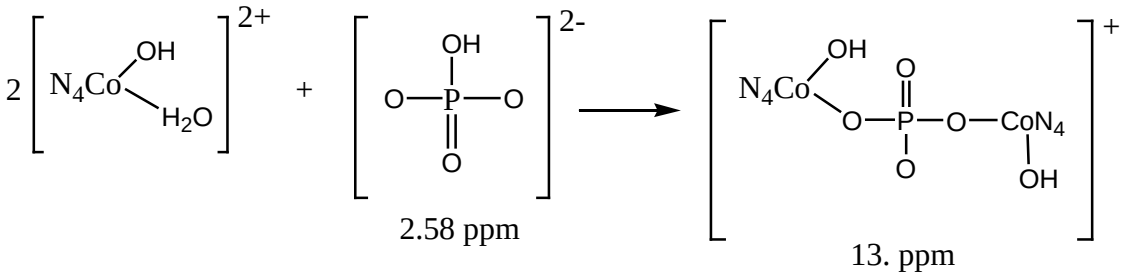

The reaction is due to the simultaneous attack of the cobalt center by the phosphate oxygen. The intermediate complex then undergoes the following plausible reaction,

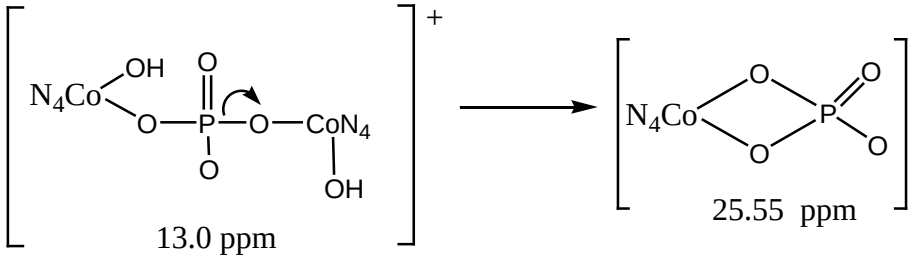

The possibility of forming double four membered chelate is also considered in line with literature evidence[67,68] .The peak at 34.2ppm is presumably due

to to the presence of the more stable double four membered chelate. No peak was observed for the monodentate chelate species in solution. By a similar analogy, 3:1 reaction solution with respect to the enzyme model to phosphate ratio showed additional trace peak at 12.30 ppm in addition to the other chemical shifts. It is after careful study that this determination was made as the trace peak is not very different from noise. We attribute this trace peak to the formation of transient species shown below in line with literature evidence[68].

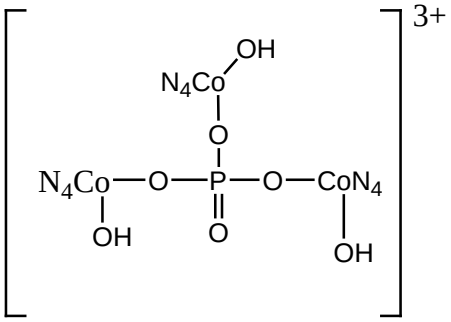

4.3 Results and discussion for the dephosphorylation studies

Results of the dephosphorylation studies showed a similar profile to that of the phosphate substrate, but with additional chemical shifts. The major observations of the study are;

(1) The same chemical shifts observed with the reaction of $[CoN_4(OH)(H_2O)]^{2+}$ and $[HPO_4]^{2-}$ were evident for reaction of $[O_2NC_6H_4PO_4]^{2-}$ with $[CoN_4(OH)(H_2O)]^{2+}$. We attribute this to dephosphorylation of NPP which is

brought about by $[CoN_4(OH)(H_2O)]^{2+}$. The oxygen of $[O_2NC_6H_4PO_4]^{2-}$ presumably attack the cobalt center in the following fashion.

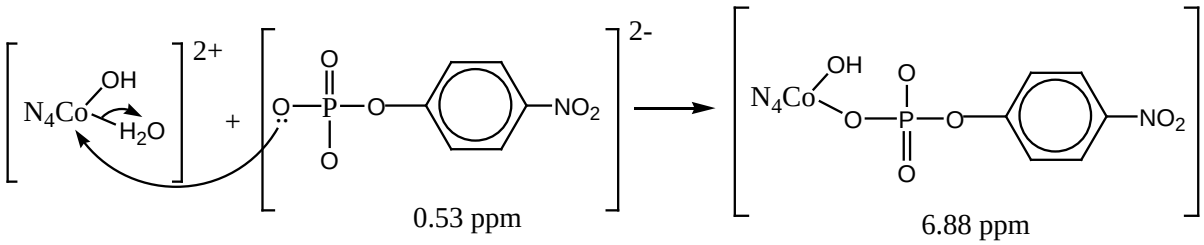

An attack on the phosphorus atom of the complex $[O_2NC_6H_4PO_4]^{2-}$ by the coordinate hydroxide, results in dephosphorylation with the production of nitrophenol.

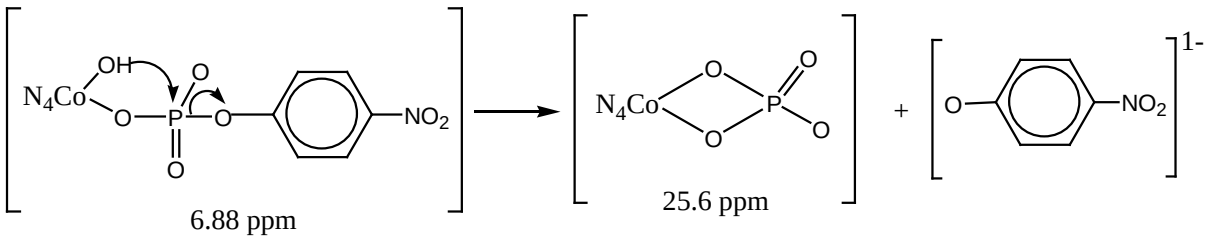

(2) Dephosphorylation of $[O_2NC_6H_4PO_4]^{2-}$ in the presence of $[CoN_4(OH)(H_2O)]^{2+}$ complexes indicates at least two competitive paths. One involves the cleavage of p-nitrophenol, and the other involves cleavage of the chelate ring at one Co-O bond. In addition, there could be a process which involves the cleavage of the monodentate p-nitrophenylphosphate from the Co(III) center as has been reported[69]. The stereochemistry of the monodentate species was not ascertained in this study. Other studies[70] with bis-(trimethylenediaminecobalt(III) ions indicate that the *cis-trans* rearrangement favour the *cis* configuration.

4.4 Pyrophosphorylation studies

The different systems monitored for the pyrophosphorylation studies are; (a) the reactions between $[O_2NC_6H_4O]^-$ and $[(OH)_2(PO_2)_2O]^{2-}$ (abbreviated as $[H_2P_2O_7]^{2-}$) for 1:1, 2:1 and 3:1 $[(OH)_2(PO_2)_2O]^{2-}$ to $[O_2NC_6H_4O]^-$ ratios. (b) the reaction between $[\{CoN_4(OH)(OH_2)\}]^{2+}$ and $[(OH)_2(PO_2)_2O]^{2-}$ for 1:1, 2:1 and 3:1 $[\{CoN_4(OH)(OH_2)\}]^{2+}$ to $[(OH)_2(PO_2)_2O]^{2-}$ ratios. (c) reaction of $[CoN_4P_2O_7]$ and $[O_2NC_6H_4O]^-$ for 1:1, 2:1 and 3:1 $[CoN_4P_2O_7]$ to $[O_2NC_6H_4O]^-$ ratios·

4.4.1 Results and discussion for the dephosphorylation studies

The chemical shifts observed in the different systems studied denoted as δ* for the various pyrophosphorylated species are depicted in table 6. Again, comparison with literature data [66-68] leads to a plausible interpretation of all major signals.

Table 6. ^{31}P $\{^{1}H\}$ NMR chemical shifts for various pyrophosphorylated species. (0.01 M, 25° C and pH 7)

Structure	Chemical shifts ((δ ppm))
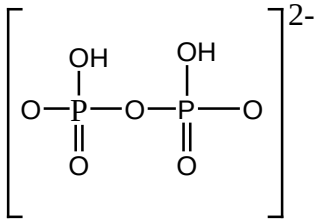	-6.66*, -4.39[66]
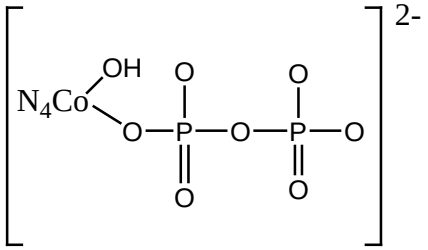	34.15*, 35.0[67], 34.0[68]
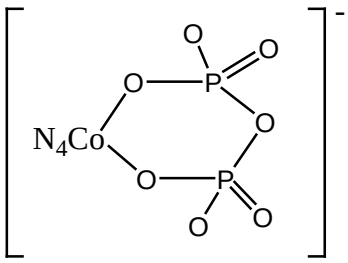	5.57*, 5.15[67], 4.4[68]
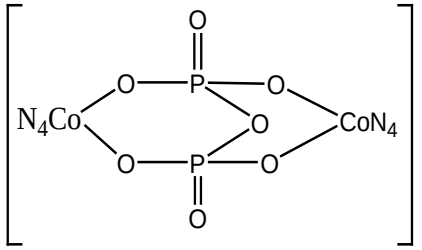	12.30*, 12.2[68]

Note: δ* is chemical shifts observed in our study

(1) In solutions that were 1:1 in $[CoN_4(OH)(H_2O)]^{2+}$ to $[H_2P_2O_7]^{2-}$ ratio at pH 7.0 and 25° C, the initial reaction involves the formation of the monodentate complex by the loss of water from the $[CoN_4(OH)(H_2O)]^{2+}$ species. The pyrophosphate oxygen then probably attacks the cobalt center to complete the chelate formation. The formation of the six-membered chelate as a major product is expected due to the stability of this ring system. Alternatively, the generation of four membered chelates can give rise to some inorganic phosphate. But this mode of attack is not preferred in the reaction as evidenced by very small hydrolysis leading to the production of inorganic phosphate. Since coordinated water is a poor nucleophile compared to coordinated hydroxide, intramolecular attack by coordinated water on phosphorus centers is considered to be unimportant in the reaction just described. The loss of the coordinated water and attack at the cobalt center by oxygens of the complex $[H_2P_2O_7]^{2-}$ to produce the six-membered chelate $[CoN_4(P_2O_7]^-$ is expected to be the major reaction pathway as shown below,

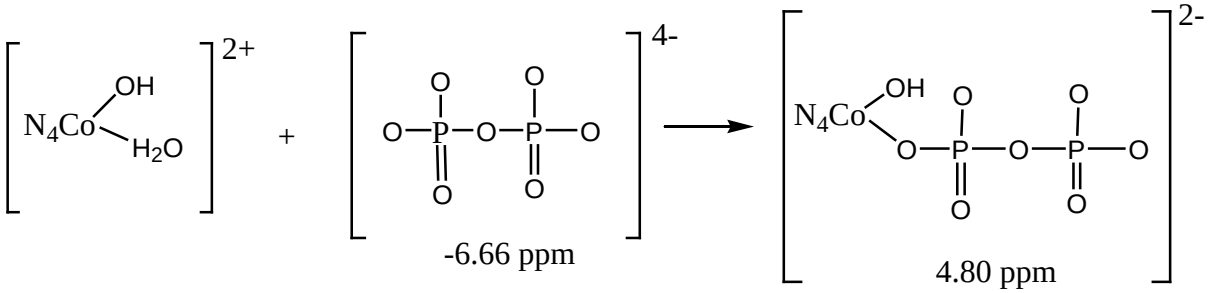

The transient species results in a six or four membered chelate from the attack of the phosphorus center by the coordinate hydroxide,

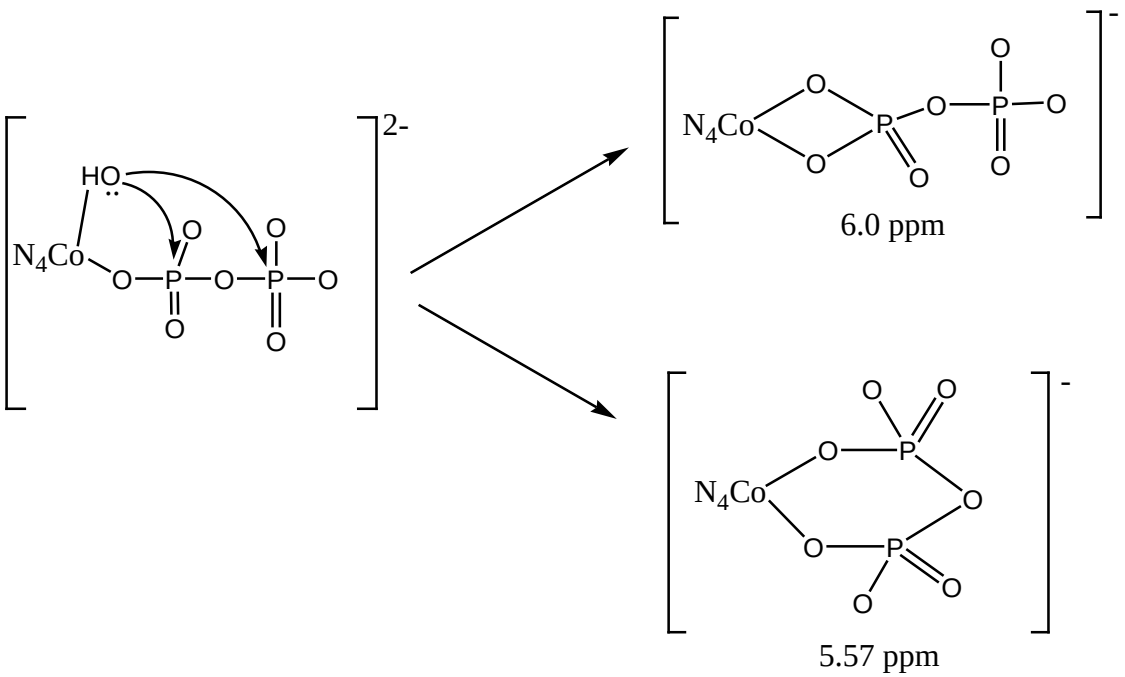

(2) The addition of 1 mole ratio of $[CoN_4(OH)(H_2O)]^{2+}$ species to the preformed six-membered chelate, $[CoN_4(P_2O_7)]^-$, results in the formation of a double six-membered chelates. The plausible reaction pathway is;

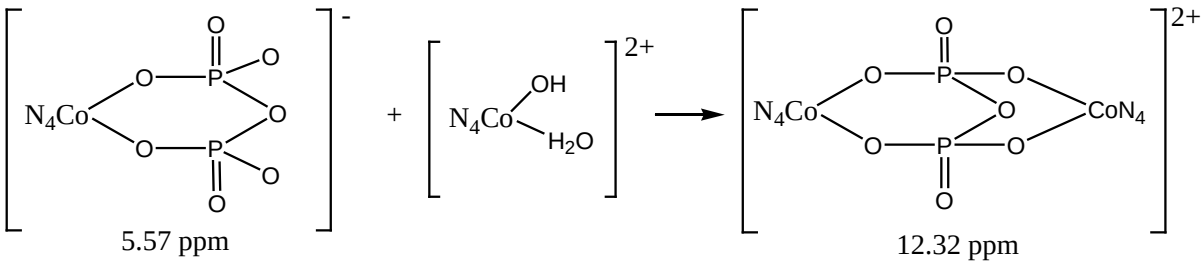

The new weak peak around 12.32 ppm observed in the spectra is presumed due to the formation of the double six membered chelate. The existence of the single and double six membered chelates in solution has been shown by previous ^{31}P NMR studies[70]. The chelates are relatively stable in solution at room temperature in the middle pH region, as evidenced by the slow degree

of hydrolysis for solutions that predominantly contain these species. For solutions of 3:1 $[CoN_4(OH)(H_2O)]^{2+}$ to $[CoN_4(OH)(P_2O_7)]^{2-}$, the spectra are generally similar to those of the 2:1 series.

(3) NPP^{2-} was reacted with preformed $[CoN_4(OH)(P_2O_7)]^{2-}$, anticipating pyrophosphorylation reaction in accordance with the following reaction pathway,

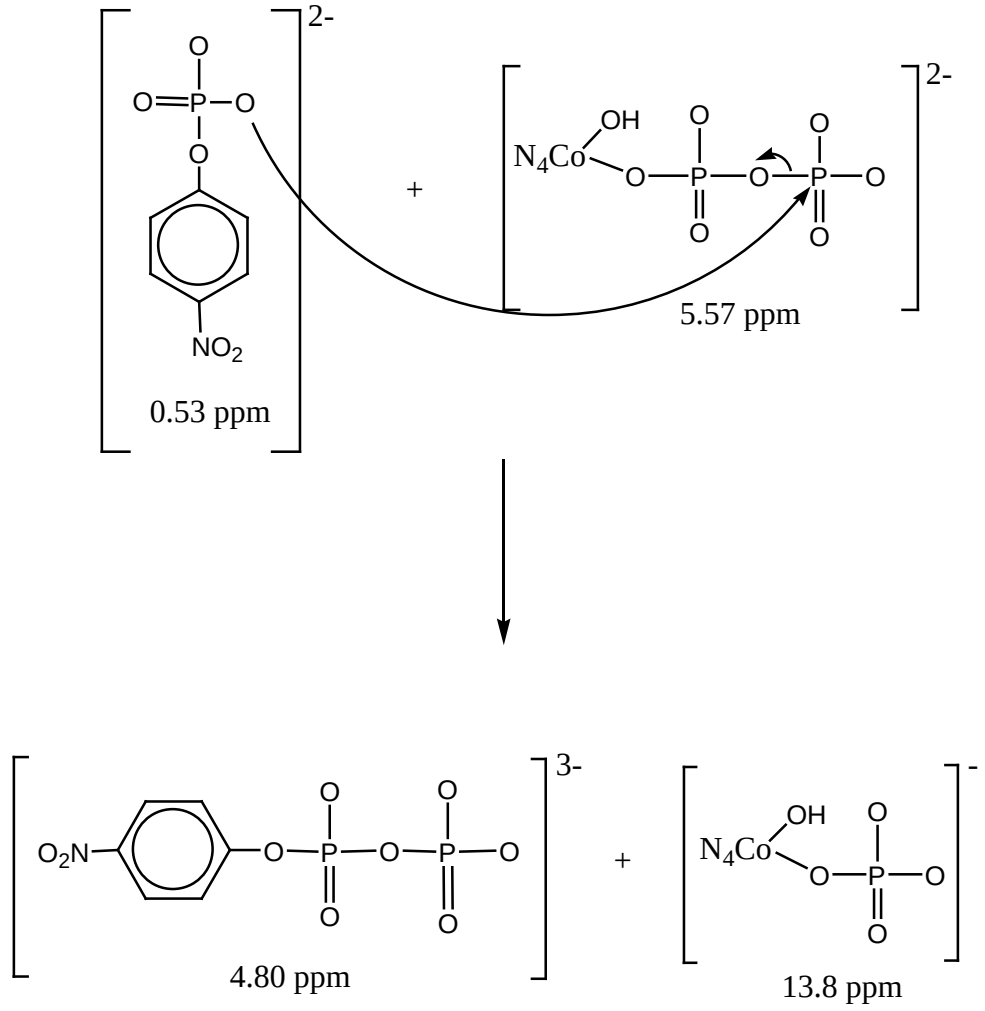

for the formation of metal coordinated nitrophenylphosphate complex [CoN_4NPP] or metal coordinated nitrophenylpyrophosphate complex [CoN_4NPPP]$^-$ as depicted below,

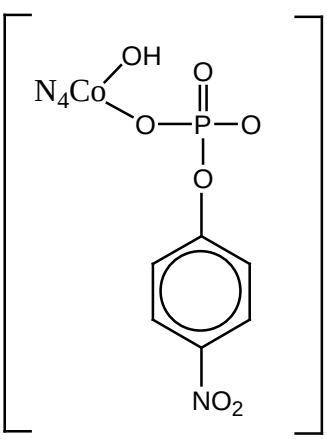

~ 25.0 ppm

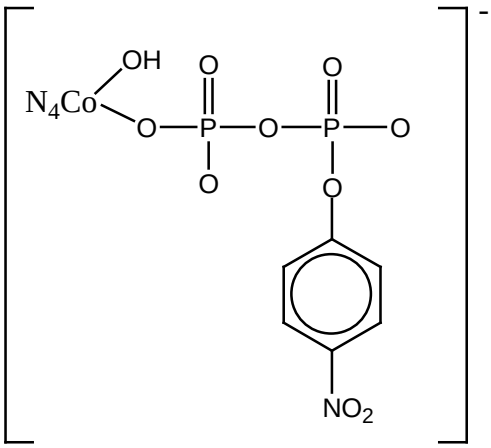

~ 25.0 ppm

The reaction for higher ratios of the preformed pyrophosphate complex to that of NPP gave very broad spectra which was difficult to interpret.

CHAPTER FIVE

Monitoring phosphorylation, dephosphorylation, pyrophosphorylation and depyrophosphorylation reactions by surface enhanced Raman scattering (SERS) in model compounds

Raman spectroscopy is based on the inelastic scattering of radiation. Scattering occurs due to collisions between photons and molecules. Irradiation of light with the frequency ν_o upon a certain molecule transfers a number of photons with the energy $E = h\nu_o$. These photons include photons colliding with molecules as well as those that pass without interacting with the molecules. Most photons colliding with molecules do not change their energy after the collision (elastic collision) and the ensuing radiation is called Rayleigh scattering. Only a very small number of the photons that collide with the molecule exchanges energy during collision (inelastic collision). Scattering phenomenon in which incident photons exchange energy with a molecule is known as Raman scattering[71]. Depending on the frequency of the scattered light, after collision with the molecule, it could be stokes Raman scattering or anti-Stokes Raman scattering. If an incident photon delivers a quantum of energy to the molecule, and the energy of the scattered photon is reduced to $(h\nu_o-\nu)$, the scattering phenomenon is known as Stokes scattering. Otherwise, when an incident photon receives the energy from the molecule, the energy of the scattering photon rises to

($h\nu_o+\nu$). This is known as anti-Stokes scattering. The change in wavelength that is observed when a photon undergoes Raman scattering is attributed to the excitation (or relaxation) of vibrational modes of a molecule. Since different functional groups have distinctive characteristic vibrational energies; every molecule has a unique Raman spectrum. Raman signals are associated with vibrations that cause a change in polarizability.

Surface enhanced Raman scattering is an embodiment of Raman spectroscopy that has all molecular fingerprint capabilities of Raman and extremely high sensitivity. The SERS effect occurs when the targeted molecules reside at appropriate sites or near nano-structured systems composed of certain metals, such as silver or gold. SERS involves the adsorption of incident laser photons within nanoscale metal structures, generating surface Plasmon's, which couple with nearby molecules (the analyte) and thereby enhancing the efficiency of Raman scattering by six orders of magnitude or more[71,72]. In addition to affording high levels of sensitivity, the rich molecular vibrational information provided by SERS scattering yields exceptional selectivity and allows the identification of virtually most compound[73]. It also affords the ability to distinguish constituents of chemicals in mixtures[74]. A detailed highlight on the advantages of SERS as a promising vibrational spectroscopic technique for probing our model compounds is given below.

(i) Because it is a vibrational spectroscopic technique, a SERS spectrum is capable of providing more information about molecular structure and the local environment than an electronic spectroscopic technique.

(ii) As the SERS analyte must be on or near a noble metal, which provides nonradiative pathways for the decay of the excited states, fluorescence interference is quenched[74]. Hence fluorescent chromophores can be studied easily with SERS technique which used to be difficult to monitor by traditional Raman scattering.

(iii) Minor changes in the orientation of an adsorbate can be discerned, because slight variations yield measurable shifts in the locations of SERS spectral peaks.

(iv) The abrupt decay of the electromagnetic fields ensures that only adsorbed molecules on or near the noble-metal substrate are probed. This makes SERS an ideal tool for surface studies and trace analyses.

(v) Water exhibits extremely weak SERS signals and silver substrates are compatible with aqueous solutions. This makes the SERS technique employing Ag colloids well suited for analysis performed on molecules in aqueous media.

(vi) Initially, Raman spectroscopy was not utilized for detection and monitoring of phosphates because it failed to provide the sensitivity required for the detection of trace quantities. This was because of high background

levels of fluorescence arising from either the sample or substrate which swamp the weak Raman signals. Subsequently, it has been found that surface enhancement effects can be achieved with silver colloids in order to improve the sensitivity needed for the detection and monitoring of phosphates.

5.1 Theory of surface enhanced Raman scattering (SERS)

Surface Enhanced Raman Scattering (SERS) is based on enhancing the Raman signal of molecules adsorbed on a metal covered surface. SERS was observed in 1974 by Fleischman et al[75]. It was reported that strong Raman scattering from pyridine adsorbed on a silver surface. In 1977, Jeanmaire and Van Duyne[76] noted that scattering intensity from the adsorbed molecules is 10^5-10^6 times stronger than those of the nonadsorbed molecules. Even higher enhancements (10^{14}-10^{15}) have been reported[77]. The enhancement factor depends on the metal surface and type of the molecules. The most commonly used metal surfaces for SERS are based on silver (Ag) and gold (Au) colloid nanoparticles[78-80].

Metal surfaces are covered with electrons. When a light beam interacts with these electrons, they begin to oscillate as a collective group across the surface, in a phenomenon termed surface plasmon. Surface Plasmon's from small uniform particles have a resonance frequency at which they absorb and scatter light most efficiently. The frequency varies with the metal and the nature of the surface. Both silver and gold Plasmon's oscillate at

frequencies in the visible region and are reported to be suitable for use with visible laser excitations[81]. It has also been observed that on a smoothed surface, the oscillation occurs along the plane of the surface, and only absorption of light can occur, but no light will be scattered[81].

5.2 The principles of SERS effect

The enhancement mechanism of SERS can be explained as an electromagnetic field and a chemical enhancement[82,83]. The chemical enhancement is derived from electronic interactions between the molecules and the metal substrate and can provide an order of magnitude increase in signal[83]. However, the more dominant effect that contributes to the SERS signal is due to enhanced electromagnetic fields at the metal roughened surface[84]. These enhanced fields are well known to originate from localized surface plasmon resonance of the nanoparticles, in which incident lights leads to a collective oscillation of the surface conduction electrons of the nanoparticle. This collective oscillation results in strongly enhanced electromagnetic fields that are confined to within several nanometers of the silver colloid[85,86]. Only molecules that enter this zone of enhanced fields experience significant enhancement of their Raman scattering. A single metal Ag colloid typically offers SERS signal enhancements on the order of 10^2-10^6 as has been reported[85]. However, when two metal Ag colloids are in close proximity, their dipoles can couple[87,88], leading to stronger overall field enhancements, reported to be as high as 10^{10} – 10^{14}. As such, Ag colloids are often considered an optimum SERS substrate, even though they lack

well-defined structure[88]. A detailed discussion of the electromagnetic and chemical enhancements is described below.

5.2.1 Electromagnetic enhancement

This is the most well-studied enhancement mechanism in SERS measurement. As has been mentioned, most enhancement factors of SERS can be due to an electromagnetic enhancement mechanism that is a direct consequence of the presence of metal roughness features at the metal surface. These features can be developed in a number of ways, for example: oxidation-reduction cycles on electrodes surfaces[89,90], vapor deposition of metal particles onto substrates[91,92] or metal colloids[93]. All of these methods leave the metal surface with small metal particles or colloids (aggregates of particles) that are capable of SERS. When a small metal sphere is subjected to an applied electric field from the incident light, the intensity of Raman scattering I_R is proportional to the square of the magnitude of the total electromagnetic fields (E_T) on the molecule[94].

$$I_R \alpha E_T^2$$

$$E_T = E_M + E_P$$

Where E_T is the total electromagnetic fields on the molecule, E_M is the electromagnetic field on the molecule in the absence of roughness features and E_P is the electromagnetic field emitted from the particulate metal roughness feature. E_M is related with classical Raman scattering and is relatively small. This is one of the reasons why Raman scattering has a weak

signal. However, the presences of metal features provide electromagnetic field from the metal particle itself. This electromagnetic field is quite proximate as the molecule is adsorbed onto the roughness features and will contribute a large factor to the total electromagnetic field. The magnitude of the total electromagnetic fields of the particle is thus crucial to the intensity of Raman signal. It also depends on the size of the metal features and type of molecule. The most efficient SERS substrate is Ag and Au colloid aggregates with range of 50 – 70 nm size[95]. On the other side, to achieve the highest enhancement, the molecule must be in close proximity to the surface (typically within ~ 10 nm from the surface)[94].

5.2.2 Chemical enhancement

As postulated by Moskovits[96], the difference of enhancement factor between CO and N_2 could not be explained by the electromagnetic model alone. Also, the experimentally obtained maximum enhancement factor was higher than that of the theory by five orders of magnitude. A dynamic charge transfer mechanism was postulated for the chemical effects[97]. It is currently accepted that one mechanism cannot fully explain the enhancement factor. Their combination gives a proper sense of the huge enhancement factor of 10^{14} in SERS[98,99].

5.3 Experimental

5.3.1 Instrument and reagents

All reagents used were either analytical reagent grade or the purest available commercially and were used without further purification. Measurement of pH was made with the Metrohm 635-pH meter equipped with a combination electrode. The pH electrode was conditioned prior to use in a pH range 4 to 9. The pH of the reaction mixture was maintained by adding drops of 0.1 M, 0.01 M and 0.001 M of NaOH or $HClO_4$. The temperature of the reaction was controlled using a thermostated water bath, which allows the water to circulate via a jacketed reaction vessel maintained at 25^{o} C. The Raman spectra were recorded with Bruker FT-Raman Model GC 7890A/5975C spectrometer equipped for the collection of fluorescence free Raman spectra in the near infrared region at 1064 nm excitation. The instrument was configured with a dual channel option for a further excitation line. It has a spectral range of 3600-70 cm^{-1} Stoke shift RT-InGaAS detector and 3500-70 cm^{-1} Stoke shift Liquid N_2 cooled Ge detector with a 50 cm^{-1} option which gives it a resolution of 0.8 cm^{-1}. The instrument is also equipped with an integrated air-cooled diode pumped Nd:Yag laser 1064 nm, polarized with a laser power of 500 Mw, 1000Mw, fully software controlled.

5.4 Preparation of the silver colloids (Ag sol gel)

Colloidal silver has been the most widely employed for SERS, possibly because its preparation requires no specialized apparatus. Silver colloids can be prepared by chemical reduction with either sodium borohydride or sodium citrate. Citrate reduced colloids are more stable and many analyst have prepared these using published protocols[100]. Batch to batch reproducibility is difficult to achieve by this method and the stability (shelf life) is variable. Preparation requires the use of ultra clean glassware and accurately controlled temperatures, stirring speed etc. A published modification[100] has led to some improvements in the properties of the silver colloids but long term stability can still be a problem. Metal colloids have been prepared by many methods in the past three decades. The preparation of colloids is directly related to the type of target molecule, the system of analysis and the availability of equipment to prepare them. Even once the colloids are prepared, keeping in view the analytical parameters, the performance of colloids remain variable due to other reasons, such as the slight change in the preparation protocol or the presence of impurities. Five hundred millilitres of 1.0 x 10^{-3} M silver nitrate solution was brought to boiling. To this, 10 mL of 3.4 x 10^{-2} M citric acid solution was added slowly. The mixture was kept at boiling for about one hour. The final volume was adjusted to 500 mL with deionized water. The resulting colloids are greenish yellow. The colloids were transferred to a 500 mL graduated cylinder, covered and allowed to fractionate by sedimentation over a 10-day period. Sedimentation provides a simple and inexpensive method for obtaining

coagulated and homogenous colloids, suitable for surface enhanced Raman scattering. The fraction of aliquots between 100 and 300 mL (measured from bottom of the cylinder) were utilized as the active colloidal silver sol.

5.5 Protocol for SERS studies

The same protocol adopted in the UV-Visible studies in the preparation of both the enzyme and substrate model compounds and the reactions of the different systems were also employed in the SERS studies. Note that for the SERS studies, the initial stoichiometric concentrations of phosphates (or pyrophosphates) were always 1 M. The final concentration after mixing was 10^{-1} M. 1.0 mL of the active silver sol was mixed with the same quantity of the analyte in a 2 mL ampoule. After vigorous mixing, the ampoule was placed in the sample holder of the Raman instrument for monitoring. The samples were run with a laser power of 450 Mw at a maximum of 1000 counts and 512 scans.

5.6 Phosphorylation studies

The different systems monitored for the phosphorylation studies are; (a) the reactions between $[HPO_4]^{2-}$ and $[O_2NC_6H_4O]^-$ for 1:1, 2:1 and 3:1 $[HPO_4]^{2-}$ to $[O_2NC_6H_4O]^-$ ratios. (b) the reaction between $[\{CoN_4(OH)(OH_2)\}]^{2+}$ and $[HPO_4]^{2-}$ for 1:1, 2:1 and 3:1 $[\{CoN_4(OH)(OH_2)\}]^{2+}$ to $[HPO_4]^{2-}$ ratios. (c) reaction of $[CoN_4PO_4]$ and $[O_2NC_6H_4O]^-$ for 1:1, 2:1 and 3:1 $[CoN_4PO_4]$ to $[O_2NC_6H_4O]^-$ ratios.

***** Note that the same methods employed in the previous (UV-Visible and

^{31}P {^{1}H} NMR studies) were also adopted in the SERS studies. In this case, the initial stoichiometric concentrations of phosphates (or pyrophosphate) were always 1 M. The final concentration after mixing was 10^{-1} M.

5.7 Results and discussion for the phosphorylation studies

In aqueous solutions, PO_4^{3-} ion has a tetrahedral symmetry (Td), and the vibrational spectrum is made up of four modes. The most intense band is related to the totally symmetric (A1) stretching vibration $v_s(PO_4)$. Considerably lower intensity bands are associated with the triple-degenerate asymmetric (F2) stretching mode $v_{as}(PO_4)$, the triple-degenerate asymmetric deformation mode $\delta_{as}(PO_4)$, and the double degenerate symmetric (E) deformation mode $\delta_s(PO_4)$. For solutions in which the dominant ionic species is HPO_4^{2-}, three stretching modes of the vibrational spectra were observed. The bonding of hydrogen ion to PO_4^{3-}, results in reduced symmetry in the HPO_4^{2-} ion. The OH group is treated as a point mass, and the symmetry is modeled as C_{3v}, where the degenerate asymmetric stretching mode (F2) splits into the symmetric and asymmetric stretches of the PO_3 group. Bonding of two hydrogen ions to the PO_4^{3-} ion further reduces the symmetry to C_{2v} in the $H_2PO_4^-$ ion, where the OH groups are treated as point masses[101]. It should be noted that in some of the reactions studied, both hydrolysis and phosphorylation reactions are possible to a varying degree. However, the spectra profiles indicate which products prevail in the solution after reaction. It is to be noted that the relative intensities of

the bands from the SERS spectra differ significantly from those of the normal Raman spectra owing to the specific selection rules[101]. Surface selection rules suggest that, for a molecule adsorbed flat on the metal surface, it's out of plane vibrational modes will be more enhanced when compared to their in-plane counterparts and vice versa, when it is adsorbed perpendicularly to the surface. Table 7 summarizes the interpretation of the spectra.

Table 7. Interpretation of SERS and Raman spectra from adsorbed phosphate species in solution.

Phosphate species	Vibrational frequency (cm^{-1})	Assignments
PO_4^{3-}	296	v(Ag-O)
	420	$\delta_s(PO_4)$
	567.3	$\delta_{as}(PO_4$
	926.9	$v_s(PO_4)$
	1076	$v_{as}(PO_4)$
HPO_4^{2-}	309	v(Ag-O)
	546	$\delta_{as}(PO_4)$
	931	v(P-O)
	1001.2	$v_{as}(PO_n)$
$H_2PO_4^-$	307	v(Ag-O)
	907	v(P-(OH)2
	975	v(P-O)
$H_2P_2O_7^{2-}$	730	v(P-O-P)
	1025	v(P-O)

The basis for interpreting the SERS spectra of adsorbed phosphate anions include the relationship of these spectra to Raman spectra of similar phosphates[101,102] IR spectra of metal coordinated phosphate complexes in aqueous solution[103] and results from the literature showing effects of adsorption on vibrational spectra[104-106]. General features of the adsorbed phosphate anion vibrational spectra on silver sol gel suggest an influence of adsorption include (a) the increased number of bands observed in the SERS spectra relative to the Raman spectra, (b) the shifts in frequencies of the SERS spectra, (c) the broadening of the P-O stretching vibrations in the frequency region 800-1200 cm^{-1} relative to the Raman spectra[107] and (d) the appearance of the low frequency band at 230-320 cm^{-1} (absent in the Raman phosphate spectra) indicating the formation of the silver-anion bond as inferred by earlier investigators[108]. The NO_2 group in nitrophenylphosphate has a strong SERS band at 1345 cm^{-1} and a weak band at 1532 cm^{-1}. These two bands are due to the symmetric and asymmetric stretching modes of the NO_2 group. The complex $[CoN_4(OH)(OH_2)]^{2+}$ shows peaks at 1626 and 1599 cm^{-1} due to the amine groups. The band around 1037 cm^{-1} is attributed to the P-O-C present in nitrophenylphosphate complexes. The P=O bonds show bands around 1250 cm^{-1}. Due to interference from the coordinated moieties, shifts of the bands for P=O bonds is seen in some of the complexes. Figure 3 depicts a system where there is little difference between spectra of a saturated solution of an analyte and the same solution with the Ag colloid mixture. A

peak at a low wavenumber of 244 cm^{-1} appears. This peak can be ascribed to the v(M-O) mode.

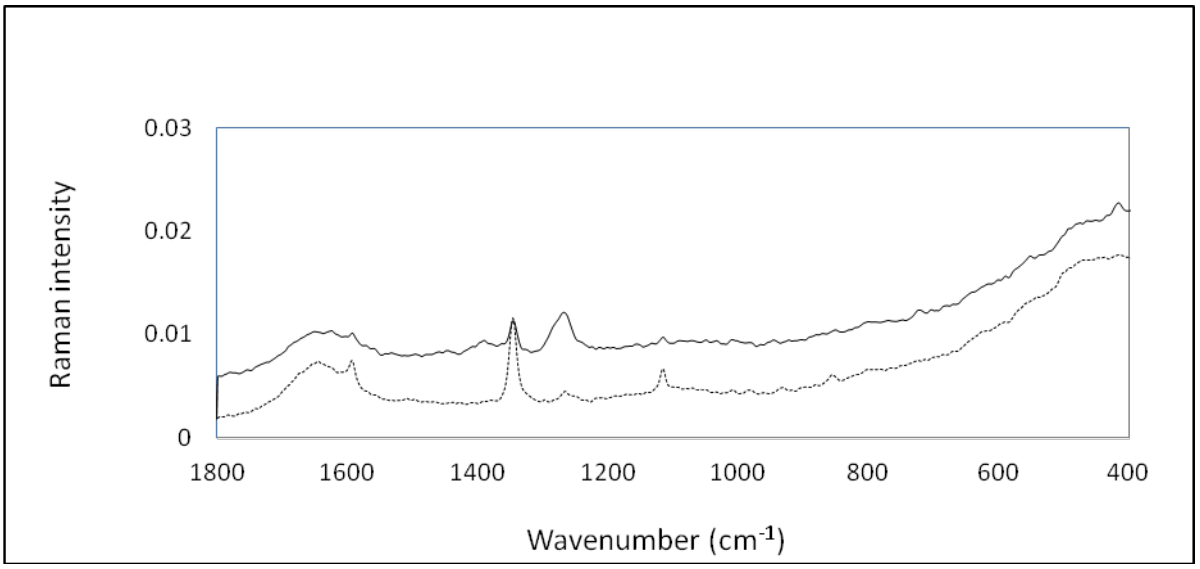

Figure 3. FT-Raman spectra of a saturated solution of $Na_2HPO_4.7\ H_2O$ (bottom) and the same solution with the Ag colloid mixture (top). Note the peak at 244 cm^{-1} due to the v(M-O) mode

A considerable enhancement, including a shift of some of the peaks, is evident for a solution of nitrophenol when the Ag colloid mixture is added. This can be seen in Figure 4.

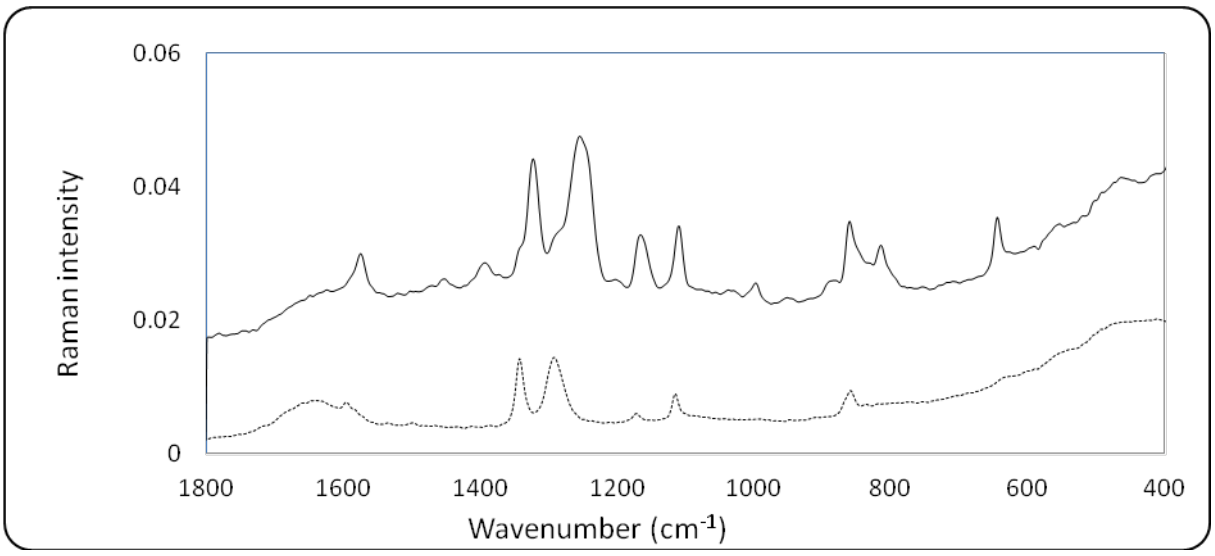

Figure 4. Raman spectra of a solution of nitrophenol in solution (bottom), and of the same solution with the silver colloid mixture (top).

As can be seen from the above examples, an enhancement of the vibrational peaks is not always possible. Monitoring of the reaction was possible by identifying those characteristic peaks in the corresponding reactions given by the values in table 7. The following deductions were made from the SERS spectra of the reaction between the enzyme and substrate models:

(1) The reactions of the preformed $[CoN_4(OH)PO_4)]^-$ with $[O_2NC_6H_4O]^-$ resulted in the disappearance of the phosphate band at the frequency region 936 cm^{-1} and the shifting of the band to around ~996 cm^{-1}. This band is associated with metal coordinated P-O stretching vibrations which normally appear in the frequency region 960-1000 cm^{-1}. This frequency shift is presumably attributed to the metal coordinated P-O stretching vibrations. Such observed frequencies are in accord with the view that coordination with a metal increases the double bond character of the P-O bond. This causes a decrease in the bond length and an increase in the corresponding frequency. The shift of the metal coordinated P-O stretching vibration from 936 cm^{-1} to the region of 996 cm^{-1} indicates the possibility of a phosphorylation reaction occurring in the system. The reactions of the complexed phosphates with nitrophenol can be rationalized as the attack of the phosphorus center of $[CoN_4(OH)PO_4)]^-$ by oxygen of the $[O_2NC_6H_4O]^-$ to produce a metal coordinated nitrophenylphosphate, which can abbreviated as $[CoN_4(OH)$-NPP].

(2) The addition of 2:1 molar ratio of $[CoN_4(OH)(H_2O)]^{2+}$ and $[HPO_4]^{2-}$ under the experimental condition is presumed to produce largely $[\{CoN_4OH\}_2PO_4]^{+}$. The additional metal ions per phosphate will force the phosphorus center to adapt an increased electrophillic character thereby facilitating the attack of nitrophenolate on phosphorus as discussed in the previous chapters. The bands at 300-320 cm^{-1} are interpreted to indicate the formation of metal phosphate complex in line the literature values. Possible adsorption geometry for the H_2PO_4 anion on the silver colloid is depicted below

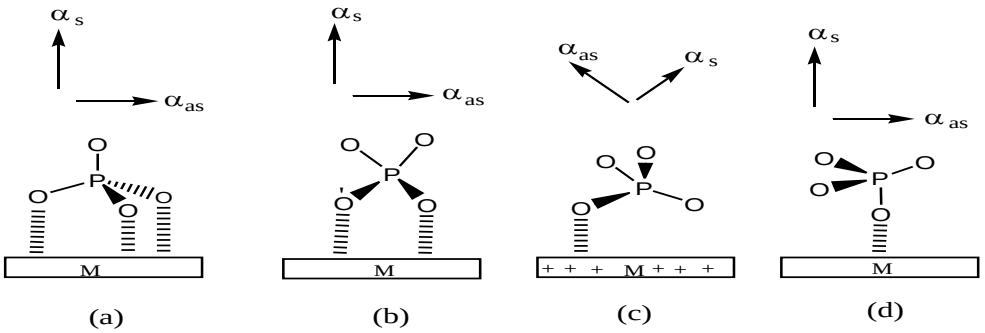

(3) The SERS spectrum of nitrophenylphosphate is shown in figure 5. The spectrum reveals a band around 893 cm^{-1} which is assumed as the P-O stretching mode in line with the information in table 7.

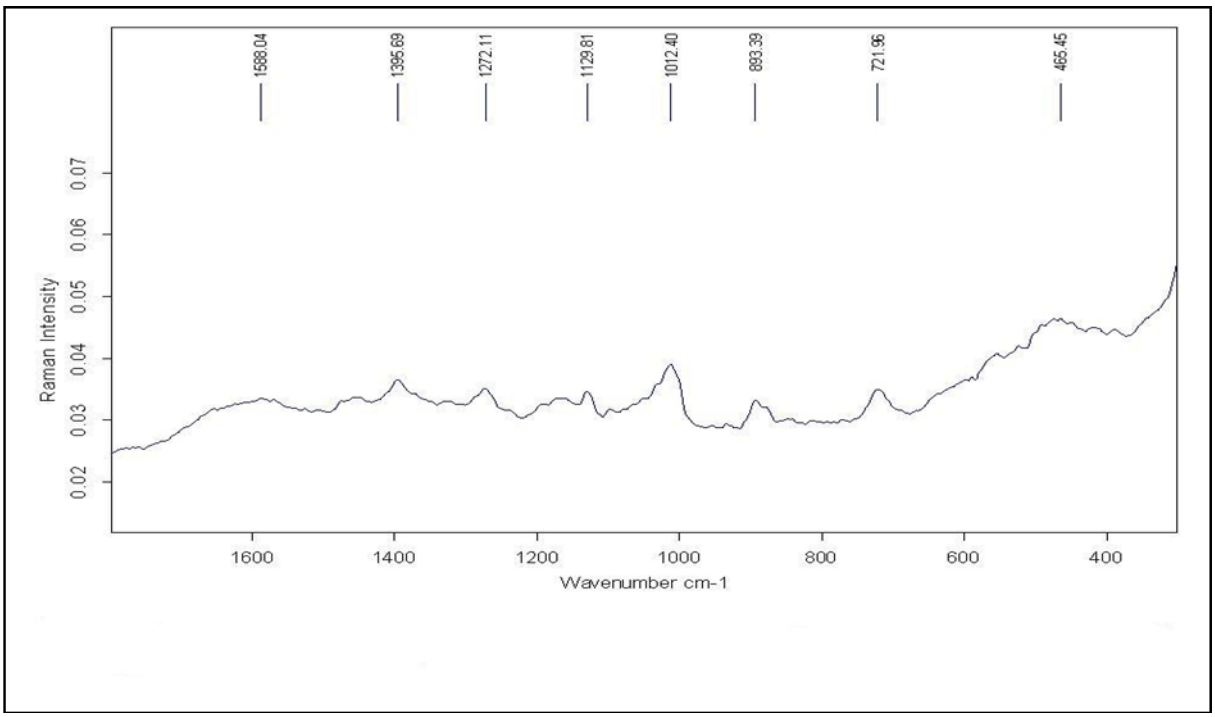

Figure 5. SERS spectrum on nitrophenylphosphate (pH 7.0, 25^{o} C and 0.1M final concentration)

5.8 Results and discussion for the dephosphorylation studies

The SERS spectrum for the reaction of $[CoN_4(OH)(OH_2)]^{2+}$ and NPP^{2-} is depicted in Figure 6 below. The new bands that appear around 1345 and 1260 cm^{-1}

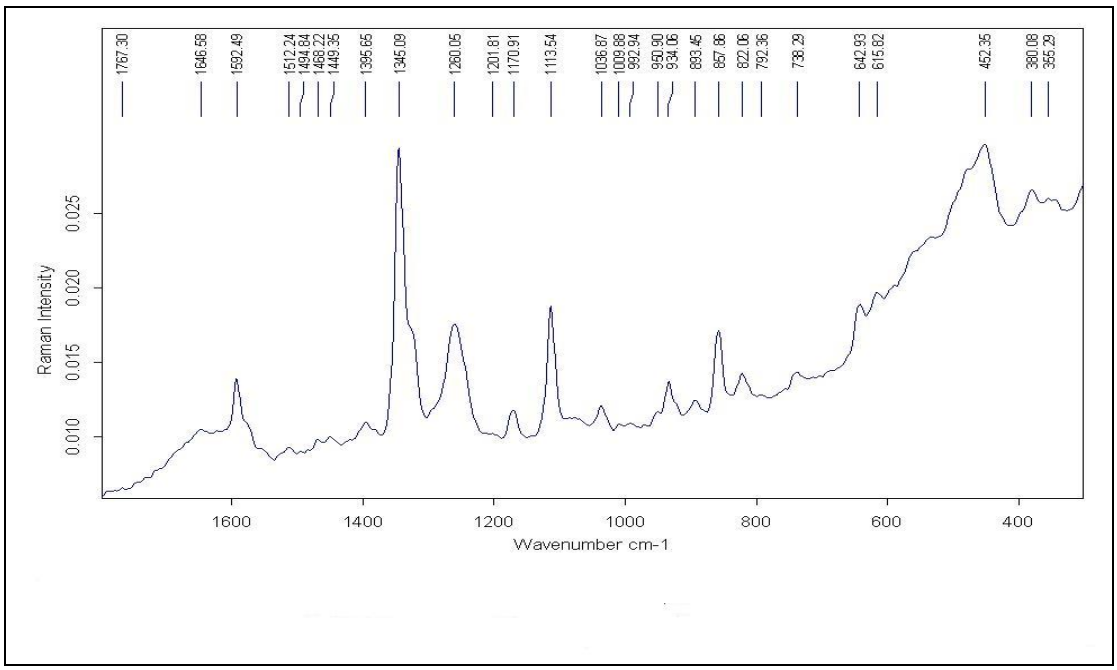

Figure 6. SERS spectrum of the complex formed between $[CoN_4(OH)(H_2O)]^{2+}$ and nitrophenylphosphate (pH 7.0, 25° C and 0.1 M final concentration

are attributed presumably to the formation of the bidentate phosphate complex $[CoN_4PO_4]$ and the metal-coordinated nitrophenylphosphate complex $[CoN_4(OH)O_2NC_6H_4PO_2(O)(OH)]$ as illustrated by the following reaction pathway,

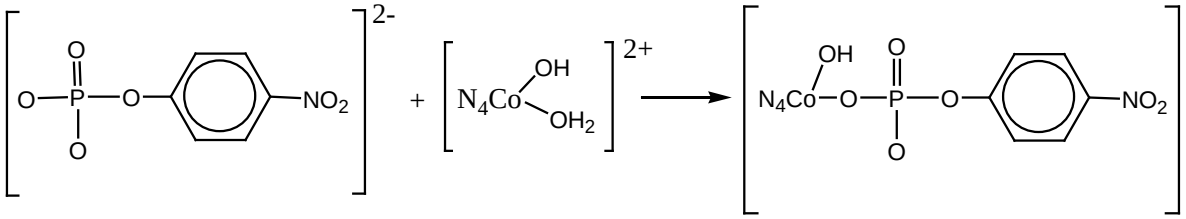

The transient species then undergoes an intramolecular attack of the phosphorus center by the cobalt coordinated hydroxide in the following fashion,

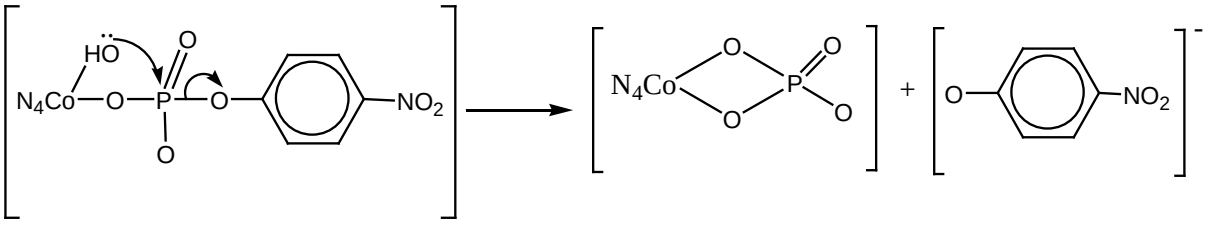

The reaction illustrates the dephosphorylation of nitrophenylphosphate by the cobalt(III) amine complex $[CoN_4(OH)(H_2O)]^{2+}$.

5.9 Results and discussion for the pyrophosphorylation studies

(1) The reaction of $[O_2NC_6H_4O]^-$ with the unactivated pyrophosphate $[H_2P_2O_7]^{2-}$ gave a SERS spectrum similar the SERS spectrum of nitrophenol depicted in Figure 4. The absence of the band in the region of 730 cm^{-1} which is characteristics of v(P-OP) stretching vibration is an indication of pyrophosphorylation reaction not occurring in the reaction solution.

(2) For the reaction of $[H_2P_2O_7]^{2-}$ with $[CoN_4(OH)(OH_2)]^{2+}$ complexes, is presumed to have produced different preformed cobalt(III) amine pyrophosphate complexes $[\{CoN_4(OH)\}(P_2O_7)]^{2-}$, $[\{CoN_4(OH)\}_2(P_2O_7]$ and $[\{CoN_4(OH)\}_3(P_2O_7]^{2+}$ in the reaction solution. The SERS spectra were recorded in solution at pH 7 and 0.1 M concentration after mixing. The spectrum for the 2:1 reaction solution of $[CoN_4(OH)(H_2O)]^{2+}$ and $[H_2P_2O_7]^{2-}$ to produce the $[\{CoN_4(OH)\}_2(P_2O_7]$ complex is depicted in Figure 7 below,

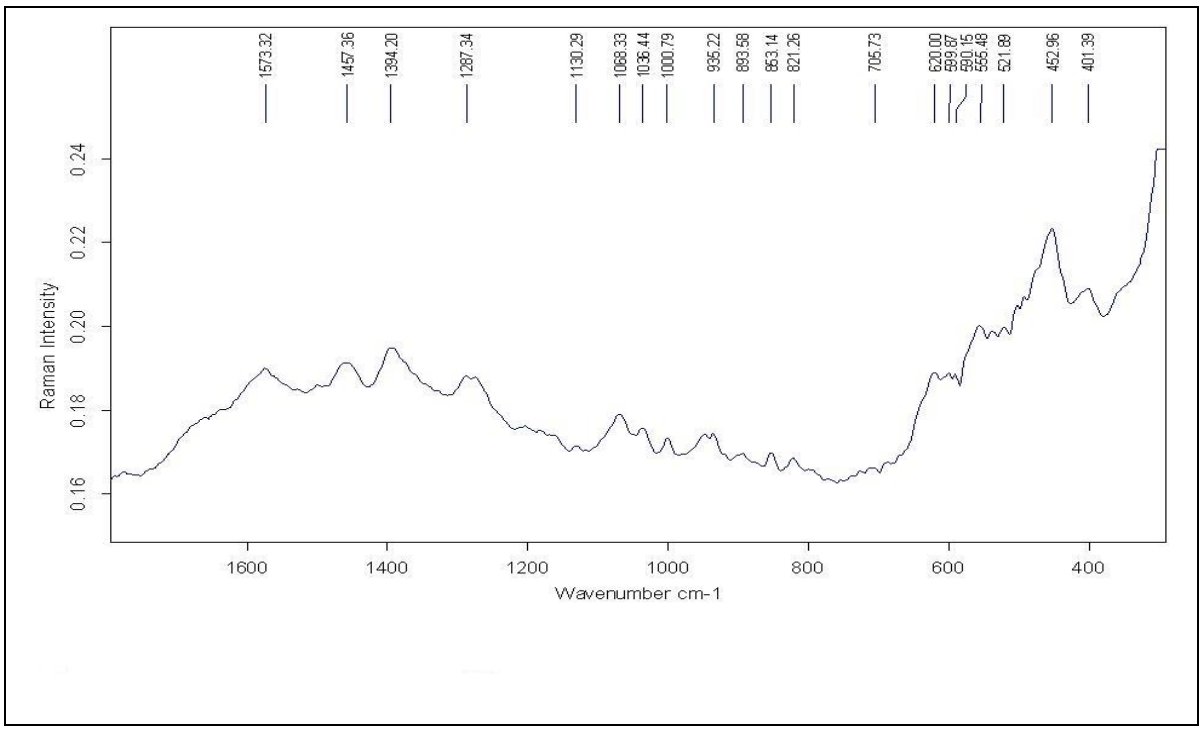

Figure 7. SERS spectrum of the preformed $[\{CoN_4(OH)\}_2(P_2O_7]$ complex at pH 7.0, 25° C and 0.1 M concentration

The plausible pathways for the formation of the coordinated cobalt(III)amine pyrophosphate complex is given below,

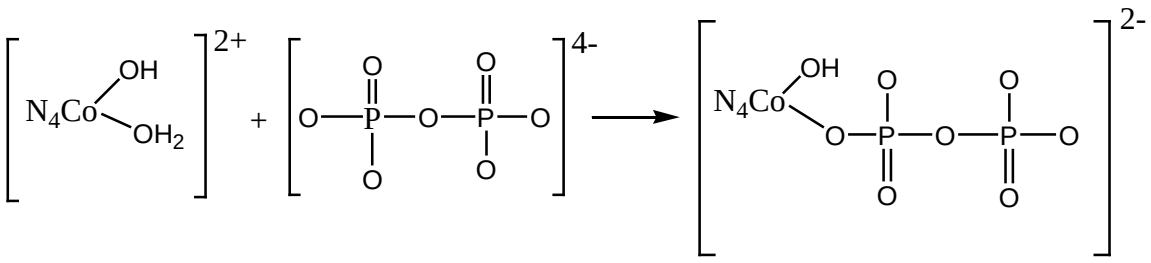

An intramolecular attack of the phosphorus center results largely in the formation of a six membered chelate as shown below,

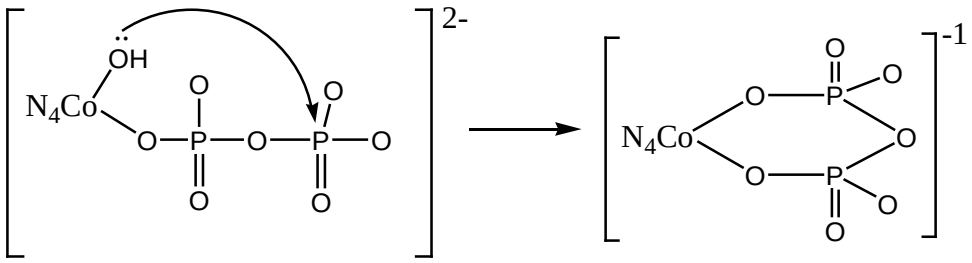

With 2:1 and 3:1 $[CoN_4(OH)(H_2O)]^{2+}$ to $[H_2P_2O_7]^{2-}$, the free oxygens will presumably be coordinated to give additional species in the solution. The band around 1036 cm^{-1} indicates the existence of coordinated pyrophosphates. As can be seen, coordination shifts the vibration peak from around 1000 to 1036 cm^{-1}. Another band located at ~1068 cm^{-1} observed in the spectrum is assigned to the stretching vibration ν(P-O) of the surface diphosphate ion. The symmetric stretching vibration at around 1068 cm^{-1} has been observed as the most intense band in the solutions containing diphosphate anions in previous studies [109,110].

(3) For the reaction of $[O_2NC_6H_4O]^-$ with preformed metal coordinated pyrophosphate complexes, different preformed cobalt(III)amine pyrophosphate complexes $[\{CoN_4(OH)\}P_2O_7]^{2-}$, $[\{CoN_4(OH)\}_2P_2O_7)]$ and $[\{CoN_4(OH)\}_3(P_2O_7)]^{2+}$ were prepared and reacted with nitrophenol. The SERS spectra were recorded in solution at pH 7 and 0.1 M concentration after mixing. The spectrum for the 1: 1 reaction solution of $[\{CoN_4\}P_2O_7]^-$ and $[O_2NC_6H_4O]^-$ is depicted in Figure 8 below,

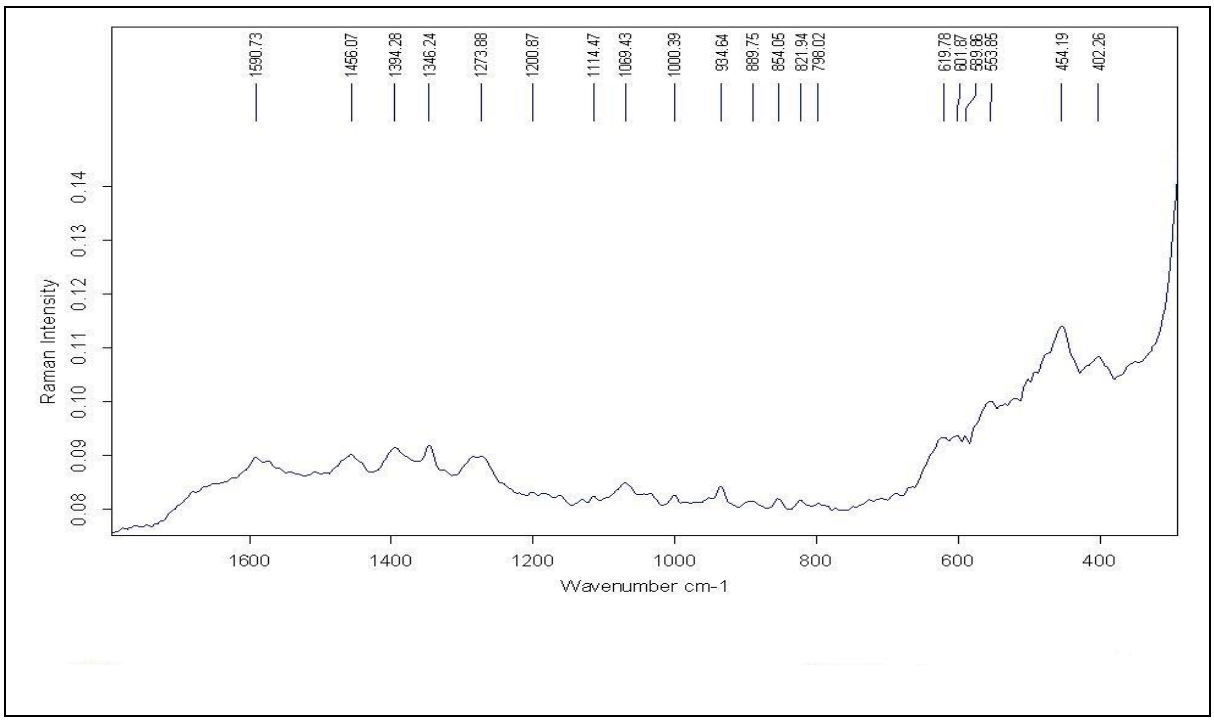

Figure 8. SERS spectrum of the complex formed between the reactions of $[CoN_4(OH)(P_2O_7)]^{2-}$ and NP (pH 7.0, 25^{o} C and 0.1 M final concentration.

Interpretation of this spectrum is complicated due to the presence of numerous coordinated species. Some of the features may be attributed to the formation of metal coordinated nitrophenylpyrophosphate in the reaction solution. The hydroxyl group picks up a proton from the surrounding to form the aquo complex. An attack by the oxygen of the nitrophenolate anion is effeted as shown in the reaction pathway,

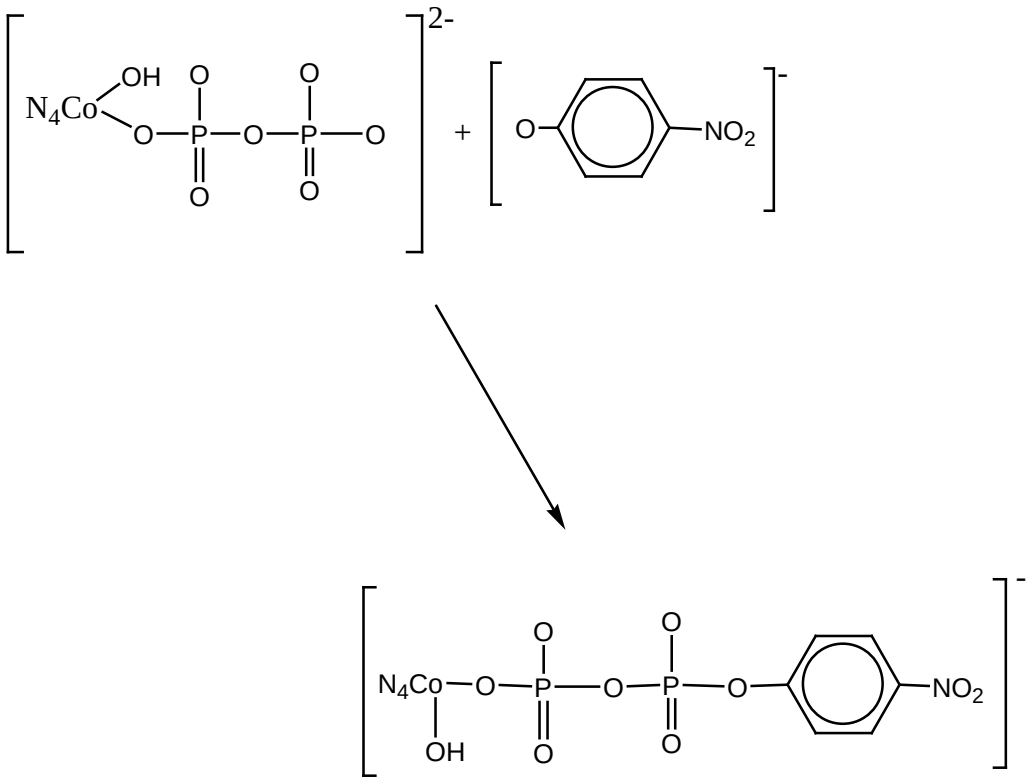

The band around 1000 cm^{-1} is characteristics of coordinated P-O-P stretching vibration.

(4) The presence of a band in the region 350-400 cm^{-1} in Figure 6 suggests the monodentate coordination with the upper silver surface for PO_4^{2-} ion through the oxygen atom O. If the coordination was bidentate, a considerably lower frequency for the v(Ag-O) mode should have been observed[110]. Simultaneous peaks associated with the v(Ag-O) mode ~230-250 cm^{-1} and the v(P-O) mode ~920-930 cm^{-1} as depicted in Table 7 suggest the possibility of both pyrophosphorylation and dephosphorylation reactions occurring in the reaction solution.

(5) The results from various systems studied to monitor the associated reactions in the model compounds were very difficult to interpret under the experimental conditions. For some systems, there were enhancements. Hence resolving the spectra was easy. For others, there was no difference between the Raman and SERS spectra and resolving the spectra was difficult. Maybe with a different silver colloid formulation, better enhancements can be achieved, and hence the reactions can be monitored easily. Further investigation is needed in this regard.

CHAPTER SIX

GENERAL CONCLUSIONS

Phosphorylation, dephosphorylation, pyrophosphorylation and depyro-phosphorylation reactions brought about by the reactions of cobalt(III) bis-trimethylenediamine phosphate/pyrophosphate complexes as the enzyme model with nitrophenol/nitrophenylphosphates as the substrate models in the biologically important middle pH region have been studied using (i) UV-Visible absorption spectroscopy (ii) ^{31}P NMR spectroscopy and (iii) Surface Enhanced Raman Scattering (SERS).

The advantage associated with UV-Visible absorption spectroscopy as an analytical technique and a method of detection emanates from the fact that UV-Visible spectroscopy is firstly, non-destructive to the sample and has a high sensitivity for detecting organic and inorganic compounds. Secondly, cobalt(III)amine phosphates and pyrophosphate complexes have the ability to react with nitrophenol/nitrophenylphosphate to form transient complexes which absorb in the ultraviolet and visible region. This provides the basis for the quantitative spectrometric analysis of the presumed chelates formed in solution employing UV-Visible absorption spectroscopy.

The reaction of $[O_2NC_6H_4O]^-$ with $[HPO_4]^{2-}$ showed no remarkable change in the absorption characteristics of the UV-Visible spectra. The addition of NP

to the preformed bis-(trimethylenediaminecobalt(III) phosphate complex $[CoN_4(OH)(PO_4)]^-$ under the experimental condition showed a decrease in the absorbance maxima at 400 nm and an increase at 310 nm. These changes are consistent with the assertion that NP is being depleted and NPP being formed in solution resulting in phosphorylation. The addition of 2:1 and 3:1 molar ratio of $[CoN_4(OH)(H_2O)]^{2+}$ and $[HPO_4]^{2-}$ under the experimental condition is presumed to produce largely the complexes $[\{CoN_4(OH)\}_2PO_4]^+$ and $[\{CoN_4(OH)\}_3PO_4]^{3+}$ respectively. In these complexes, the additional metal ions per phosphate will force the phosphorus center to adopt an increased electrophilic character, thereby facilitating the attack of nitrophenol on phosphorus. The results show an increased percentage phosphorylation of about 72% for the NP + $[\{CoN_4(OH)\}_2PO_4]^+$. An observed decrease in the percentage phosphorylation for the reactions of NP + $[\{CoN_4(OH)\}_3PO_4]^{2+}$ is as a result of both phosphorylation and dephosphorylation reactions presumably occurring simultaneously in solution. The above reactions mimic the activation and deactivation of phosphorylase enzymes by metal ions in biological system.

The addition of 1:1 molar ratio NPP^{2-} to $[CoN_4(OH)(H_2O)]^{2+}$ under the experimental condition showed an increase in the absorbance maxima at 400 nm and a decrease at 310 nm. These changes are consistent with the assertion that NPP^{2-} is being depleted and NP^- being formed in solution resulting in dephosphorylation. An enhancement of the rate of dephosphorylation of about 54 % was observed in the reaction solutions

that contained 2:1 metal ion to NPP^{2-} ratio. This can be rationalized by the fact that the second metal ion available in the solution coordinates to one of the available oxygens on the NPP^{2-} thereby creating a possibility of intramolecular attack on the phosphorus center by the coordinated hydroxide of the metal ion. The rate of enhancements observed in the system NPP^{2-} + $[CoN_4(OH)(H_2O)]^{2+}$could be attributed to stoichiometric reasons as the rate enhancements were observed only as the metal ion to NPP ratios were increased from 1:1, 2:1 and 3:1 molar ratios. The highest rate enhancement of about 54% was observed in the in the 2:1 metal to NPP^{2-} ratio.

Finally, the use of UV-Visible absorption spectroscopy in the monitoring of phosphorylation, dephosphorylation and pyrophosphorylation has proven to be an effective technique for quantitative studies. UV-Visible spectroscopy provided us with a limited insight into mechanistic features. To gain a better insight on the mechanistic aspects of these biochemical processes in our model studies, ^{31}P $\{^{1}H\}$ NMR absorption spectroscopy was employed.

^{31}P NMR was also employed as an analytical technique because apart from the advantages mentioned in chapter four, it also has the added advantage that the spectra of specific biological molecules can usually be observed in solution without interference from solvent. This advantage does circumvent the serious complications that may arise in observing ^{1}H NMR spectra in H_2O[111]. In complexes with macromolecules such as enzymes, the protons of

interest, unlike phosphorus are usually observed by the many protons in the spectrum arising from the macromolecules. Hence the possibility of readily distinguishing and assigning each phosphorus atom in the formed complexes as well as the state of ionization of their respective terminal phosphates by ^{31}P NMR is probable. Investigators like Cohn and Hughes[28] have shown that the metal chelates of ATP could be distinguished from the free ligating species by a significant change in the chemical shifts of the β-^{31}P of ATP. ^{31}P $\{^{1}H\}$ NMR absorption spectroscopy was capable in providing information which relates to the (i) stoichiometry, (ii) the state of metal chelation, (iii) the ionization state of the preformed complexes, (iv) and possibly the conformational changes in the substrate produced by interaction with the metal ion.

The formation of the preformed metal phosphate species requires a deprotonated water *cis* to the coordinated complex to attack the phosphorus centre. The resultant four membered ring chelate species can then react with nitrophenol to give presumably the metal coordinated nitrophenylphosphate. A logical route for the production of nitrophenylphosphate is via the conjugate dissociative (S_N1) mechanism which is frequently found in cobalt(III)amine chemistry[112]. It is characterized by the production of presumed four-coordinate cobalt intermediate which is able to compete for the nucleophiles in aqueous solution. This mechanism is consistent with known chemistry and accommodates the observed rate enhancements. The intramolecular nucleophile therefore gives rise to a very substantial rate enhancement for addition of nitrophenol, and for the

formation of nitrophenylphosphate in the solution. The preformed metal phosphate species generated by the intramolecular attack of the hydroxyl is depicted as a five coordinate with trigonal-bipyramidal geometry. Alternatively, square-pyramidal[113,114] or octahedral[115,116] phosphorus intermediates could arise from this step. The trigonal-bipyramidal complex could readily react with nitrophenoxide ion or nitrophenol via exocyclic P-O cleavage to produce the metal coordinated nitrophenylphosphate which has a ^{31}P $\{^{1}H\}$ NMR chemical shift of ~6.88 ppm in 0.1M solution[117,118]. An important mechanistic aspect of the system is that phosphate complex formation occurs exclusively via an intramolecular pathway. The intermolecular attack of hydroxide ion at the phosphorus center does not compete with this process even under the concentration of study. This result is consistent with the chemistry observed[127] for $[Co(NH_3)_5O_3POC_6N_4NO_2]^+$ and *cis*-$[(Co(en)_2(OH_2)O_3POC_6H_4NO_2]^+$. The results also provide a unique opportunity to assess the effect that simultaneous coordination to two metal centers has on the rate of phosphorylation reactions. The presence of a second cobalt center is responsible for the increase in rate over that observed for the mononuclear complexes. The conclusion from the analyses is that monodentate coordination of a phosphate to a metal ion will not, by itself, lead to a large acceleration in the rate of complex formation although rate enhancements has been observed in the kinetic studies. The dominant role of metal ions in these reactions might then be seen to be several fold. Firstly, they can group the reactants and provide a coordinated nucleophile for an efficient intramolecular attack[119]. Secondly, they can polarize the phosphorus centers to enhance attack by nucleophile. This effect must also

be coupled with the effects of negative charge neutralization on the phosphate derivatives. Finally, the metal ions bound to the phosphorus oxygen atom may also assist P-O bond rupture as a leaving group effect. For example, in E.coli alkaline phosphatase, it is conceivable that two Zn^{2+} ions are bound to the phosphate complex and/or to the intermediate in order to assist their phosphoryl transfer characters.

For the 1:1 mixtures of $[CoN_4(OH)(H_2O)]^{2+}$ and NPP^{2-}, production of NP^- is clearly dominant. With increased metal complex to NPP^{2-} ratio, we observe evidence for the dinuclear complexes at 25 ppm and 34.15 ppm. It therefore seems clear that efficient dephosphorylation of nitrophenylphosphate requires the formation of complexes containing one or two metal centers. For the (tn) system, the significantly greater dephosphorylation rates observed for the 2:1 complex compared to the 1:1 and 3:1 mixtures points to the 2:1 complex being much more reactive. Indeed, we can quantitatively explain the enhanced rate behaviour on the basis that the reaction proceed entirely through a 1:1 and 2:1 species. Geometrical considerations render it unlikely that 4:1 or higher complexes are of any importance. It is worth mentioning that there are similarities in the mechanisms of phosphorylation and pyrophosphorylation reactions as observed in our experiments. For a 1:1 ratio of $CoN_4(OH)(P_2O_7)]^{2-}$ with NP^-, at the appropriate pH 7, a rate enhancement of close to 60% for the formation of the metal complexed pyrophosphate species was observed. At the 2:1 and 3:1 ratio, we have obtained up to about 17% and 1% respectively of the metal complexed

pyrophosphate. Again the limiting factors are the high reactivity towards hydrolysis to orthophosphate especially for the 3:1 complex as well as the stability of the presumed complexes formed in solution. The formation of the polynuclear pyrophosphate in solution species is pH dependent. We believe this aspect is the main contributor to the pH dependency of the overall pyrophosphorylation process. The requirement of polynuclear metal complexation for efficient pyrophosphorylation is paramont. The present study demostrates a dramatic enhancement in the rate of pyrophosphorylation for the biologically important neutral pH region. This is, to our knowledge, the first case where an enhancement of this magnitude has been observed in pyrophosphorylation reaction processes involving P-O-P linkages in a homogenous model system.

Only few experiments are feasible at concentrations appreciably lower than 1 mM using this technique. This is perhaps the single, most serious limitation in using ^{31}P NMR more widely in bioinorganic chemistry. The second limitation related to ^{31}P NMR spectroscopy, especially in relation to some of the experiments in this investigation, is the unavailability of a reliable theory to relate the chemical shifts to structural features of the phosphorus-containing biological molecules. It should be pointed out that a value of the chemical shift for metal ions bound complexes cannot be used to specify the anionic complexes. This is because; many shifts arising from unknown perturbations are far downfield in the metal ion chelated complexes. Progress in overcoming these two limitations would undoubtedly

enhance the utility of this powerful technique by orders of magnitude. With the development of Fourier transform (FT) ^{31}P NMR spectroscopy, the sensitivity of instruments and the accuracy of the data produced have dramatically improved [120] and it is now possible to detect and identify quite low concentrations of phosphorus containing complexes. Indeed, by using all the instrumental aids available to enhance sensitivity, it has been possible to estimate phosphorus complexes at the 200 and even the 5 ppm levels[121,122]. This capability has been put to rapid use in the bio-inorganic field, as the phosphorus atom is involved directly in many vital biochemical reactions that include phosphorylation, dephosphorylation pyrophosphorylation and depyrophosphorylation reactions.

The last phase of the investigation employed the use of Surface Enhanced Raman Scattering as an analytical spectrophotometric technique in probing phosphorylation, dephosphorylation, pyrophosphorylation and depyro-phosphorylation reactions in the model compounds with the aim of unravelling additional features that take place in the reaction. The technique is expected to provide both structural and electronic insights into the species of interest. The SERS spectra obtained provided more information about the molecular structure of the different complexes formed in solution. The enhancement mechanism of SERS is considered in two ways: a chemical enhancement and an electromagnetic field enhancement. The chemical enhancement is derived from electromagnetic interactions between the molecules and the metal substrate, which can provide an order of magnitude increase in signals. However, the more dominant effect that

contributes to the SERS signal enhancement is due to enhanced electromagnetic fields at the metal colloid surface. These enhanced fields are well known to originate from the localized surface plasmon resonance of the Ag colloid, in which incident lights lead to a collective oscillation of the surface conduction electrons of the metal colloid aggregates. This collective oscillation results in strongly enhanced electromagnetic fields that are confined to within several nanometers of the silver colloid surface[123-125]. Only molecules that enter this zone of enhanced field experience significant enhancement of their Raman scattering. A single metal colloid typically offers SERS signal enhancements on the order of 10^2-10^6 as have been reported[126]. However, when a colloid made up of two metal aggregate are in close proximity[127], their dipoles can couple, leading to stronger overall field enhancements, reported to be as high as 10^{10}-10^{14}. As such colloid aggregates are often considered an optimum SERS substrate, even though they lack well-defined structure[128]. The use of SERS as an analytical technique for studies of phosphorylation, dephosphorylation, pyrophosphorylation and depyrophosphorylation in model systems is a relatively new field, yet it is one that has provided diverse results and insights into both structure and dynamic processes involved in these biochemical reactions. The SERS technique has proved to be a very effective analytical tool because of its high sensitivity, selectivity, and fluorescence-quenching properties. It is our presumption that this will someday provide an insight to what is taking place within cells in living systems.

6.1 FUTURE OUTLOOK

One of the greatest challenges that are yet to be overcome is achieving a uniform distribution of the colloid aggregates in the solution for effective SERS amplification. An interesting approach to this may be to use hybrid magnetic-metallic nanoparticles that allow the nanoparticles to be repositioned within the reaction matrix through the use of an external magnet as proposed in the literature [128]. The current limitation of SERS for studying naturally occurring intracellular species is that it is difficult to provide absolute information about which biomolecules are nearby. However, the technique is well suited to reporting on differences in environment, including changes in SERS spectra as a function of structure of the molecules under study.

At present, the ability to make unambiguous assignments of various SERS bands to specific biological molecules is a distinct challenge due to overlap in structural motifs present in a number of different molecules. However, the future looks bright for intracellular SERS, especially with development of probes that target specific analytes, either within the intracellular matrix or through surface functionalization. The structural information provided by SERS allows us to know with absolute certainty when a particular target analyte is within the zone of enhancement of metallic nanoparticles. By designing SERS probes that have a specific reporter function for intracellular behaviour, it would in principle be possible to measure specific properties of the intracellular matrix. As nanoparticle synthesis continues to

improve, SERS will evolve into an even more robust, and ultimately ubiquitous, intracellular analytical technique.

REFERENCES

(1) Marshall, C. J.; Leevers, S. J.; *Methods Enzymol.* **1995**, 255, 273-290.

(2) Pines, J.; *Biochem. Soc. Trans.* **1993**, 21, 921-925.

(3) Frimpong, K.; Darnay, B. G.; Rodwell, V. W.; *Protein Express Purif.* **1993**, 4, 337-344.

(4) Fisher, E. H.; Krebs, E. G.; *J. Bio. Chem.* **1955**, 216, 121-132.

(5) Johnson, L. N.; Bartford, D.; *Annu. Rev. Biophys. Biomol. Struct.* **1993**, 22, 199-232.

(6) Stoud, R. M.; *Curr. Opin. Struct. Biol.* **1993**, 1, 826-835.

(7) Hunter, C. F.; Rodwell, V. W.; *J. Lipid Res.* **1980**, 21, 399-405.

(8) Kennelly, P. J.; Rodwell, V. W.; *J. Lipid Res.* **1985**, 26, 903-914.

(9) Shin, N.; Cohn, M.; Nick, J.; *J. Biol. Chem.* **1982**, 13, 7646-7649.

(10) Cohn, M.; Jaffee, K.; Nick, J.; *J. Biol. Chem.* **1982**, 57, 7650-7656.

(11) Springs, B.; Cooperman, B S.; Panakal, A.; Hamm, D J.; *Biochemistry.* **1981**, 20, 6051-6060.

(12) Liu Zu, D.; Hider, R. C.; *Coord. Chem. Rev.* **2002**, 232 (1-2), 151-171.

(13) Klabunde, T.; Krebs, B.; Lipscomb, W. N.; Strater, N.; *Angew. Chem. Int. Ed. Eng.* **2004**, 35, 2025-2055.

(14) Vichard, C.; Kaden, T. A.; *Inorg. Chim. Acta.* **2002**, 337, 173-180.

(15) Vichard, C.; Kaden, T. A.; *Inorg. Chim. Acta.* **2004**, 357, 2285-2293.

(16) Mildvan, A. S.; *Adv. Enzymol. Relat. Areas Mol. Biol.* **1979**, 49, 103-126.

(17) Mildvan, A. S.; Grisham, C. M.; *Struct. Bonding (Berlin).* **1974**, 20 1-20.

(18) Benkovic, S. J.; Bruice, T. C.; *Bioorganic Mechanisms*. W.A. Benjamin Edition, New York, **2010**.

(19) Williams, A.; Naylor, R. A.; *J. Chem. Soc*. **1971**, 10, 1973-1979.

(20) Kirby, A. J.; Jencks, W. P.; *J. Am. Chem. Soc.* **1965**, 87, 3209-3216.

(21) Kirby, A. J.; *Adv. Phys. Org. Chem.* **1980**, 17, 183-278.

(22) Page, M. I.; Angew. Chem. **1977**, 89, 456-467.

(23) Jencks, W. P.; *Adv. Enzymol. Relat. Areas Mol. Biol.* **1975**, 43, 219-410.

(24) Ramirez, F.; Marecek, J.; Minore, S.; LeNoble, W.; *J. Am. Chem. Soc.***1986**, 108, 348-349.

(25) Westheimer, F. H.; *Phosphorus Chem.* **1981**, 22, 65-68.

(26) Smikjo, A.; *Chemical Kinetics and Inorganic Reaction Mechanisms*, 2nd edition, Springer, **2003**, 40-41.

(27) Ramirez, F.; Marecek, J. F.; *Biochim. Biophys. Acta.* **1980**, 598, 21-29.

(28) Cohn, M.; Hughes, T. R,; *J. Biol. Chem.* **1962**, 237, 176-181.

(29) Chang, R. K.; *Ber, Bunsen-Ges. Phys. Chem.,* 1987, 91, 296-305.

(30) Sigman, D. S.; Jorgensen, C. J.; *J. Am. Chem. Soc.* **1972**, 94, 1720-1730.

(31) Sigel, H.; *Chemia. Anal (Warsaw).* **1967**, 21, 489-500.

(32) Pilipenko, A. T.; Tananaiko, M. M.; *Khim. Proct-st (Moscow).* **1973**, 28, 745-778.

(33) Dean, E. W.; *Chem. Rev.* **1996**, 96, 2435-2458.

(34) Ling, Y.; Rong-Zhen, L.; Jian-Guo, Y.; Ruo-Zhang, L.; *J. Phys. Chem. B.* **2009**, 113, 6505-6510.

(35) Novak, T.; Mildvan, A. S.; Kenyon, G. L.; *Biochemistry*. **1973**, 12, 1690-1701.

(36) Shray, K. J.; Mildvan, A. S.; *J. Biol. Chem.* **1972**, 247, 2034-2037.

(37) David, L. N.; Michael, M. C.; *Principles of Biochemistry* (4th Edition), **2010**.

(38) Tymoczko J. L.; Berg, J. M.; Stryer, L.; Biochemistry: *A Short Course*. W.H. Freeman & Co, New York, **2012**.

(39) Kornbey, A.; *DNA replication*. W.H. Freeman & Co, **1980**.

(40) Wotterman, G. M.; Scott, R. M.; Haight, G. P.; *J. Am. Chem. Soc.* **1974**, 96, 7569-7574.

(41) Creaser, I. I.; Dubs, R. V.; Sargeson, A. L.; *Aust. J. Chem.* **1984**, 37, 1999-2003.

(42) Haight, G. P.; Hambley, T. W.; Hendry, P.; Sargeson, A. M.; *J. Chem. Soc. Chem. Commun.* **1985**, 8, 488-491.

(43) Michael, J. K.; Thomas, D. J.; *Ultraviolet and Visible Spectroscopy*, Wiley, London, **1987**.

(44) Lumir, S.; *Analytical Absorption Spectrophotometry in the Visible and Ultraviolet: The Principles,* Elsevier, London, **1989**.

(45) Ronald, C. D.; Roy, S.; *Visible and Ultraviolet Spectroscopy,* Wiley, London, **1987**.

(46) Daniel, C. H.; *Qualitative chemical analysis,* Freeman, **1982**.

(47) Burgess, C.; Knowles, A.; *Techniques in Visible and Ultraviolet Spectrometry, Practical Absorption Spectrometry, Ultraviolet Spectrometry,* Chapman & Hall, **1984**.

(48) Jones, D. R.; Lindoy, L. F.; Sargeson, A. M, *J. Am. Chem. Soc.* **1984**, 106, 7807-7819.

(49) Eguzozie, K. U.; *MSc dissertation*. **2008**.

(50) Bauer, H. F.; Drinkard, W.C.; *J. Am. Chem. Soc.* **1960**, 82, 5031-5032.

(51) Hubner, P.W.A.; Milburn, R. M.; *Inorg. Chem.* **1980**, 19, 1267-1272.

(52) Lincoln, S. F.; Stranks, D. R.; *Aust. J. Chem.* **1968**, 21, 37-56.

(53) Jones, D. R.; Lindoy, L. F.; Sargeson, A. M.; *J. Am. Chem. Soc.* **1983**, 105 25, 7327-7336.

(54) Haight, G. P.; Hambley, T. W.; Sargeson, A. M.; Hendry, P. L.; *J. Chem. Soc. Chem. Commun.* **1984**, 23, 1568-1571.

(55) Stranks, D. R.; Vanderhoef, N.; *Inorg. Chem.* **1976**, 15, 2639-2642.

(56) Massoud, S. S.; Milburn, R. M.; *Inorg. Chim. Acta.* **1988**, 146, 3-4.

(57) Tafesse, F.; Massoud, S. S.; Milburn, R. M, *Inorg. Chem.* **1985**, 24, 2591-2593.

(58) Tafesse, F.; Massoud, S. S.; Milburn, R. M.; *Inorg. Chem.* **1993**, 32, 1864-1865.

(59) Hediger, M.; Milburn, R. M.; *Phos. Chem.***1981**, 171, 211-216

(60) Creaser, I. I.; Haight G. P.; *J. Chem. Soc. Chem. Commun* **1984**, 23, 1568-1571.

(61) Epp, J. B.; *Biochem. Biophysc. Res. Commun.* **2004**, 429, 60-70.

(62) Chao, C. C.; *Clin. Exp. Immunol.* **2001**, 8, 446-448.

(63) Redfield, A. G.; *Methods in Enzymology* (C.H.W Hirs & S.N Timasheff eds), Academic press, New York, **1978**.

(64) Harold, G.; *Introduction to Phosphorus Chemistry,* Cambridge University Press, **1981**.

(65) Corbridge D. E. C.; *Phosphorus 2000: Chemistry, Biochemistry & Technology,* Elsevier, London, **2000**.

(66) Stranks, D. R.; Lincoln, S. F.; *Aust. J. Chem.* **1968**, 21, 1745-1751.

(67) Jackson, W. G.; Harrowfield, J. M.; Vowles, P. D.; *Int. J. Chem. Kinet.* **1977**, 9, 535-48.

(68) Milburn, R. M.; Hediger, M.; *Inorg. Chem.* **1982**, 16, 165-182.

(69) Jonasson, I. R.; Lincoln, S. F.; Stranks, D. R.; *Aust. J. Chem.* **1970**, 23, 2267-2278.

(70) Jonasson, I. R.; Murray, R. S.; Stranks, D. R.; Yandell, J. K.; *Proc. Int. Conf. Coord. Chem.* **1969**, 32, 1144-1169.

(71) Furtak, T. E.; Chang. R. K.; *"Surface enhanced Raman scattering",* Plenium, New York, **1982**.

(72) Weaver, M. J.; Farquharson, S.; Tadayoni, M. A.; *J. Chem. Phys.,* **1985**, 82, 4867-4874.

(73) Garrel, R. L.; *Anal. Chem.* **1989**, *61*, 401-402.

(74) Storey, J. M. E.; Barber, T. E.; Shelton, R. D.; Wachter, E. A.; Carron, K. T.; Jiang, Y.; *Spectroscopy.* (Duluth, MN, United States), **1995**, 10, 20-25

(75) Fleischmann, M.; Hendra, P. J.; McQuillan, A. J, *Chem. Phys. Lett.* **1974**, 26, 163-166.

(76) Jeanmaire, D. L.; VanDuyne, A. P.; *J. Electroanal. Chem.* **1977**, 84, 1-20

(77) Nie, S.; Emory, S. R.; *Science.* **1997**, 275, 1102-1106.

(78) Smith, E.; Dent, G.; *Modern Raman Spectroscopy: A practical approach,* John Wiley & Sons Ltd, **2005**.

(79) LeRu, E. C.; Etchegoin, P. G.; *Anal. Chem.* **2009**, 81, 682-688.

(80) Hering, K.; Cialla, D.; Ackermann, K.; *Anal. Bioanal. Chem.* **2009**, 390, 113-124.

(81) Moskovits, M.; *Rev. Mod. Phys.* **1985**, 57, 783-826.

(82) Schatz, G. C.; Young, M. A.; VanDuyne, R. P.; *Top. Appl. Phys.* **2006**, 103, 19-46.

(83) Otto, A.; *J. Raman Spectrosc.* **2005**, 36, 497-509.

(84) Hao, E.; Schatz, G. C; *J. Chem. Phys.* **2004**, 120, 357-366.

(85) Stiles, P. L.; Dieringer, J. A.; Shah, N. C; *Annu. Rev. Anal. Chem.* **2008**, 1, 601-626.

(86) Whitney, A. V.; Elam, J. W.; Zou, S.; *J. Phys. Chem.* B. **2005**, 109, 20522-20528.

(87) Dieringer, J. A.; Lettan, R. B.; Scheit, K. A.; *J. Am. Chem. Soc.* **2007**, 129, 16249-16256.

(88) Michaels, A. M.; Nirmal, M.; Brus, L. E.; *J. Am. Chem. Soc.* **1999**, 121, 9932-9939.

(89) Saito, H.; Ikezawa, Y.; Toda, G.; *Chem. Phys. Lett.* **1984**, 110, 291-293.

(90) Tushel, D. D.; Pemberton, J. E.; Cook J. E; *Langmuir.* **1986**, 2, 380-388.

(91) Yan, W.; Bao, L.; Mahurin, Dai S.; *Appl. Spectrosc.* **2004**, 58, 18-25.

(92) Morgan, S. H.; *J. Raman. Spectrosc.* **2005**, 36, 1082-1087.

(93) Sutherland, W. S.; Winefonder, J. D.; *J. Raman. Spectrosc.* **1991**, 22, 541-549.

(94) Smith, E.; Dent, G.; *Modern Raman Spectroscopy- a practical approach.* John Wiley and Sons Ltd (**2005**).

(95) Kneip, K.; Moskovits, M.; Kneip, H.; *Top. Appl. Phys.* **2006**, 103, 147-184.

(96) Moskovits, M.; *J. Am. Chem. Soc.* **1985**, 107, 6826-6829.

(97) Myers, A. B.; Mathies, R. A.; Biological Applications of Raman Spectroscopy, Spiro TG (Ed), Wiley: New York, **2007**.

(98) Creighton, J. A.; *Surf. Sci.* **1983**, 124, 209-219.

(99) Wang, Z; Lu, C.; Yun, B.; *Proc. SPIE-Int. Soc. Opt. Eng.* **2008**, 6826, 1-6.

(100) Hao, E.; Schatz, G. C.; *J. Chem. Phys.* **2004**, 120, 357-366.

(101) Chapman, A. C; Thirlwell, L. E; *Spectrochim. Acta,* **1964**, 20, 937-942.

(102) Preston, C. M; Adams, W. A; *J. Phys. Chem,* **1979**, 83, 814-821.

(103) Lincoln, S. F.; Stranks, D. R.; *Aust. J. Chem.* **1968**, 21, 1745-1755.

(104) Weber, M.; Nart, F. C.; *Electrochim. Acta.* **1996**, 41, 653-659.

(105) Nart, F. C.; Iwasita, T. J.; *J. Electroanal. Chem. Interfacial Electrochem.* **1992**, 322, 289-296.

(106) Niaura, G.; Gaigalas, A. K.; Vilker, V. L.; *J. Phys. Chem. B.* **1997**, 101, 9250-9262.

(107) Nart, F. C.; Iwasita, T.; *Electrochim. Acta.* **1992**, 37, 385-392.

(108) Gao, P.; Weaver, M. J.; *J. Phys. Chem. B.* **1986**, 90, 4057-4063.

(109) Lim, K.T.; Eysel, H. H.; *J. Raman. Spectrosc.* **1988**, 19, 525-539.

(110) Gao, X.; Davies, J. P.; Weaver, M. J.*; J. Phys. Chem. B,* **1990**, 94, 6858-6864.

(111) Gorenstein, D. G.; *Phosphorus 31 NMR: Principles and Applications,* Academic press, NY, **1984**.

(112) Sargeson, A. M.; *Pure Appl. Chem.* **1973**, 33, 527-544.

(113) Holmes, R. R.; *J. Am. Chem. Soc.* **1974**, 96, 4143-4149.

(114) Holmes, R. R.; *J. Am. Chem. Soc.* **1975**, 97, 5379-5385.

(115) Chang, B. C.; Denney, D. B.; Powel, R. L.; White, D. L.; *J. Chem. Soc. Chem. Commun.* **1971**, 18, 1070-1071.

(116) Ramirez, F.; *J. Am. Chem. Soc.* **1968**, 90, 751-755.

(117) Harrowfield, J. M.; Lindoy, L. F.; Jones, D. R.; Sargeson, A. M.; *J. Am. Chem. Soc.* **1980**, 102, 7733-7741.

(118) Jones, D. R.; *J. Am. Chem. Soc.* **1983**, 105, 7327-7336.

(119) Knowles, J. R.; *Rev. Biochem.* **1980**, 49, 877-919.

(129) Krusic, P. J.; San Fillipo, J.; Hutchinson, B. Hans, R. L.; Daniels, L. M.; *J. Am. Chem. Soc.* **1981**, 103, 2129-2131.

(120) Braun, S.; Kalinowski, H. O.; Berger, S.; *100 or more Basic NMR Experiments*. VCH, Weinheim, **1990**.

(121) Quin, L. D.; Verkade, J. G.; *Phosphorus-31 NMR Spectral Properties in Compounds Characterization and Structural Analysis*. Wiley-VCH, **1994**.

(122) Schlucker, S.; *Surface Enhanced Raman Spectroscopy. Analytical, Biophysical & Life Science Applications.* Elsevier, **2010**.

(123) Weatherby, S.; *Surface Enhanced Raman Spectroscopy,* Royal Society of Chemistry, **2006**, Cambridge, United Kingdom.

(124) Kneipp, K.; Moskovits, M.; Kneipp, H.; *Surface Enhanced Raman Scattering. Phys & Applications,* Springer, Berlin, Heidelberg, **2006**.

(125) Aroca, R. F.; *The observed spectrum in Surface Enhanced Vibrational Spectroscopy Abstract,* 58th, Southeast regional meeting of the American Chemical Society, Augusta, G.A United States, **2006**.

(126) Kerker, M.; Thompson, B. J.; *Selected Papers on Surface Enhanced Raman Scattering. Society of Photo Optics*, San Francisco, United States, **1990**.

(127) Dieringer, J. A.; *Faraday Discuss*, **2006**, 132, 9-26.

(128) Stiles, P. L.; Dieringer, J. A.; Shah, N. C.; VanDuyne, R. P.; *Annu. Rev. Anal. Chem.* **2008**, 1, 601-626.